Nonlinear Dynamics of Annular and Circular Plates under Thermal and Electrical Loadings

Waleed F. Faris

Dissertation submitted to the Faculty of the Engineering
Virginia Polytechnic Institute and State University
in partial fulfillment of the requirements for the degree of

Doctor of Philosophy
in
Engineering Mechanics

Ali H. Nayfeh, Chairman
Werner Kohler
Liviu Librescu
Saad A. Ragab
Alfred Wicks

December, 2003
Blacksburg, Virginia

Keywords: Nonlinear Dynamics, Circular, Annular, Thin Plates, Thermal, Electrostatic

Nonlinear Dynamics of Annular and Circular Plates under Thermal and Electrical Loadings

Waleed F. Faris

(ABSTRACT)

The nonlinear static and dynamic response of circular and annular plates under electrostatic, thermal, and combined loading is investigated. The main motivation for the study of these phenomena is providing fundamental insights into the mechanics of micro-electro-mechanical-systems (MEMS). MEMS devices are usually miniaturization of the corresponding macro-scale devices. The basic mechanics of the components of many MEMS devices can be modeled using conventional structural theories. Some of the most used and actively researched MEMS devices- namely pressure sensors and micropumps- use circular or annular diaphragms as principle components. The actuation and sensing principles of these devices are usually electrostatic in nature. Most MEMS devices are required to operate under wide environmental conditions, thus, a study of thermal effects on the performance of these devices is a major design consideration.

There exists a wide arsenal of analytic, semi-analytic, and numerical tools for nonlinear analysis of continuous systems. The present work uses different tools for the analysis of different types of problems. The selection of the analysis tools is guided by two principles. The first consideration is that the analysis should reveal the fundamental mechanics and dynamics of the problem rather than simply generating numerical data. The second consideration is numerical efficiency. Guided by the same principles, the basic structural model adopted in this work is the von-Karman plate model. This model captures the basic nonlinear phenomena in the plate with minimal complexity in the equations of motion, thus providing a balance between simplicity and accuracy.

We address a wide array of problems for a variety of loading and boundary conditions. We start by analyzing annular plates under static electrostatic loading including the variation of the plate natural frequencies with the applied voltage. We also analyze parametric resonances in plates subjected to sinusoidally varying thermal loads. We investigate the prebuckling and postbuckling static thermal response and the corresponding variation of the natural frequencies. Finally, we close by investigating the problem of a circular plate under a combination of thermal and electrostatic loading. The results of this investigation demonstrate the importance of including nonlinear phenomena in the modeling of MEMS devices both for correct quantitative predictions and for qualitative description of operations.

Dedication

To my mother who could not wait to see this moment.

To my father who tries to hold.

To Heba, Mariem, and Yomna my only joy in this life.

Acknowledgement

I would like to thank all who helped and supported me during the past four years in my research. Special thanks goes to my academic advisor Dr. Ali Nayfeh for his help, guidance, and unfailing support without which the completion of this work would have been impossible. I would also like to express my thanks to my committee members for their support and valuable suggestions, especially Professor Ragab.

Contents

List of Figures

List of Tables

Chapter 1

Introduction and Literature Review

1.1 Motivation

Since the electronic revolution in the sixties, miniaturization has become an important goal of technology. This is quite clear in the doubling of the number of transistors per chip every two years since the sixties (Michalicek, 2000). Since the first bulk-etched silicon wafers were used as pressure sensors in the 1970*s*, a new discipline arose known as *Microelectromechanical Systems* (MEMS) in the USA and *integrated systems* in Europe (Michalicek, 2000). MEMS are usually defined as highly miniaturized devices or array of devices combining electrical and mechanical components that are fabricated using integrated circuit (IC) batch-processing techniques (Michalicek, 2000). MEMS have received a great deal of attention in recent years. This is due not only to the excitement naturally associated with a new emerging technology, but also to the great promise of increased miniaturization and improved performance of these devices over conventional devices. Miniaturization means less energy input, increased reliability, reduced cost, and a room for more complicated and advanced applications.

Applications of MEMS are very wide. In automotive engineering applications, MEMS-based sensors are used as coolant pressure sensors, manifold gas pressure sensors, airbag accelerometers, and speedometers. In medical applications, MEMS sensors are used for measuring blood pressure and micropumps (MEMS pumps) are used for drug delivery (Sensors Magazine, 1997). In defense

applications, MEMS are used in inertial navigation, as distributed unattended sensors for security surveillance and process control, as integrated fluidic systems for propellant and combustion control, as mass data storage devices, and in active and conformal surfaces for distributed aerodynamic control of aircraft (Michalicek, 2000).

The worldwide MEMS market is growing at a very fast rate. In 1993, it was less than 1 Billion US Dollars and in 2000 it approached 14 Billion US Dollars. The lion's share in 2000 was for pressure sensors, which constituted about one quarter of the worldwide market, and for microfluidic devices, which constituted slightly less than one quarter of the worldwide market (Michalicek, 2000).

The main theme of this dissertation is micromachined devices, especially sensors and micropumps. Many micromachined sensors are miniaturized versions of their macroscopic counterparts. Thus, it is quite instructive to take a look at the macroscopic versions of these devices.

For pressure sensors it is reported (Sensors Magazine, 1997) that many of these devices were based on diaphragms. Other devices were also sought to improve the amount of deflection of a simple diaphragm, such as capsules and bellows. Strain gauges are commonly used to measure the deflections of diaphragm-based devices. Some diaphragm sensors have elaborate systems of levers, which are linked to electric switches or potentiometer winding. Others, instead of having strain gauges mounted directly on the diaphragm itself, have a piston, which is driven into a mounted strain gauge by the motion of the diaphragm. Most sensors for greater than atmospheric pressure share the common characteristic of deformable diaphragm. In diaphragm-based pressure sensors, the applied pressure is determined by the deflection it produces in the diaphragm. The shape of the diaphragm is arbitrary, but generally takes the form of a square or a circle.

Macroscale pumps are generally classified into dynamic-type pumps and positive-displacement pumps. Dynamic-type pumps include centrifugal, axial, and turbine pumps. Positive-displacement pumps include reciprocating and rotary pumps. Reciprocating pumps, which are most common, include piston and diaphragm pumps (Tay and Phoon, 1997).

Micropump technology is currently one of the most advanced technologies in MEMS. They are designed to handle small and precise volumes in various medical, biomedical, and chemical applications. The function of a micropump is to raise the pressure of a certain volume of gas or liquid.

Usually, micropumps are integrated with other microflow devices and sensors to allow precise control and sensing of flow of the order of microliters. Several pumping principles are available in the literature and most of them mimic macroscale pumps. Figure 1.1 shows a diagram for a diaphragm micropump.

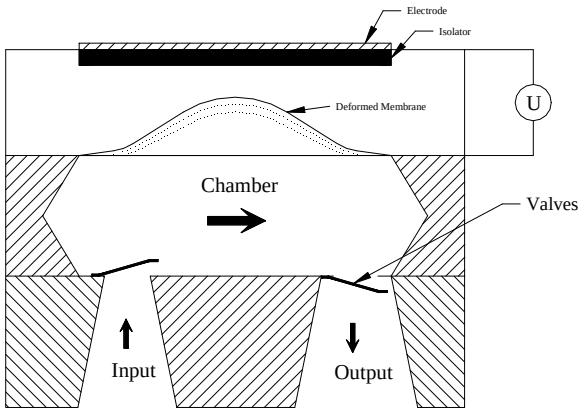

Figure 1.1: Diagram for a diaphragm micropump.

Generally, micropumps are classified into two categories (Tay and Phoon, 1997): mechanical and non-mechanical. Mechanical micropumps include reciprocating and peristaltic pumps, and non-mechanical micropumps include electrohydrodynamic pumps. Reciprocating micropumps with different actuating techniques are widely used. Piezoelectric, pneumatic, electrostatic, and thermopneumatic actuation principles are used. Electrostatic actuation is gaining popularity because of its simplicity and high-flow output pressures (Tay and Phoon, 1997). Different shapes of electrostatic actuating elements are reported in the literature, such as rectangular, square, circular, and annular (Saif et al., 1999; Tay and Phoon, 1997). They are also used in other MEMS devices, such as sensors, valves, deformable micromirrors, and micro-turbo generators.

Several transduction techniques have been used for micromachined devices, in general, and micropumps and sensors, in particular. These include piezoelectric, capacitive, optics, and resonance.

So, it is clear now that diaphragm-based MEMS devices are among the most common devices. Also, capacitive or electrostatic actuation is commonly used in commercial applications because they suffer less losses and need less mechanisms for their operation. Temperature affects the

sensitivity and performance of such devices to a considerable extent, especially sensors used in high-temperature environments, such as exhaust manifolds in cars, propulsion engines, and steel making industry. Also, temperature affects the measurement accuracy of other MEMS devices, such as accelerometers and resonance-based calibration instruments.

The main objective of this dissertation is to analyze the mechanical response, static and dynamic, of circular diaphragms under electrostatic and/or thermal loading.

1.1.1 Problem Statement

Analysis of the structural dynamics of MEMS devices poses new challenges. Classical analysis in structural dynamics does not lend itself easily to the new types of forcing and nonlinearities one encounters in dealing with MEMS. New approaches have to be developed to deal with these challenges, combining the rigor of theory and the practicality of engineering design approaches.

In this dissertation, we study the linear and nonlinear problems of thin circular and annular plates under electrostatic and/or thermal loading. We use different solution techniques to study the local and global behavior of the dynamic responses. For the local analysis, we use a combination of perturbation and numerical techniques. For the global analysis, we use a reduced-order model based on the Galerkin approximation.

1.2 A Review of Plate Theories

Plates are flat structures whose thickness h is small compared to the other in-plane dimensions. For a circular plate, the only in-plane dimension is the radius R.

Plate theories are classified in many ways. One way of classification is based on the thickness (Bairagi 1986); that is, thin- and thick-plate theories. We focus on thin-plate theories because most of the applications that we address in this work are thin plates. Since we are concerned with circular and annular plates, the theoretical development we present here is based on the cylindrical coordinate system (r, θ, z). Geometrically, a plate is said to be *thin* if its *thinness ratio* h/R remains less than $1/20$, otherwise, the plate is said to be *thick*. In thin-plate theories, the stresses σ_z, τ_{rz},

and $\tau_{\theta z}$, which are directed towards the z-axis across the thickness, are considered to be of negligible magnitude compared to the other stresses. In thick-plate theories, the stress components σ_z, τ_{rz}, and $\tau_{\theta z}$ are comparable to the other stresses and cannot be neglected. The various in-plane stresses σ_r, σ_θ, τ_{rz} do not remain proportional to the distance z measured from the neutral plane though the variation of the stresses τ_{rz} and $\tau_{\theta z}$ across the thickness can still be assumed to be parabolic.

Thin plates can withstand external loads and moments and develop resistive loads and moments which can be classified into two distinct groups of action:

1. Membrane (in-plane) action.
2. Bending (transverse) action.

Thin-plate theories are classified according to the transverse deflection w relative to the thickness h as follows:

1. Plates with small deflection.

   In this case, w is small compared to the plate thickness. In theory w must be $\leq 0.2h$ for the application of thin-plate theory with small deflections to give accurate results, but in practice this theory is used for deflections up to the order of the plate thickness with fairly good results for the static case. Because of the smallness of the deflection, the slope and any higher-order terms in the slope or deflection are neglected. Accordingly, in small-deflection theory, the bending effect is dominant whereas the membrane effect is totally disregarded.

   Though, there are several trials to derive theories within the small deflection framework, the most in use is the Kirchoff plate theory, which is sometimes referred to as the classical plate theory or (CPT).

2. Plates with large deflections.

   When $w \geq h$, the results calculated by the small-deflection theory are usually not in good agreement with the observed results. Such cases are better treated by using theories developed on the basis of large deflection.

   Large deflections should be accounted for, also, in cases that do not necessarily involve deflections larger than the plate thickness. For example, as the thickness of the plate tends to

be thinner and thinner, there is considerable reduction in the bending rigidity $D = \frac{Eh^3}{12(1-\nu^2)}$, causing the plate to be more flexible. Another example is plates subjected to the action of in-plane loads. A third example is plates operated in the elasto-plastic range. In the case of large deflection, both membrane and bending forces take part in resisting the action of the loads. The larger the deflection is, the greater are the curvature and the membrane actions and vice versa.

There are several theories for plates under large deflections, the most commonly used of them is the von Karman plate theory which is sometimes referred to as the Kirchoff-Foppel plate theory, we use this theory in this thesis. Berger in 1955 (Chia, 1980) proposed an alternate formulation for the nonlinear static isotropic theory of plates, in which he disregarded the elastic energy due to the second invariant of the membrane strain compared to the square of the first invariant. This hypothesis came to be known in the literature as Berger's approximation or hypothesis and the resulting plate equations are known as Berger's plate equations or model. Nowinski and Ohnabe (1972) showed that the Berger approximation may lead to grave inaccuracies and even become meaningless if the edge of the plate is free to move in the in-plane directions.

3. Plates with excessive large deformations.

   Plates having very thin sections offer practically no bending resistance to deformation. Also, plates subjected to excessive loads particularly towards the stage of collapse, are susceptible excessive deflections. In such cases, a plate will behave as a perfectly flexible structure known as *membrane*.

1.3 Literature Review

There is a large number of publications concerning plate theories and plate dynamics, which can not be covered here. The key issues in our research are nonlinear dynamics of plates and plates under thermal and/or electrostatic loading. Hence, in the following sections, we review the main works on the nonlinear dynamics of plates, plates under thermal loading, plates under electrostatic loading, plates under both loadings, and finally postbuckling analysis of plates under both loadings.

The review is limited to literature written in English unless otherwise indicated.

1.3.1 Nonlinear Dynamics of Plates

Here, we review the static and dynamic postbuckling of circular plates. We classify the literature according to the method of solution to make it easier for the reader.

Perturbation and Series Methods

One of the earliest works on the nonlinear vibration of plates is that of Herrmann (1952) in which, starting from the fundamental equations of the general three-dimensional nonlinear theory of elasticity for the case of small elongation and shears but moderately large rotations, he derived a set of plate equations of motion for an isotropic material obeying linear Hooke's law. The equations are solved for the case of propagation of straight-crested waves and the wave velocities are computed for values of the parameters involved.

Chu and Herrmann (1956) studied the large-amplitude free vibrations of a rectangular plate. By applying a perturbation method, they showed that the in-plane inertia and buoyancy terms can be neglected, and obtained equations which are the dynamic analogues of the von Kármán equations of static equilibrium. With appropriate choices for the displacement functions, the space variables were eliminated and the remaining ordinary-differential equations in terms of the time variable were solved in terms of elliptic functions.

Sridhar et al. (1975,1978) in two consecutive publications studied the symmetric and asymmetric responses of a circular plate to a harmonic excitation when the frequency of the excitation is near one of the natural frequencies. They used the dynamic analogue of the von Kármán equations. The response was expressed as an expansion in terms of linear, free-oscillation modes, and the amplitude was considered to be small but finite. The method of multiple scales was used to find an approximate solution of the nonlinear equations governing the time-dependent coefficients in the expansion. It was shown that, if there is no internal resonance, only the mode having a frequency near that of the excitation is strongly excited.

Hadian and Nayfeh (1990) used the method of multiple scales to study the response of circular plates to a harmonic external excitation. They found out that the multi-mode response loses stability through a Hopf bifurcation, resulting in harmonically and chaotically modulated motions.

Oh and Nayfeh (1998) have shown experimentally a complicated dynamic behavior of a cantilever (90/30/-30/-30/30/90)s graphite-epoxy plate. The plate was base excited using a 2000-lb table shaker near its seventh (third torsional) mode. They monitored the excitation using a base-mounted accelerometer and the plate response using a laser vibrometer. For some excitation amplitudes and frequencies, they observed the activation of a low-frequency (first bending) mode accompanied by amplitude and phase modulations of the seventh mode. Therefore, they concluded that this type of modal interactions is possible for all ranges of structural stiffnesses and configurations whenever there exist modes whose natural frequencies are much lower than the natural frequencies of the directly excited modes. In addition, they also observed simultaneous activation of a two-to-one internal resonance along with the high- to low-frequency modal interactions for some excitation amplitudes and frequencies. They used time-history, power-spectra, and force-response plots to characterize the dynamics of the plate.

Yu et al. (2001) used the method of multiple scales to analyze the nonlinear vibrations of a simply supported thin rectangular plate and derived a set of ordinary-differential equations governing the modulation of the amplitudes and phases of the response. They discussed heteroclinic bifurcation in details.

Azrar et al. (2002) investigated the nonlinear forced vibrations of thin elastic rectangular plates using an asymptotic-numerical method. Various types of harmonic excitations were considered. Using the method of harmonic balance and Hamilton's principle, they converted the equations of motion into an operational formulation. They used the finite-element method to obtain a nonlinear solution for a given frequency and amplitude of excitation. Applying perturbation techniques in the vicinity of this solution, they transformed the nonlinear governing equation into a sequence of linear problems having the same stiffness matrix, which can be easily computed.

Nath and Alwar (1980) studied the nonlinear dynamic response of orthotropic circular plates for both clamped and simply supported boundary conditions. They expressed the response in terms of Chebychev polynomials. They focused on the effect of the orthotropic parameter on the nonlinear

response of the plate under three types of dynamic loadings: step function, sinusoidal, and N-shaped pulse. Nath (1982) studied the nonlinear dynamic response of circular plates resting on Winkler and Pasternak type elastic foundations. He used Chebychev polynomials and the implicit Houbolt technique for solving the problem in space and time, respectively. He investigated the effect of the foundation parameters on the nonlinear response of the plate with clamped and simply supported boundary conditions. Nath and Kumar (1995) studied the nonlinear dynamic response of cylindrically orthotropic, symmetrically laminated, cross-ply moderately thick plates using Chebychev polynomials. They demonstrated the effects of transverse shear, rotary inertia, material properties, number of layers, and boundary conditions on the static and dynamic responses of plates.

Galerkin Method

Yamaki (1961) used Galerkin single-mode expansion to solve the von Kármán equations directly for circular plates. He considered simply supported and clamped cases, both with movable and immovable edges.

Nowinski (1962) utilized the von Kármán dynamic equations to investigate of the free nonlinear axisymmetric vibrations of a circular plate built-in at the boundary. He represented the deflections using a series of separable terms and used an orthogonalization procedure to eliminate the space variable. Confining the study to one term of the series, the solution in the time variable was found in the form of elliptic functions.

Wah (1963) used Berger's approximation of the von Kármán equations to study large-amplitude free vibrations of clamped and simply supported circular plates. He used a single-mode Galerkin expansion and studied the ratio between the linear frequencies and their respective nonlinear ones.

Leung and Mao (1995) discretized the Lagrangian of continuous systems by Galerkin's method to obtain the discrete Hamiltonian and Hamilton's equations. They applied symplectic numerical integration schemes to the resulting ordinary-differential equations to construct the phase diagram. They showed that, due to modal coupling, bounded quasi-periodic and non-periodic free vibrations are very common for continuous systems. Comparison is made with the Runge-Kutta method. They showed that the Runge-Kutta integration reduces the total energy of an undamped

system while symplectic integration almost preserves it. The symplectic schemes are extended to ordinary-differential equations by means of the Lagrangian and Hamiltonian, and they used them to investigate the nonlinear vibrations of beams and plates. Nonlinear modal coupling is emphasized. They noted that extension of these schemes to shell structures involves the complication of curvature effects.

Abe et al. (1998) used a single-mode Galerkin procedure to reduce the equations of motion of a laminated plate to a Duffing-type equation in terms of the transverse displacement. They analyzed solutions of the resulting equation using the method of multiple scales. They investigated the influence of the lamination sequence, the thickness ratio, the number of layers, and the in-plane boundary conditions on the subharmonic-resonance response. Abe et al. (1998) investigated three-mode responses of simply supported laminated plates to harmonic excitations by using a combination of the Galerkin procedure and the method of multiple scales. They compared their analytical results with numerical integration results and found good agreement.

Wei (2001) analyzed the global bifurcations and chaos of the response of a simply supported rectangular thin plate to a parametric excitation by applying the Galerkin procedure to the von Kármán equations. The method of multiple scales was used to obtain the variational equations. Based on the averaged equations, they used the theory of normal forms to derive an explicit expression of the normal form and used it to carry out a global bifurcation analysis.

Zhang (2001) studied the global bifurcations and chaotic dynamics of a parametrically excited simply supported rectangular thin plate. The Galerkin approximation was used to reduce the von Kármán equations into a system of nonlinear ordinary-differential equations. Then, they used the method of multiple scales to obtain the variational equations. They used the method of normal forms to obtain an explicit normal form and used it to analyze global bifurcations.

Ritz and Kantorovitch Methods

Srinivasan (1966) applied the Ritz method to solve free and forced harmonic vibrations of beams and plates with immovable boundary conditions. For plates, he used the Ritz method to reduce Berger's equation into a system of nonlinear algebraic equations. His results are limited to the

nonlinear static deflection and harmonic response of plates.

Huang and Sandman (1971) studied the free and forced vibrations of a circular plate with a clamped and immovable boundary. Steady-state sinusoidal oscillations were assumed, and then the time variable was eliminated by applying the Kantorovich method. Thus the basic governing equations for the problem were reduced to a pair of ordinary-differential equations, which form a nonlinear eigenvalue problem. A computational method was used to solve these equations. The effects of large amplitudes on the transverse shape of vibration and the induced stresses were studied and illustrated and the dynamic response curves of the plate under applied loading were presented.

Dumir et al. (1985) studied the large-amplitude responses of axisymmetric cylindrically orthotropic thin circular plates resting on elastic foundations. They considered clamped immovable and simply supported, movable and immovable, boundary conditions. They also considered linear and nonlinear Winkler elastic foundations and Pasternak elastic foundations. Time was eliminated through the Kantorovich averaging method and an orthogonal point collocation method was used for spatial discretization. The results demonstrated the effects of the foundation parameters, the orthotropic parameter, and the edge conditions on the nonlinear responses. In a subsequent paper, Dumir et al. (1986) studied the large-amplitude response of an axisymmetric cylindrically orthotropic thin circular plate of varying thicknesses and elastically restrained edge against rotation and in-plane displacement. The results demonstrated the effects of taper ratio, the orthotropic parameter, and in-plane and rotational stiffnesses on the nonlinear response.

Other Approximate Methods

Ramesh and Krishnamoorthy (1995) investigated the application of the dynamic relaxation (DR) method to the analysis of geometrically nonlinear plates and shells involving large deflections and small rotations and strains. They reviewed the merits and demerits of two types of approaches suggested for the reevaluation of the parameters of the DR method. They developed an accurate shallow shell element using Marguerre's shallow shell theory. The total Lagrangian (TL) approach is used for an explicit derivation of element internal force vectors by an energy approach considering all higher-order terms both in the membrane strain-displacement relations and in the curvature expressions. They illustrated the efficiency of the proposed shallow shell element in combination with

the DR method for prebuckling and postbuckling analyses of structures through various numerical examples. Also, they studied the effect of these higher-order terms in the membrane and curvature expressions on the overall accuracy of the solution for geometrically nonlinear problems.

Zhu et al. (1995) presented a technique combining the modal expansion with the finite-element representation of a finite region containing defects to analyze the transient response of a laminated composite plate. As an illustration, a model problem of a laminated plate containing a normal surface breaking crack was studied in detail. They presented numerical results showing the effect of the crack depth on the transient response.

Exact Solution

Maganty and Bickford (1987) derived an accurate set of geometrically nonlinear equations of motion of circular rings. They concluded that, for nonresonant motions, the initial out-of-plane amplitude has a marginal effect on the initial in-plane oscillation, whereas the effect of the initial in-plane amplitude on the out-of-plane oscillation is significant. For resonance motions, they indicated that there is an exchange of energy between the in-plane and out-of-plane motions.

1.3.2 Plates under Thermal Loading

Although thermal loading of plates is an old subject, very few surveys do exist on the subject. The most recent of them is by Tauchert (1991) who covers a wide range of topics, such as composite plates, buckling, and post-buckling. Thornton (1993) reviewed the thermal buckling of plates and shells since the fifties till the time of his publication. Thermal induced vibrations of isotropic plates occupy a small portion of the survey. In the following, we present an extensive survey. The literature on this subject can be classified into two categories. The first category focuses on the static behavior and the second focuses on thermally induced vibrations. In the following, we review each category, starting with the first.

Static Behavior due to Thermal Loading

Marguerre (1935) formulated the linear decoupled thermoelastic plate equation. Sokolnikoff and Sokolnikoff (1939) studied linear thermal stresses in clamped elastic plates under constant linear temperature distributions and showed that the solution is similar to that of an equivalent transversely loaded elastic plate.

Heldenfels and Roberts (1952) studied, experimentally and theoretically the thermal stresses induced in a flat rectangular plate due to nonuniform heating. They derived an approximate theoretical model for the plate under small deflections, solved it using energy methods, and compared the results with experimental results.

Gatewood (1957) solved the thermal flat plate problem for small deflections and constant temperature distributions and concluded that, for the cases he considered, temperature has negligible effect.

Newman and Forray (1962) developed an exact mathematical formulation for the axisymmetric deflection of a circular plate in the framework of the von Kármán large-strain displacement relations. A finite-difference procedure, utilizing the relaxed iterations technique, was used to solve the problem of combined thermomechanical loading. They presented results for the case of a simply supported plate with immovable edge, including the static behavior and the change in the tangential and radial membrane forces and bending moments.

Pal (1969) applied Berger's approximation to derive simplified, decoupled equations for large deflections of circular and annular plates and solved them by the successive approximations method. The deformations of circular and annular flat plates with different boundary conditions and subjected to an arbitrary symmetric temperature were analyzed considering the effect of temperature gradient through the thickness under transient heating conditions.

Lin et al. (1994) used the generalized differential quadrature method to solve for the large deflections of a rectangular plate under thermal load. The weighing coefficients for the approximation of the derivatives were calculated and then implemented in a straightforward manner to include different boundary conditions. They compared their results for the case of no thermal loads to known solutions and found good accuracy.

Rossit and Laura (1997) determined the static deflections for two different thermoelastic problems using the Ritz method employing a unified approach that consists of using polynomial coordinate functions that satisfy the governing boundary conditions. The first problem was thermoelastic stresses and deflections in a thin rectangular plate with edges restrained against rotation. The second problem was thermoelastic plane stress in a rectangular plate with stress-free edges. Both problems were solved within the framework of linear plate theory.

Thermally Induced Vibrations

Altay and Dokmeci (1997) developed nonlinear two-dimensional dynamic equations of motion for an elastic plate under thermomechanical loading. The nonisothermal plate equations, formulated in invariant differential and variational forms, were derived from the three-dimensional equations of coupled thermoelasticity together with Mindlin's kinematic hypothesis of elastic plates. Some cases involving special material, motion, and geometry were indicated, and presented a theorem on the uniqueness of the solutions of the fully linearized thermoelastic plate equations.

Verma (2001) studied the propagation of plane harmonic thermoelastic waves in a thin, flat, infinite homogeneous, transversely isotropic plate of finite width. The study was carried out within the context of generalized theory of thermoelasticity.

Irie and Yamada (1978) studied thermally induced vibrations of circular and annular plates within the framework of linear plate theory. The plate was assumed to be subjected to a sinusoidally varying heat flux on one surface, while the other surface was thermally insulated. The temperature distribution due to the heat input was analyzed using the Fourier heat conduction equation. Then, they calculated the thermal moment due to temperature and then the resulting static deflection. Also, they presented the frequency response of an annular plate to a sinusoidal heat flux, which confirms the expectations of the linear theory of vibrations.

Pal (1970) studied the free vibrations of heated circular plates with simply supported and clamped boundary conditions by using Berger's approximation. He used two methods: an exact method in terms of elliptic integrals and the other is approximate using the successive approximation method. Subsequently, Pal (1973) studied the static and dynamics of heated orthotropic circular plates

with simply supported and clamped boundary conditions. Jones et al. (1980) examined the large-amplitude vibrations and buckling behavior of a rectangular plate under elevated temperatures including viscoelastic effect by using Berger's approximation. Chang and Wan (1986) analyzed analytically large-amplitude thermomechanically coupled vibrations of rectangular elastic thin plates with different boundary conditions using Berger's approximation. They carried out a one-term Galerkin approximation and found that the effect of coupling is negligible as long as the damping effect is not required.

Sunakawa (1964) solved approximately the fundamental equations of nonlinear flexural vibration for a rectangular elastic plate by the method of successive approximation and demonstrated the influences of temperature changes and large amplitudes on the period of free vibrations. Some numerical examples were given for a rectangular plate with hinged and immovable edges. He emphasized the considerable effect of even small temperature differences.

Buckens (1979) examined small deflections of rectangular plates under thermal loads and analyzed their buckling. Then, he studied the postbuckling behavior using the von Kármán equations.

Mansfield (1982) gave an exact analysis of certain large-amplitude free vibrations of unsupported elliptical plates of lenticular section, whose middle surfaces may be flat or have small constant curvatures. The temperature in the plates may vary quadratically in the plane and linearly through the thickness. Biswas and Kapoor (1985) studied the effect of temperature on the time period of vibration of nonlinear orthotropic circular plates with clamped boundary conditions. They used the von Kármán equations written in terms of tranverse and radial displacements and solved them using a one-term Galerkin approximation.

Sathyamoorthy (1986) studied the effect of thermal loading on large-amplitude free vibrations of orthotropic clamped plates. He assumed a temperature distribution and solved the von Kármán equations to find the mechanical response using a single-mode Galerkin approximation.

Trajkovski and Cukic (1999) studied thermoelastic vibrations of free supported and clamped thin circular plates caused by a thermal shock impinging on their surface. The system of partial-differential equations of motion of the coupled system was reduced to a system of first- and second-type Volterra integral equations in the time domain. In both cases, the solutions were given in the

form of a series of Bessel functions of the first kind.

Xuefeng et al. (1999) analyzed the problem of free vibrations of circular plates when the temperature and stress fields are coupled. Using a one-term Galerkin approximation, they obtained a system of nonlinear ordinary-differential equations in time. They compared the time history of the vibration amplitude with those obtained for the case of decoupled temperature and stress fields. They found that the natural frequency in the coupled case is larger (smaller) than that in the uncoupled case when the initial displacement is small (large).

Qiang et al. (1999) studied the chaotic motion of an elliptic plate under both thermal and mechanical loading. They formulated the problem using the von Kármán large-strain approach. The Melnikov function was used to give the critical condition for chaotic motion. Then, they demonstrated the results by Poincare maps, phase portraits, and time histories. Yeh et al. (2002) reduced the partial-differential equations governing plate motions to a set of three ordinary-differential equations using a single-mode Galerkin approximation. They studied the chaotic and bifurcation dynamics of a simply supported rectangular plate under thermo-mechanical coupling using the fractal dimensions and maximum Lyapunov exponents.

1.3.3 Plates under Electrostatic Force

The electrostatic load applied to a plate has an upper limit beyond which the mechanical restoring force is overcome by the opposing electrostatic force and the structure collapses. This structural instability phenomenon is known as 'pull in,' and the critical voltage associated with it is called the 'pull in voltage.'

The literature on plates under electrostatic loading is increasing rapidly due to their wide applications. Microphones, micropumps, sensors, and microswitches are only examples of such vast range of applications.

One of the earliest works on the subject is that of Warren et al. (1972) who presented nonlinear equations for the static deflection of the moving electrode due to the electrical field between the electrodes in capacitance microphones. The equations were solved numerically for circular and annular membranes. Because of the nonlinearity of the electrical attraction forces, certain values

of the microphone parameters exist for which the deflections can become unstable. Warren et al. (1973) studied the dynamic response of a membrane to an acoustic excitation using finite differences. They included the effects of static deflections and thin air film between the electrodes.

Wang and Hadaegh (1996) studied micromachined deformable mirrors modeled by either membrane or plate equations with nonlinear electrostatic actuation. They used numerical methods to compute the mirror deformation caused by a given actuator voltage and the actuator voltage required for producing the desired deformations at the actuator locations. They applied their technique to circular deformable mirrors whose surfaces are modeled by elastic membranes.

Cozma and Puers (1997) investigated the possibility of using electrostatic forces to actuate the membrane of a pressure sensor in order to create self-testing features. It was shown that the electrostatic pressure is small compared with the external pressure, unless large voltages or electrical charges are used. The sensor diaphragm was modeled as a membrane and the finite-element method was used to solve for the membrane deflection under electrostatic actuation.

Bourouina and Grandchamp (1996) modeled a square-shape micropump under electrostatic loading using the electrical analogy and the idea of equivalent network. They assumed the micropump diaphragm to behave like a nonlinear membrane. However, they did not consider the dynamic behavior of the membrane, as their main interest was the calculation of the flow rate.

Francais et al. (1997) developed a mechanical law with a simple elementary model of the membrane deflection that approximates the micropump square diaphragm. They demonstrated the static instability (pull-in) of such a system under electrostatic actuation and provided an analytical solution for the membrane deflection. Also, they proposed a parameter optimization procedure for the dimensions of the electrostatically actuated membrane in order to achieve maximum volume displacement. Francais and Defour (1998) studied a micropump made of a square diaphragm for medical applications. They modeled the diaphragm as a membrane and included two nonlinear characteristics: the pull-in effect and the hysteresis phenomenon. They solved the problem using circuit analogy.

Jiang et al. (2000) studied a micropump actuated by a electrostatic force. They used the boundary-element method to solve the Laplace equation governing the potential difference. A combination

of the assumed-mode method and the boundary-element method was employed to solve for the diaphragm deflections. They presented numerical results showing the time history of the transverse deflection.

Rajalingham and Bhat (1998) studied in two steps the vibration of a microphone diaphragm subjected to an electrostatic force field, which induces a deflection-dependent load intensity. The diaphragm was modeled using linear circular plate theory. First, they calculated the static deflection due to the electrostatic load and found that it increases with the field strength. It was noted that, as the field strength reaches a critical value, it destabilizes the static deflection and causes the plate to buckle. Second, they solved for small vibrations around the static deflected position.

Saif et al. (1999) presented a methodology based on energy methods to analyze electrostatically actuated micropumps. The micropump diaphragm was modeled as a linear membrane. The methodology was used to analyze two different types of micropumps: paraboloid and annular cavity membranes. The relation between the pressure and deflection was demonstrated, but no dynamic analysis was carried out.

Francais and Dufour (1999) proposed a complete normalized study the behavior of a diaphragm under classical excitations encountered in microsystem: pneumatic, electrostatic, piezoelectric, and magnetic. They presented a traditional approximate analytical solution based on energy minimization through the use of a polynomial solution technique. They used both membrane and linear plate formulations to study the pull-in phenomenon and the relation between the deflection and the electrostatic loading for different diaphragm shapes.

Konig and Wachutka (1999) analyzed the instability inherent in electrostatically driven microdevices. Starting from a simplified lumped model of two rigid plates under electrostatic loading, they formulated the governing differential equations and analyzed the stability of their solutions. They presented a homotopy method that overcomes the stiffness of the problem. They presented numerical results for micromirrors and membranes.

Seeger and Boser (2002) characterized parallel-plate actuators for oscillations near the mechanical resonant frequency and amplitudes comparable to the actuator gap. They showed that, at resonance, the structure can move beyond the static pull-in limit, which they calculated as one-third of

the gap, but it is still limited to 56 percent of the gap by resonant pull-in. Above the resonant frequency, the structure is not limited by pull-in and can theoretically oscillate across the entire gap. They developed a function model, which included an amplitude-dependent model for electrostatic spring tuning, to predict the steady-state frequency response and they verified it experimentally

1.3.4 Postbuckling Behavior of Plates

Here, we review the static and dynamic postbuckling of circular plates. We classify the literature according to the method of solution to make it easier for the reader.

Perurbation Techniques and Power Series

Friedrichs and Stoker (1942) studied the problem of buckling and postbuckling of a thin circular plate under uniform radial pressure, assuming radial symmetry. They investigated simply-supported circular plates. Buckling takes place at a critical value of the radial pressure. They introduced a nondimensional load parameter defined as the ratio of the radial load to the critical radial load. They transformed the von Kármán plate equations into a simpler form by a change of variables. They first obtained a fifth-order perturbation expansion in terms of a small parameter, the square root of the difference between the load parameter and unity. They solved the same problem by expanding the solution in a power-series in terms of the plate radius. Comparing both solutions, they found that the perturbation solution is of limited usability for load ratios beyond two but the power-series solution is accurate up to a load ratio of five. They did not compare the analytical results with numerical solutions. Hence, the comparison between the two methods of solution does not provide enough evidence for their credibility. Bodner (1954) extended the work of Friedrichs and Stoker (1942) to the case of a clamped circular plate. He reached the same conclusion, with the only difference that the computation for his case was more tedious due to the slow convergence of the power series.

Dombourian et al. (1976) examined the modal coupling behavior of a compressed imperfect rectangular plate modeled as a six-degrees-of-freedom structural system. They developed a direct variational approach using the total potential energy of the system to generate a system of nonlin-

ear algebraic equations. A perturbation procedure was used to examine the effect of imperfection and aspect ratio on the static transverse deflection of a plate subjected to an in-plane edge displacement. They expressed each unknown in powers of a perturbation parameter, which reduced the nonlinear equations to a system of equations that can be solved successively by elementary linear algebra techniques. The segmented deflection history was developed for a variety of imperfection compositions and aspect ratios.

Brewster (1991) derived an asymptotic expansion for the solution of the axisymmetric von Kármán thin circular plates equations under transverse and compressive in-plane loads, with the edge elastically supported against rotation. The equations were reformulated in a form amenable to solution by singular perturbation techniques, where the perturbation parameter was proportional to the plate thickness. Solutions of this nonlinear singular perturbation problem were related to the Foppel membrane solutions and exhibited global breakdown. His formal analysis suggested that the relationship between compressive membrane and plate solutions does not extend to the case of clamped plates.

Shen (1997) studied the thermal postbuckling of a simply supported composite laminated rectangular plate subjected to uniform and non-uniform tent-like temperature loadings. The formulation is based on Reddy's higher-order shear-deformation plate theory with inclusion of thermal effects. The analysis was carried out using a mixed Galerkin-perturbation technique to determine the thermal buckling loads and postbuckling equilibrium paths. The solution procedure starts by substituting assumed summations of the plate equations variables; namely, the deflection and stress function. The assumed summations are multiplied by a small perturbation parameter, which upon substitution yield a system of perturbation equations that are solved step by step using the Galerkin approximation. The effects of transverse shear deformation, thermal load ratio, plate aspect ratio, total number of plies, fiber orientation, and initial geometric imperfections were studied.

Wang (2000) obtained an analytic axisymmetric postbuckling equilibrium path for circular plates under uniform radial compression using a power-series method. The solution procedure is based on a second-order differential equation in the vicinity of the normal singular point. He also investigated the problem of asymmetric bifurcation buckling from the axisymmetric postbuckling deformation state using the adjacent equilibrium criterion. The von Karman nonlinear equations in the incre-

mental form had been solved using power-series and Fourier-series expansions in the circuferencial direction.

Galerkin Approximation

Gossard et al. (1953) studied the static behavior of flat and initially imperfect rectangular plates subjected to thermal buckling. They used the von Kármán model for the plates and a one-term Galerkin expansion. The method was used to determine the deflections of a simply supported panel subjected to a tent-like temperature distribution over the plate surface. The theoretical and experimental results were in good agreement for the range of temperatures and deflections considered in the test.

Shulman (1958) derived equations of motion for thermally stressed plates both before and after initial buckling. He used a linear plate model for prebuckling and the von Kármán model for postbuckling. For prebuckling, he solved the problem exactly. For postbuckling, he separated the static part from the dynamic part by assuming that the deflection is the sum of the static deflection and a dynamic part around this deflection. The stress function also was expressed similar to the deflection. These equations were solved by the assumed mode method, which is to a great extent similar to the Galerkin approximation. These equations yield the free-vibration characteristics around the two equilibrium states produced by the temperature rise. They considered uniformly heated plates with two opposite edges simply supported and generalized support conditions on the other two edges.

Ahmad (1970) developed a one-term Galerkin approximation to study the postbuckling response of a thin elastic circular plate under the action of an axisymmetric, time-dependent radial thrust, assuming that the thrust produces resonance of only the principal mode of vibration. He showed that this assumption is valid for certain simple cases of loading history and for small penetrations of the postbuckling domain. He presented the radial variation of the stresses and the time history of the deflection for the case of pulse loading.

Dumir (1986) developed an approximate solution for the large axisymmetric responses of isotropic thin circular plates resting on Winkler, Pasternak, and nonlinear Winkler foundations, taking into

account the in-plane displacement. He considered plates with edges elastically restrained against rotation. The von Karman plate equations in terms of the transverse deflection and the stress function were employed. A one-term mode shape was used to approximate the transverse deflection and Galerkin's approximation was used to obtain an equation for the central deflection in the form of Duffing's equation. He determined the nonlinear frequencies, postbuckling response to a radial load at the edge, and the maximum transient response to a transverse step load.

Ritz Method

Ng and White (1988) studied the dynamic behavior of postbuckled isotropic rectangular plates through four main steps. First, they derived a simple formula using a one-term Rayleigh method to give a simple preliminary solution; this solution does not give accurate results for a plate with a multi-mode imperfection and for vibration modes different from the critical mode. Second, they used a multi-mode Rayleigh-Ritz approach. Third, they used the finite-element method. And the final step was to use experiments to validate the theoretical solutions. Comparison showed that the one-term simple formula was not adequate and that the multi-mode Rayleigh-Ritz and finite-element results were quite similar. The experimental results showed a clear discrepancy with all of the three theoretical methods.

Analytic Approaches

Mansfield (1962) gave an exact solution for the bending, buckling, and curling of a thin circular plate of lenticular section with a uniform temperature gradient through its thickness. The behavior of such a plate with an initial spherical curvature, susceptible to a further possibility of snap-through buckling, was also studied.

Gauss and Antman (1984) studied the global properties of the buckled states of nonlinear thermoelastic beams and plates heated at their ends and edges. For plates, they considered axisymmetric circular plates only. Their analysis relied much on the combination of classical results of ordinary-differential equations theory and that of bifurcation theory. They emphasized the crucial role of the constitutive assumptions.

1.4 Contributions

1. We investigate the nonlinear response of a circular plate to a thermal loading consisting of a steady component and a sinusoidal component. We base the analysis on the heat-conduction equation and the dynamic analogue of the von Kármán equations. We neglect the dissipation terms in the heat equation and solve it for the temperature distribution. Then, we substitute the resulting distribution into the equations describing the displacement and stress function. We use the method of multiple scales to determine a first-order approximation of the plate response for two cases. In the first case, we treat the case of principal parametric resonance of an axisymmetric mode of a simply supported plate with movable edges. In the second case, we treat the case of combination parametric resonance of two axisymmetric modes of a clamped plate with immovable edges. The case of principal parametric resonance of an axisymmetric mode is treated as a special case. These investigations are the first in the literature on circular plates.

2. We investigate the shift in the natural frequencies of circular plates due to a temperature loading. This work is very important for diaphragm-based measurement devices.

3. We study the mechanical behavior of an electrostatically actuated micropump. We model the actuating element as an annular plate using the von Kármán nonlinear plate equations to account for in-plane stresses and moderate large deformations. This is the first time in the literature that this model is used for this problem. The electrostatic forcing adds another nonlinearity to the model. We solve for the nonlinear static deflection first and then solve the linearized eigenvalue problem around the calculated deflected shape. We present results describing the static characteristics and the linear natural frequencies and their corresponding mode shapes of the actuating element under two different boundary conditions.

4. We investigate the behavior of circular plates under thermal and electrostatic loadings for the first time in the literature. We study the static and dynamic behavior, including the natural frequencies, of plates undergoing large deformations.

5. We study the postbuckling behavior of circular plates under thermal loading. We compare the results with those obtained with a single-mode Galerkin approximation and a power-series

method. We conclude that a single-mode approximation might give erroneous results and that implementation of the multi-mode approximation is easier and faster than the power-series method.

6. We illustrate the importance of including nonlinearity in modeling sensors and other similar diaphragm-based devices .

Chapter 2

General von Kármán Formulation of Circular and Annular Plates under Thermal and Electrostatic Loadings

2.1 Basic Assumptions

The derivation in this chapter is for an isotropic axisymmetric von Kármán plate. We first list the assumptions underlying the Kirchoff classical plate theory (CPT) and the von Kármán plate theory. The Kirchoff plate theory assumptions are (Ugural, 1981):

1. The deflection of the midplane is small compared with the thickness of the plate. The slope of the deflected surface is therefore very small and the square of the slope is negligible in comparison to unity.
2. The midplane remains unstrained subsequent to bending.
3. A straight line (fillament) initially normal to the midsurface remains straight and normal to that surface after bending.
4. The stress σ_z normal to the midplane is small compared with the other stress components

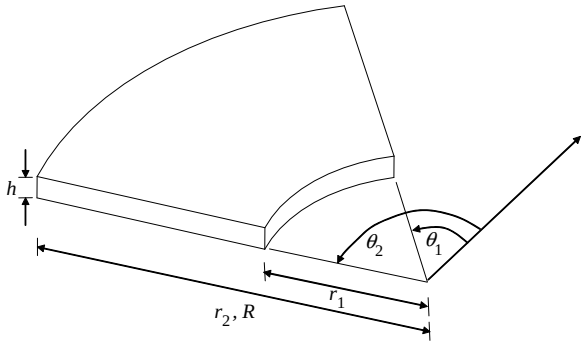

Figure 2.1: Main features of plate geometry.

and may be neglected.

For the von Kármán plate theory, the deflection is the order of the plate thickness, though it is still smaller than the other plate dimensions, and as a result the first two assumptions in the CPT do not hold anymore, meanwhile the third and fourth assumptions still hold.

2.2 Problem Formulation

The displacement field is assumed to have the form (Librescu, 2001; Reddy, 1999)

$$u_r(r,\theta,z,t) = u(r,\theta,t) - z\frac{\partial w}{\partial r} \tag{2.1}$$

$$u_\theta(r,\theta,z,t) = v(r,\theta,t) - z\frac{1}{r}\frac{\partial w}{\partial \theta} \tag{2.2}$$

$$u_z(r,\theta,z,t) = w(r,\theta,t) \tag{2.3}$$

where u, v, and w are the radial, angular, and transverse displacements of the plate middle surface, respectively. The nonlinear strains according to von Kármán are

$$\epsilon_{rr} = \frac{\partial u_r}{\partial r} + \frac{1}{2}\left(\frac{\partial u_z}{\partial r}\right)^2 \tag{2.4}$$

$$\epsilon_{\theta\theta} = \frac{u_r}{r} + \frac{1}{r}\frac{\partial u_\theta}{\partial \theta} + \frac{1}{2}\left(\frac{1}{r}\frac{\partial u_z}{\partial \theta}\right)^2 \tag{2.5}$$

$$\epsilon_{zz} = \frac{\partial u_z}{\partial z} = 0 \tag{2.6}$$

$$2\epsilon_{r\theta} = \frac{1}{r}\left(\frac{\partial u_r}{\partial \theta} - u_\theta\right) + \frac{\partial u_\theta}{\partial r} + \frac{1}{r}\frac{\partial u_z}{\partial r}\frac{\partial u_z}{\partial \theta} \tag{2.7}$$

$$\epsilon_{\theta z} = \frac{1}{2}\left(\frac{\partial u_\theta}{\partial z} + \frac{1}{r}\frac{\partial u_z}{\partial \theta}\right) = 0 \tag{2.8}$$

$$\epsilon_{rz} = \frac{1}{2}\left(\frac{\partial u_r}{\partial z} + \frac{\partial u_z}{\partial r}\right) + \frac{1}{2}\frac{\partial u_z}{\partial r}\frac{\partial u_z}{\partial z} = 0 \tag{2.9}$$

We note that ϵ_{zz}, $\epsilon_{\theta z}$, and ϵ_{rz} given by Equations (2.6), (2.8), and (2.9) are identitically zero in the thin-plate theory approximation. Substituting the displacement field into Equations (2.4), (2.5), and (2.7) yields

$$\epsilon_{rr} = \frac{\partial u}{\partial r} + \frac{1}{2}\left(\frac{\partial w}{\partial r}\right)^2 - z\frac{\partial^2 w}{\partial r^2} \tag{2.10}$$

$$\epsilon_{\theta\theta} = \frac{u}{r} + \frac{1}{r}\frac{\partial v}{\partial \theta} + \frac{1}{2r^2}\left(\frac{\partial w}{\partial \theta}\right)^2 - \frac{z}{r}\left(\frac{\partial w}{\partial r} + \frac{1}{r}\frac{\partial^2 w}{\partial \theta^2}\right) \tag{2.11}$$

$$\epsilon_{r\theta} = \frac{1}{2}\left(\frac{1}{r}\frac{\partial u}{\partial \theta} + \frac{\partial v}{\partial r} - \frac{v}{r} + \frac{1}{r}\frac{\partial w}{\partial r}\frac{\partial w}{\partial \theta} - z\frac{2}{r}\left(\frac{\partial^2 w}{\partial r \partial \theta} - \frac{1}{r}\frac{\partial w}{\partial \theta}\right)\right) \tag{2.12}$$

The principle of virtual displacements can be expressed as

$$\delta W = 0 \tag{2.13}$$

where W is the total work: the strain energy, kinetic energy, and work done by the external loads (Ugural, 1981). In polar coordinates, this principle becomes

$$\begin{aligned}\delta W = &\int_0^T \int_{\Omega_0} \int_{-\frac{h}{2}}^{\frac{h}{2}} (\sigma_{rr}\delta\epsilon_{rr} + \sigma_{\theta\theta}\delta\epsilon_{\theta\theta} + \sigma_{r\theta}\delta\gamma_{r\theta}) dz r dr d\theta dt \\ &- \int_0^T \int_{\Omega_0} \int_{\frac{-h}{2}}^{\frac{h}{2}} \rho(\dot{u}_r\delta\dot{u}_r + \dot{u}_\theta\delta\dot{u}_\theta + \dot{u}_z\delta\dot{u}_z) dz r dr d\theta dt \\ &- \int_0^T \int_{\Omega_0} q(r,\theta,t)\delta w r dr d\theta dt\end{aligned} \tag{2.14}$$

where $q(r,\theta,t)$ is the distributed transverse load, T is the final time, and Ω_0 denotes the domain of the plate.

We define

$$N_{rr} = \int_{-\frac{h}{2}}^{\frac{h}{2}} \sigma_{rr} dz \tag{2.15}$$

$$N_{\theta\theta} = \int_{-\frac{h}{2}}^{\frac{h}{2}} \sigma_{\theta\theta} dz \tag{2.16}$$

$$N_{r\theta} = \int_{-\frac{h}{2}}^{\frac{h}{2}} \sigma_{r\theta} dz \tag{2.17}$$

$$M_{rr} = \int_{-\frac{h}{2}}^{\frac{h}{2}} \sigma_{rr} z dz \tag{2.18}$$

$$M_{\theta\theta} = \int_{-\frac{h}{2}}^{\frac{h}{2}} \sigma_{\theta\theta} z dz \tag{2.19}$$

$$M_{r\theta} = \int_{-\frac{h}{2}}^{\frac{h}{2}} \sigma_{r\theta} z dz \tag{2.20}$$

$$\gamma_{r\theta} = 2\epsilon_{r\theta} \tag{2.21}$$

where $N_{rr}, N_{\theta\theta}, N_{r\theta}$ are the in-plane forces and $M_{rr}, M_{\theta\theta}, M_{r\theta}$ are the out-of-plane moments. Substituting Equations (2.10)-(2.12) and (2.15)-(2.20) into Equation (2.14), we obtain

$$\begin{aligned}\int_0^T \int_{\Omega_0} \Bigg[& N_{rr}\left(\frac{\partial \delta u}{\partial r} + \frac{\partial w}{\partial r}\frac{\partial \delta w}{\partial r}\right) + N_{\theta\theta}\left(\frac{1}{r^2}\frac{\partial w}{\partial \theta}\frac{\partial \delta w}{\partial \theta} + \frac{1}{r}\frac{\partial \delta v}{\partial \theta} + \frac{\delta u}{r}\right) \\ & + N_{r\theta}\left(\frac{1}{r}\frac{\partial \delta u}{\partial \theta} + \frac{\partial \delta v}{\partial r} - \frac{\delta v}{r} + \frac{1}{r}\frac{\partial w}{\partial r} + \frac{\partial \delta w}{\partial \theta}\right) - M_{rr}\frac{\partial^2 \delta w}{\partial r^2} - M_{\theta\theta}\frac{1}{r}\left(\frac{\partial \delta w}{\partial r} + \frac{1}{r}\frac{\partial^2 \delta w}{\partial \theta^2}\right) \\ & - 2M_{r\theta}\frac{1}{r}\left(\frac{\partial^2 \delta w}{\partial r \partial \theta} - \frac{1}{r}\frac{\partial \delta w}{\partial \theta}\right) - I_0\left(\dot{u}\delta\dot{u} + \dot{v}\delta\dot{v} + \dot{w}\delta\dot{w}\right) \\ & - I_2\left(\frac{\partial \dot{w}}{\partial r}\frac{\partial \delta \dot{w}}{\partial r} + \frac{1}{r^2}\frac{\partial \dot{w}}{\partial \theta}\frac{\partial \delta \dot{w}}{\partial \theta}\right) - q\delta w\Bigg] r dr d\theta dt = 0\end{aligned} \tag{2.22}$$

where I_0 is the mass moment of inertia and I_2 is the rotary inertia. Integrating Equation (2.22) by parts in space and time to relieve δu, δv, and δw from any differentiations, we find that each individual term simplifies as follows:

$$\int_{\Omega_0} N_{rr}\frac{\partial \delta u}{\partial r} r dr d\theta = \int_{\Omega_0} (rN_{rr})\frac{\partial \delta u}{\partial r} dr d\theta = (rN_{rr})\,\delta u|_{r_1}^{r_2} - \int_{\Omega_0}\left(N_{rr} + r\frac{\partial N_{rr}}{\partial r}\right)\delta u dr d\theta \tag{2.23}$$

$$\begin{aligned}\int_{\Omega_0} N_{rr}\frac{\partial \delta w}{\partial r}\frac{\partial w}{\partial r} r dr d\theta &= \int_{\Omega_0}\left(rN_{rr}\frac{\partial w}{\partial r}\right)\frac{\partial \delta w}{\partial r} dr d\theta \\ &= \left(rN_{rr}\frac{\partial w}{\partial r}\right)\delta w|_{r_1}^{r_2} - \int_{\Omega_0}\frac{\partial}{\partial r}\left(rN_{rr}\frac{\partial w}{\partial r}\right)\delta w dr d\theta\end{aligned} \tag{2.24}$$

$$\int_{\Omega_0} N_{\theta\theta}\frac{1}{r}\frac{\partial \delta v}{\partial \theta} r dr d\theta = \int_{\Omega_0} N_{\theta\theta}\frac{\partial \delta v}{\partial \theta} dr d\theta = N_{\theta\theta}\delta v|_{\theta_1}^{\theta_2} - \int_{\Omega_0}\frac{\partial N_{\theta\theta}}{\partial \theta}\delta v dr d\theta \tag{2.25}$$

$$\begin{aligned}\int_{\Omega_0}\frac{1}{r^2}N_{\theta\theta}\frac{\partial \delta w}{\partial \theta}\frac{\partial w}{\partial \theta} r dr d\theta &= \int_{\Omega_0}\left(\frac{1}{r}N_{\theta\theta}\frac{\partial w}{\partial \theta}\right)\frac{\partial \delta w}{\partial \theta} dr d\theta \\ &= \left(\frac{1}{r}N_{\theta\theta}\frac{\partial w}{\partial \theta}\right)\delta w|_{\theta_1}^{\theta_2} - \int_{\Omega_0}\frac{\partial}{\partial \theta}\left(\frac{1}{r}N_{\theta\theta}\frac{\partial w}{\partial \theta}\right)\delta w dr d\theta\end{aligned} \tag{2.26}$$

$$\int_{\Omega_0} N_{r\theta}\frac{\partial \delta v}{\partial r} r dr d\theta = \int_{\Omega_0} \left(r N_{r\theta}\right)\frac{\partial \delta v}{\partial r} dr d\theta = \left(r N_{r\theta}\right)\delta v|_{r_1}^{r_2} - \int_{\Omega_0}\left(N_{r\theta} + r\frac{\partial N_{r\theta}}{\partial r}\right)\delta v dr d\theta \tag{2.27}$$

$$\int_{\Omega_0} N_{r\theta}\frac{1}{r}\frac{\partial \delta u}{\partial \theta} r dr d\theta = \int_{\Omega_0} N_{r\theta}\frac{\partial \delta u}{\partial \theta} dr d\theta = N_{r\theta}\delta u|_{\theta_1}^{\theta_2} - \int_{\Omega_0}\frac{\partial N_{r\theta}}{\partial \theta}\delta u dr d\theta \tag{2.28}$$

$$\begin{aligned} -\int_{\Omega_0} M_{rr}\frac{\partial^2 \delta w}{\partial r^2} r dr d\theta &= -\left[\left(r M_{rr}\frac{\partial \delta w}{\partial r}\right)|_{r_1}^{r_2} - \int_{\Omega_0}\frac{\partial}{\partial r}\left(r M_{rr}\frac{\partial \delta w}{\partial r}\right) dr d\theta\right] \\ &= -\left[\left(r M_{rr}\frac{\partial \delta w}{\partial r}\right)|_{r_1}^{r_2} - \left(\frac{\partial}{\partial r}\left(r M_{rr}\right)\delta w|_{r_1}^{r_2} - \int_{\Omega_0}\frac{\partial^2}{\partial r^2}\left(r M_{rr}\right)\delta w dr d\theta\right)\right] \end{aligned} \tag{2.29}$$

$$-\int_{\Omega_0} M_{\theta\theta}\frac{1}{r}\frac{\partial \delta w}{\partial r} r dr d\theta = -\int_{\Omega_0} M_{\theta\theta}\frac{\partial \delta w}{\partial r} dr d\theta = -\left(M_{\theta\theta}\delta w|_{r_1}^{r_2} - \int_{\Omega_0}\frac{\partial M_{\theta\theta}}{\partial r}\delta w dr d\theta\right) \tag{2.30}$$

$$\begin{aligned} &-\int_{\Omega_0} M_{\theta\theta}\frac{1}{r^2}\frac{\partial^2 \delta w}{\partial \theta^2} r dr d\theta = -\int_{\Omega_0} M_{\theta\theta}\frac{1}{r}\frac{\partial^2 \delta w}{\partial \theta^2} dr d\theta = -\left[\frac{1}{r}M_{\theta\theta}\frac{\partial \delta w}{\partial \theta}|_{\theta_1}^{\theta_2} - \int_{\Omega_0}\frac{1}{r}\frac{\partial M_{\theta\theta}}{\partial \theta}\frac{\partial \delta w}{\partial \theta} dr d\theta\right] \\ &= -\left[\frac{1}{r}M_{\theta\theta}\frac{\partial \delta w}{\partial \theta}|_{\theta_1}^{\theta_2} - \left(\frac{\partial M_{\theta\theta}}{\partial \theta}\delta w|_{\theta_1}^{\theta_2} - \int_{\Omega_0}\frac{\partial^2 M_{\theta\theta}}{\partial \theta^2}\delta w dr d\theta\right)\right] \end{aligned} \tag{2.31}$$

$$\begin{aligned} &-2\int_{\Omega_0} M_{r\theta}\frac{1}{r}\left(\frac{\partial^2 \delta w}{\partial r \partial \theta} - \frac{1}{r}\frac{\partial \delta w}{\partial \theta}\right) r dr d\theta = -2\int_{\Omega_0} M_{r\theta}\left(\frac{\partial^2 \delta w}{\partial r \partial \theta} - \frac{1}{r}\frac{\partial \delta w}{\partial \theta}\right) dr d\theta \\ &= -2\left(M_{r\theta}\frac{\partial \delta w}{\partial r}|_{\theta_1}^{\theta_2} - \int_{\Omega_0}\frac{\partial M_{r\theta}}{\partial \theta}\frac{\partial \delta w}{\partial r} dr d\theta\right) + 2\left(\frac{1}{r}M_{r\theta}\delta w|_{\theta_1}^{\theta_2} - \int_{\Omega_0}\frac{1}{r}\frac{\partial M_{r\theta}}{\partial \theta}\delta w dr\right) \\ &= -2\left(M_{r\theta}\frac{\partial \delta w}{\partial r}|_{\theta_1}^{\theta_2} - \left(\frac{\partial M_{r\theta}}{\partial \theta}\delta w|_{r_1}^{r_2} - \int_{\Omega_0}\frac{\partial^2 M_{r\theta}}{\partial r \partial \theta}\delta w dr d\theta\right)\right) \\ &+2\left(\frac{1}{r}M_{r\theta}\delta w|_{\theta_1}^{\theta_2} - \int_{\Omega_0}\frac{1}{r}\frac{\partial M_{r\theta}}{\partial \theta}\delta w dr\right) \end{aligned} \tag{2.32}$$

$$\begin{aligned} -\int^T\int_{\Omega} I_0\left(\dot{u}\delta\dot{u}\right) r dr d\theta dt &= -\int^T\int_{\Omega}\left(r I_0\right)\dot{u}\delta\dot{u} dr d\theta dt \\ &= -\left[\left(r I_0\right)\frac{\partial u}{\partial t}\delta u|_{t_1}^{t_1} - \int^T\int_{\Omega}\left(r I_0\right)\frac{\partial^2 u}{\partial t^2}\delta u dr d\theta dt\right] \end{aligned} \tag{2.33}$$

$$\begin{aligned} -\int^T\int_{\Omega} I_0\left(\dot{v}\delta\dot{v}\right) r dr d\theta dt &= -\int^T\int_{\Omega}\left(r I_0\right)\dot{v}\delta\dot{v} dr d\theta dt \\ &= -\left[\left(r I_0\right)\frac{\partial v}{\partial t}\delta v|_{t_1}^{t_1} - \int^T\int_{\Omega}\left(r I_0\right)\frac{\partial^2 v}{\partial t^2}\delta v dr d\theta dt\right] \end{aligned} \tag{2.34}$$

$$\begin{aligned} -\int^T\int_{\Omega} I_0\left(\dot{w}\delta\dot{w}\right) r dr d\theta dt &= -\int^T\int_{\Omega}\left(r I_0\right)\dot{w}\delta\dot{w} dr d\theta dt \\ &= -\left[\left(r I_0\right)\frac{\partial w}{\partial t}\delta w|_{t_1}^{t_1} - \int^T\int_{\Omega}\left(r I_0\right)\frac{\partial^2 w}{\partial t^2}\delta w dr d\theta dt\right] \end{aligned} \tag{2.35}$$

$$-\int^{T}\int_{\Omega} I_2\frac{\partial^2 w}{\partial r\partial t}\frac{\partial^2 \delta w}{\partial r\partial t}rdrd\theta dt = -\big[\,(rI_2)\,\frac{\partial^2 w}{\partial r\partial t}\frac{\partial \delta w}{\partial r}|_{t_1}^{t_1} - \int^{T}\int_{\Omega}(rI_2)\,\frac{\partial^2 w}{\partial r\partial t}\frac{\partial \delta w}{\partial r}drd\theta dt\big] \tag{2.36}$$

Substituting Equations (2.23)-(2.36) into Equation (2.22) and setting each of the coefficients of $\delta u, \delta v, \delta w$ in the area integrand equal to zero, we obtain

$$\delta u : \frac{1}{r}\left(\frac{\partial(rN_{rr})}{\partial r} + \frac{\partial N_{r\theta}}{\partial \theta} - N_{\theta\theta}\right) - I_0\frac{\partial^2 u}{\partial t^2} = 0 \tag{2.37}$$

$$\delta v : \frac{1}{r}\left(\frac{\partial(rN_{r\theta})}{\partial r} + \frac{\partial N_{\theta\theta}}{\partial \theta} + N_{r\theta}\right) - I_0\frac{\partial^2 v}{\partial t^2} = 0 \tag{2.38}$$

$$\begin{aligned}\delta w : \frac{1}{r}\Big[\frac{\partial(rM_{rr})}{\partial r} - \frac{\partial M_{\theta\theta}}{\partial r} + \frac{1}{r}\frac{\partial^2 M_{\theta\theta}}{\partial \theta^2} + 2\frac{\partial^2 M_{r\theta}}{\partial r\partial\theta} + \frac{2}{r}\frac{\partial M_{r\theta}}{\partial\theta} + \frac{\partial(rN_{rr}\frac{\partial w}{\partial r})}{\partial r}\\ + \frac{1}{r}\frac{\partial(N_{\theta\theta}\frac{\partial w}{\partial\theta})}{\partial\theta}\Big] + q - I_0\frac{\partial^2 w}{\partial t^2} + I_2\frac{\partial}{\partial t^2}\left(\frac{1}{r}\frac{\partial(r\frac{\partial w}{\partial r})}{\partial r} + \frac{1}{r^2}\frac{\partial^2 w}{\partial\theta^2}\right) = 0\end{aligned} \tag{2.39}$$

And setting each of the coefficients of $\delta u, \delta v, \delta w$ in the boundary integral equal to zero, we obtain the following boundary conditions:specify

for $r = r_1, r_2$

$$N_{\theta\theta} \quad \text{or} \quad \delta u = 0 \tag{2.40}$$

$$rN_{r\theta} \quad \text{or} \quad \delta v = 0 \tag{2.41}$$

$$\left[\frac{\partial(rM_{r\theta})}{\partial r} + \frac{1}{r}\frac{\partial M_{\theta\theta}}{\partial\theta} - rM_{r\theta} + \frac{1}{r}N_{\theta\theta}\frac{\partial w}{\partial\theta} + N_{r\theta}\frac{\partial w}{\partial r}\right] = 0 \quad \text{or} \quad \delta w = 0 \tag{2.42}$$

$$\frac{1}{r}M_{\theta\theta} = 0 \quad \text{or} \quad \delta\frac{\partial w}{\partial\theta} = 0 \tag{2.43}$$

For $\theta = \theta_1, \theta_2$

$$N_{rr} \quad \text{or} \quad \delta v = 0 \tag{2.44}$$

$$N_{r\theta} \quad \text{or} \quad \delta u = 0 \tag{2.45}$$

$$\left[\frac{\partial(rM_{rr})}{\partial r} + 2\frac{\partial M_{r\theta}}{\partial\theta} - M_{\theta\theta} + rN_{rr}\frac{\partial w}{\partial r} + N_{r\theta}\frac{\partial w}{\partial\theta}\right] = 0 \quad \text{or} \quad \delta w = 0 \tag{2.46}$$

$$M_{rr} = 0 \quad \text{or} \quad \delta\frac{\partial w}{\partial r} = 0 \tag{2.47}$$

Finally, for position (r_1, θ_1),(r_2, θ_1)

$$M_{r\theta} \quad \text{or} \quad \delta w = 0 \tag{2.48}$$

We consider linear thermoelastic isotropic plates in which the elastic stiffnesses are independent of the temperature and obtain

$$\sigma_{rr} = \frac{E}{1-\nu^2}(\epsilon_{rr} + \nu\epsilon_{\theta\theta}) - \frac{E\alpha}{1-\nu}\Delta T \tag{2.49}$$

$$\sigma_{\theta\theta} = \frac{E}{1-\nu^2}(\epsilon_{\theta\theta} + \nu\epsilon_{rr}) - \frac{E\alpha}{1-\nu}\Delta T \tag{2.50}$$

$$\sigma_{r\theta} = 2G\epsilon_{r\theta} \tag{2.51}$$

where α is the coefficient of thermal expansion and $G = \frac{E}{2(1+\nu)}$. Substituting Equations (2.49-2.51) into Equations (2.15)-(2.20), we have

$$N_{rr} = \int_{-\frac{h}{2}}^{\frac{h}{2}} (\frac{E}{1-\nu^2}(\epsilon_{rr} + \nu\epsilon_{\theta\theta}) - \frac{E\alpha}{1-\nu}\Delta T)dz \tag{2.52}$$

$$N_{\theta\theta} = \int_{-\frac{h}{2}}^{\frac{h}{2}} (\frac{E}{1-\nu^2}(\epsilon_{\theta\theta} + \nu\epsilon_{rr}) - \frac{E\alpha}{1-\nu}\Delta T)dz \tag{2.53}$$

$$N_{r\theta} = \int_{-\frac{h}{2}}^{\frac{h}{2}} (2G\epsilon_{r\theta})dz \tag{2.54}$$

$$M_{rr} = \int_{-\frac{h}{2}}^{\frac{h}{2}} (\frac{E}{1-\nu^2}(\epsilon_{rr} + \nu\epsilon_{\theta\theta}) - \frac{E\alpha}{1-\nu}\Delta T)zdz \tag{2.55}$$

$$M_{\theta\theta} = \int_{-\frac{h}{2}}^{\frac{h}{2}} (\frac{E}{1-\nu^2}(\epsilon_{\theta\theta} + \nu\epsilon_{rr}) - \frac{E\alpha}{1-\nu}\Delta T)zdz \tag{2.56}$$

$$M_{r\theta} = \int_{-\frac{h}{2}}^{\frac{h}{2}} (2G\epsilon_{r\theta})zdz \tag{2.57}$$

Substituting Equations (2.4)-(2.7) into Equations (2.52)-(2.57) yields

$$N_{rr} = \frac{Eh}{1-\nu^2}\left[\left(\frac{1}{2}\left(\frac{\partial w}{\partial r}\right)^2 + \frac{\partial u}{\partial r}\right) + \frac{\nu}{r}\left(u + \frac{\partial v}{\partial \theta} + \frac{1}{2r}\left(\frac{\partial w}{\partial \theta}\right)^2\right)\right] - \frac{N_T}{1-\nu} \tag{2.58}$$

$$N_{\theta\theta} = \frac{Eh}{1-\nu^2}\left[\nu\left(\frac{1}{2}\left(\frac{\partial w}{\partial r}\right)^2 + \frac{\partial u}{\partial r}\right) + \frac{1}{r}\left(u + \frac{\partial v}{\partial \theta} + \frac{1}{2r}\left(\frac{\partial w}{\partial \theta}\right)^2\right)\right] - \frac{N_T}{1-\nu} \tag{2.59}$$

$$N_{r\theta} = G\left(\frac{\partial v}{\partial r} - \frac{v}{r} + \frac{1}{r}\frac{\partial u}{\partial \theta} + \frac{1}{r}\frac{\partial w}{\partial r}\frac{\partial w}{\partial \theta}\right) \tag{2.60}$$

$$N_T = E\alpha\int_{-\frac{h}{2}}^{\frac{h}{2}} \Delta T(r,\theta,z,t)dz \tag{2.61}$$

$$M_{rr} = -D\left[\frac{\partial^2 w}{\partial r^2} + \frac{\nu}{r}(\frac{\partial w}{\partial r} + \frac{1}{r}\frac{\partial^2 w}{\partial \theta^2})\right] - \frac{M_T}{1-\nu} \tag{2.62}$$

$$M_{\theta\theta} = -D\left[\nu\frac{\partial^2 w}{\partial r^2} + \frac{1}{r}(\frac{\partial w}{\partial r} + \frac{1}{r}\frac{\partial^2 w}{\partial \theta^2})\right] - \frac{M_T}{1-\nu} \tag{2.63}$$

$$M_{r\theta} = -(1-\nu)D\frac{1}{r}\left(\frac{\partial^2 w}{\partial r \partial \theta} - \frac{1}{r}\frac{\partial w}{\partial \theta}\right) \tag{2.64}$$

$$M_T = E\alpha \int_{-\frac{h}{2}}^{\frac{h}{2}} \Delta T(r,z) z dz \tag{2.65}$$

When the in-plane natural frequencies are large compared with the transverse natural frequencies, the in-plane inertia term can be neglected. Then, we introduce the stress function F, which sometimes referred to as the Airy function, defined by

$$N_{rr} = \frac{1}{r}\frac{\partial F}{\partial r} + \frac{1}{r^2}\frac{\partial^2 F}{\partial \theta^2}, \quad N_{\theta\theta} = \frac{\partial^2 F}{\partial r^2}, \quad N_{r\theta} = \frac{1}{r^2}\frac{\partial F}{\partial \theta} - \frac{1}{r}\frac{\partial^2 F}{\partial r \partial \theta} \tag{2.66}$$

which satisfy Equations (2.36) and (2.37) exactly. Substituting the axisymmetric form of Equation (2.66) into the axisymmetric form of Equation (2.38), we obtain

$$D\nabla^4 w + \rho h\ddot{w} = \frac{1}{r}\frac{\partial^2 w}{\partial r^2}\frac{\partial F}{\partial r} + \frac{1}{r}\frac{\partial w}{\partial r}\frac{\partial^2 F}{\partial r^2} - 2c\frac{\partial w}{\partial t} - \frac{1}{1-\nu}\nabla^2 M_T \tag{2.67}$$

In the axisymmetric case, the compatibility equation can be deduced from the following equations:

$$\epsilon_{rr} = \frac{1}{Eh}(N_{rr} - \nu N_{\theta\theta}) + \alpha\Delta T \tag{2.68}$$

$$\epsilon_{\theta\theta} = \frac{1}{Eh}(N_{\theta\theta} - \nu N_{rr}) + \alpha\Delta T \tag{2.69}$$

$$N_{rr} = \frac{1}{r}\frac{\partial F}{\partial r} \text{ and } N_{\theta\theta} = \frac{\partial^2 F}{\partial r^2} \tag{2.70}$$

$$\epsilon_{rr} = \frac{\partial u}{\partial r} + \frac{1}{2}\left(\frac{\partial w}{\partial r}\right)^2 \text{ and } \epsilon_{\theta\theta} = \frac{u}{r} \tag{2.71}$$

where u is the radial displacement. It follows from Equations (2.68)-(2.71) that

$$\frac{\partial u}{\partial r} = -\frac{1}{2}\left(\frac{\partial w}{\partial r}\right)^2 + \frac{1}{Eh}\left(\frac{1}{r}\frac{\partial F}{\partial r} - \nu\frac{\partial^2 F}{\partial r^2}\right) + \alpha\Delta T \tag{2.72}$$

$$\frac{u}{r} = \frac{1}{Eh}\left(\frac{\partial^2 F}{\partial r^2} - \frac{\nu}{r}\frac{\partial F}{\partial r}\right) + \alpha\Delta T \tag{2.73}$$

Eliminating u from Equations (2.72) and (2.73), we obtain the compatibility equation

$$r\frac{\partial^3 F}{\partial r^3} + \frac{\partial^2 F}{\partial r^2} - \frac{1}{r}\frac{\partial F}{\partial r} = -\frac{1}{2}Eh\left(\frac{\partial w}{\partial r}\right)^2 - Eh\alpha r\frac{\partial \Delta T}{\partial r} \tag{2.74}$$

Now adding the external force due to the electrostatic field to Equation (2.67), we obtain the final form

$$D\nabla^4 w + \rho h \ddot{w} = \frac{1}{r}\frac{\partial^2 w}{\partial r^2}\frac{\partial F}{\partial r} + \frac{1}{r}\frac{\partial w}{\partial r}\frac{\partial^2 F}{\partial r^2} - 2c\frac{\partial w}{\partial t} - \frac{1}{1-\nu}\nabla^2 M_T + \frac{\epsilon V^2}{2\left(d-w\right)^2} \tag{2.75}$$

$$r\frac{\partial^3 F}{\partial r^3} + \frac{\partial^2 F}{\partial r^2} - \frac{1}{r}\frac{\partial F}{\partial r} = -\frac{1}{2}Eh\left(\frac{\partial w}{\partial r}\right)^2 - Eh\alpha r\frac{\partial T}{\partial r} \tag{2.76}$$

where V is the applied voltage, d is the capacitor gap distance, and ϵ is the dielectric constant of the medium.

In the following work, we treat the electrostatic and/or thermal loadings.

Chapter 3

Annular Plate under Electrostatic Loading

In this chapter, we study the mechanical behavior of an electrostatic micropump employing an annular actuation member. We present a complete theoretical framework to enable an accurate simulation and a proper understanding of the mechanical behavior of this type of micropumps, thus enabling better pump designs. To this end, the annular plate is modeled as a distributed-mass structure deflecting in bending under electrostatic actuation. We adopt the von Kármán plate model under axisymmetric loading conditions to account for the bending stiffness and nonlinearities arising from large deflections. Two cases of boundary conditions are considered to simulate practical MEMS devices.

The equations are nondimensionalized and the design parameters of the pump are lumped into nondimensional parameters. To study both of the deflection and the pull-in phenomenon of the annular plate, we first solve the static problem numerically. The eigenvalue problem, representing the vibrations around the deflected position, is then solved numerically to obtain the natural frequencies and mode shapes.

3.1 Problem Formulation

We assume that the transverse deflection w of the plate is axisymmetric and write the equations of motion as

$$D\nabla^4 w + c\frac{\partial w}{\partial t} + \rho h\frac{\partial^2 w}{\partial t^2} = \frac{1}{r}\frac{\partial^2 w}{\partial r^2}\frac{\partial \Phi}{\partial r} + \frac{1}{r}\frac{\partial w}{\partial r}\frac{\partial^2 \Phi}{\partial r^2} + \frac{\epsilon V^2}{2\left(d-w\right)^2} \tag{3.1}$$

$$\nabla^4 \Phi = -\frac{Eh}{r}\frac{\partial^2 w}{\partial r^2}\frac{\partial w}{\partial r} \tag{3.2}$$

where t is time, ρ is the material density, c is the viscous damping, h is the plate thickness, d is the capacitor gap distance, ϵ is the dielectric constant of the medium, V is the DC voltage, and Φ is the stress function. The modulus of rigidity D is

$$D = \frac{Eh^3}{12\left(1-\nu^2\right)} \tag{3.3}$$

where E is Young's modulus and ν is Poisson's ratio. In the axisymmetric case, the differential operator ∇^4 is given by

$$\nabla^4 = \frac{\partial^4}{\partial r^4} + \frac{2}{r}\frac{\partial^3}{\partial r^3} - \frac{1}{r^2}\frac{\partial^2}{\partial r^2} + \frac{1}{r^3}\frac{\partial}{\partial r} \tag{3.4}$$

where r is the radial position.

In the axisymmetric case, the fourth-order compatibility equation (3.2) can be reduced to the following third-order equation (Chapter 2):

$$r\frac{\partial^3 \Phi}{\partial r^3} + \frac{\partial^2 \Phi}{\partial r^2} - \frac{1}{r}\frac{\partial \Phi}{\partial r} = -\frac{1}{2}Eh\left(\frac{\partial w}{\partial r}\right)^2 \tag{3.5}$$

We introduce nondimensional variables, denoted by asterisks, defined as follows:

$$r = Rr^*, \;\; w = dw^*, \;\; t = R^2\left(\frac{\rho h}{D}\right)^{1/2} t^*, b = Rb^*$$
$$c = \frac{12(1-\nu^2)}{R^4}\left(\rho h^5 D\right)^{1/2} c^*, \;\; \Phi = Ehd^2\Phi^* \tag{3.6}$$

where R is the outer radius of the annular plate. Substituting Equation (3.6) into Equations (3.1)

and (3.5) and dropping the asterisks, we obtain

$$\frac{\partial^2 w}{\partial t^2} + c\frac{\partial w}{\partial t} + \nabla^4 w = \frac{\alpha_1}{r}\Big(\frac{\partial^2 w}{\partial r^2}\frac{\partial \Phi}{\partial r} + \frac{\partial w}{\partial r}\frac{\partial^2 \Phi}{\partial r^2}\Big) + \frac{\alpha_2 V^2}{(1-w)^2} \tag{3.7}$$

$$r\frac{\partial^3 \Phi}{\partial r^3} + \frac{\partial^2 \Phi}{\partial r^2} - \frac{1}{r}\frac{\partial \Phi}{\partial r} = -\frac{1}{2}\left(\frac{\partial w}{\partial r}\right)^2 \tag{3.8}$$

where $\alpha_1 = \frac{12(1-\nu^2)d^2}{h^2}$ and $\alpha_2 = \frac{\epsilon R^4}{2Dd^3}$. They represent the ratio of the mechanical restoring force to the electrostatic force and the effective electrostatic force, respectively.

We express the plate deflection and the stress function as the summation of static components, denoted by $w_s(r)$ and $\Phi_s(r)$, and dynamic components, denoted by $u(r,t)$ and $\phi(r,t)$; that is,

$$w(r,t) = w_s(r) + u(r,t) \tag{3.9}$$

$$\Phi(r,t) = \Phi_s(r) + \phi(r,t) \tag{3.10}$$

To calculate the static deflection, we set the time derivatives in Equations (3.7) and (3.8) equal to zero and obtain

$$\nabla^4 w_s = \frac{\alpha_1}{r}\Big(\frac{\partial^2 w_s}{\partial r^2}\frac{\partial \Phi_s}{\partial r} + \frac{\partial w_s}{\partial r}\frac{\partial^2 \Phi_s}{\partial r^2}\Big) + \frac{\alpha_2 V^2}{(1-w_s)^2} \tag{3.11}$$

$$r\frac{\partial^3 \Phi_s}{\partial r^3} + \frac{\partial^2 \Phi_s}{\partial r^2} - \frac{1}{r}\frac{\partial \Phi_s}{\partial r} = -\frac{1}{2}\left(\frac{\partial w_s}{\partial r}\right)^2 \tag{3.12}$$

We generate the equations of motion governing the dynamic behavior of the plate around the deflected shape by substituting Equations (3.9) and (3.10) into Equations (3.7) and (3.8) and dropping the terms representing the equilibrium position and higher-order terms. The result is

$$\begin{aligned}\frac{\partial^2 u}{\partial t^2} + c\frac{\partial u}{\partial t} + \nabla^4 u = \frac{\alpha_1}{r}\Big(&\frac{\partial^2 u}{\partial r^2}\frac{\partial \Phi_s}{\partial r} + \frac{\partial^2 w_s}{\partial r^2}\frac{\partial \phi}{\partial r} + \frac{\partial u}{\partial r}\frac{\partial^2 \Phi_s}{\partial r^2} + \frac{\partial w_s}{\partial r}\frac{\partial^2 \phi}{\partial r^2} + \frac{\partial^2 u}{\partial r^2}\frac{\partial \phi}{\partial r} + \frac{\partial u}{\partial r}\frac{\partial^2 \phi}{\partial r^2}\Big) \\ &+ \frac{2\alpha_2 V^2}{(1-w_s)^3}u + \frac{3\alpha_2 V^2}{(1-w_s)^4}u^2 + \frac{4\alpha_2 V^2}{(1-w_s)^5}u^3\end{aligned} \tag{3.13}$$

$$r\frac{\partial^3 \phi_s}{\partial r^3} + \frac{\partial^2 \phi_s}{\partial r^2} - \frac{1}{r}\frac{\partial \phi_s}{\partial r} = -\frac{1}{2}\Big[2\frac{\partial u}{\partial r}\frac{\partial w_s}{\partial r} + \left(\frac{\partial u}{\partial r}\right)^2\Big] \tag{3.14}$$

Next, we study two cases. First, we consider an annular plate clamped along both of the outer and inner radii; this design was proposed by Saif et al. (1999). Second, we consider an annular plate clamped along the outer radius and free along the inner radius. The latter design is still under investigation.

3.2 Clamped-Clamped Case

We consider the case of immovable inner and outer edges. In this case, the radial displacement u is equal to zero. The nondimensional boundary conditions for this case are

$$\frac{\partial^2 \Phi}{\partial r^2} - \frac{\nu}{r}\frac{\partial \Phi}{\partial r} = 0 \text{ at } r = b \text{ and } 1 \tag{3.15}$$

$$w = 0 \text{ and } \frac{\partial w}{\partial r} = 0 \text{ at } r = b \text{ and } 1 \tag{3.16}$$

where b is the nondimensional inner radius.

We calculate the static deflection of the plate by solving the following boundary-value problem numerically for $w_s(r)$:

$$w_s^{iv} = -\frac{2}{r}w_s''' + \frac{1}{r^2}w_s'' - \frac{1}{r^3}w_s' + \frac{\alpha_1}{r}\left(w_s''\Phi_s' + w_s'\Phi_s''\right) + \frac{\alpha_2 V^2}{(1-w_s)^2} \tag{3.17}$$

$$r\Phi_s''' + \Phi_s'' - \frac{1}{r}\Phi_s' = -\frac{1}{2}\left(w_s'\right)^2 \tag{3.18}$$

$$\Phi_s'' - \frac{\nu}{r}\Phi_s' = 0 \quad \text{at} \quad r = b \text{ and } 1 \tag{3.19}$$

$$w_s = 0 \text{ and } w_s' = 0 \quad \text{at} \quad r = b \text{ and } 1 \tag{3.20}$$

We solved Equations (3.17)-(3.20) for a polysilicon annular plate with an outer radius $R = 50\mu m$, inner radius $R = 5\mu m$, and thickness $h = 1\mu m$, a capacitor gap $d = 2\mu m$, and a range of electrostatic forces varying from zero to the forcing level where structural instability (pull-in) develops. Figure 3.1 shows an axisymmetric cross-section of the plate as it deflects under an upward electrostatic force increasing from zero to the forcing level corresponding to $\alpha_2 V^2 = 140.6$. The evolution of the static deflection is most pronounced in the mid-region of the cross-section. Figure 3.2 shows variation of the maximum deflection W_{Max} for the same range of $\alpha_2 V^2$ as that in Figure 3.1. As the electrostatic force, represented by $\alpha_2 V^2$, increases, the maximum deflection increases.

To calculate the mode shapes and corresponding natural frequencies, we substitute $w_s(x)$ into

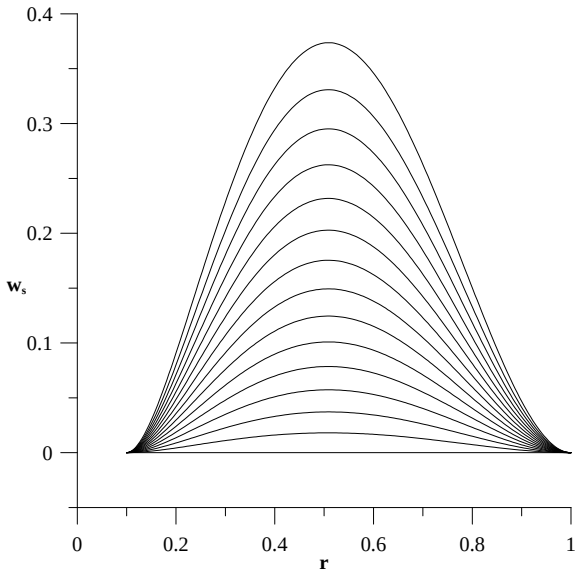

Figure 3.1: Nondimensional deflection $w_s(r)$ of the clamped-clamped plate under an electrostatic force ranging from $\alpha_2 V^2 = 0$ to 140.6.

Equations (3.13)-(3.16), drop the nonlinear and damping terms, and obtain

$$\frac{\partial^2 u}{\partial t^2} + \nabla^4 u = \frac{\alpha_1}{r}\Big(\frac{\partial^2 u}{\partial r^2}\frac{\partial \Phi_s}{\partial r} + \frac{\partial^2 w_s}{\partial r^2}\frac{\partial \phi}{\partial r} + \frac{\partial u}{\partial r}\frac{\partial^2 \Phi_s}{\partial r^2} + \frac{\partial w_s}{\partial r}\frac{\partial^2 \phi}{\partial r^2}\Big) + \frac{2\alpha_2 V^2}{(1-w_s)^3}u \tag{3.21}$$

$$r\frac{\partial^3 \phi_s}{\partial r^3} + \frac{\partial^2 \phi_s}{\partial r^2} - \frac{1}{r}\frac{\partial \phi_s}{\partial r} = -\Big[\frac{\partial u}{\partial r}\frac{\partial w_s}{\partial r}\Big] \tag{3.22}$$

$$\phi'' - \frac{\nu}{r}\phi' = 0 \quad \text{at} \quad r = b \ \text{ and } \ 1 \tag{3.23}$$

$$u = 0 \ \text{ and } \ u' = 0 \quad \text{at} \quad r = b \ \text{ and } \ 1 \tag{3.24}$$

To solve these equations for the undamped mode shapes and natural frequencies of the plate, we assume a harmonic motion in the *nth* mode in the form

$$u(r,t) = \psi_n(r)e^{i\omega_n t} \tag{3.25}$$

$$\phi(r,t) = \chi_n(r)e^{i\omega_n t} \tag{3.26}$$

where $\psi_n(r)$ is the *nth* axisymmetric mode shape, $\chi_n(r)$ is the associated stress function, and ω_n is the *nth* nondimensional natural frequency. Substituting Equations (3.25) and (3.26) into Equations

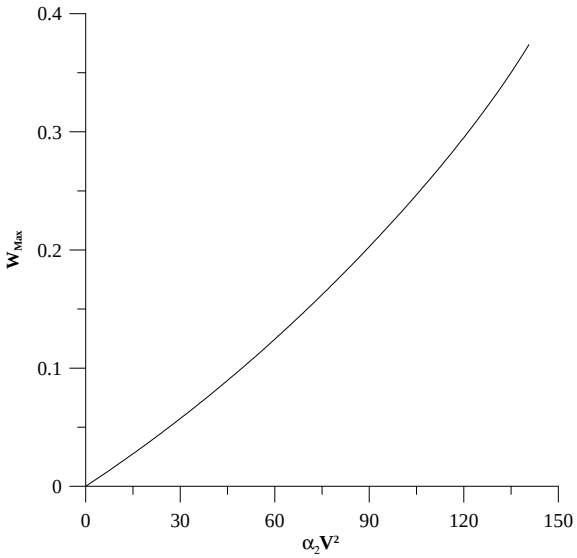

Figure 3.2: Variation of the maximum deflection W_{Max} of the clamped-clamped plate with $\alpha_2 V^2$.

(3.21)-(3.24) yields

$$\psi_n^{iv} + \frac{2}{r}\psi_n''' - \frac{1}{r^2}\psi_n'' + \frac{1}{r^3}\psi_n' - \frac{\alpha_1}{r}\left(\psi_n''\chi_n' + \psi_n'\chi_n''\right) = \left(\frac{\alpha_2 V^2}{(1-w_s)^2} + \omega^2\right)\psi_n \tag{3.27}$$

$$r\chi_n''' + \chi_n'' - \frac{1}{r}\chi_n' = -\left(w_s'\psi_n'\right) \tag{3.28}$$

$$\chi_n'' - \frac{\nu}{r}\chi_n' = 0 \quad \text{at} \quad r = b \ \text{ and } \ 1 \tag{3.29}$$

$$\psi_n = 0 \ \text{ and } \ \psi_n' = 0 \quad \text{at} \quad r = b \ \text{ and } \ 1 \tag{3.30}$$

To solve this eigenvalue problem, we release the second boundary condition at $r = 1.0$ and solve the boundary-value problem iteratively using a shooting method until ω_n, ψ_n, and χ_n converge to within predefined tolerances. This procedure is repeated for each mode shape and associated natural frequency and stress function, using various sets of initial guesses for the mode shape, natural frequency, and stress function.

Figure 3.3 shows variation of the fundamental natural frequency ω_1 of the clamped-clamped plate with $\alpha_2 V^2$. The fundamental frequency of the plate decreases at low and high levels of the electrostatic force. In the mid-range, the fundamental frequency remains nearly constant due to the counterbalance between the electrostatic force and in-plane stresses. As pull-in develops, the fundamental natural frequency is expected to approach zero. Our results do not reflect this fact because

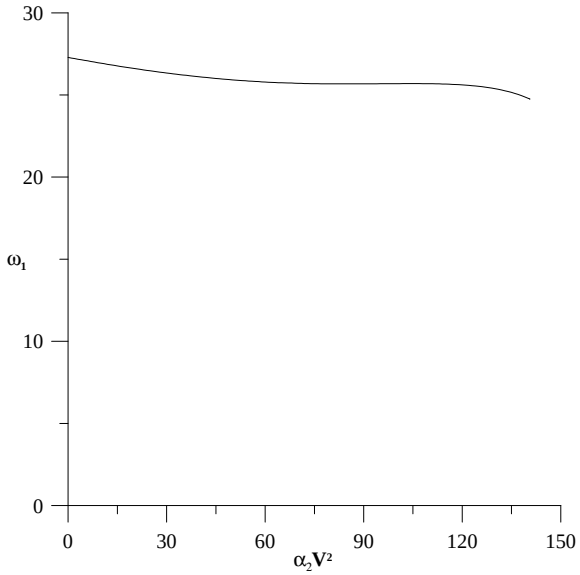

Figure 3.3: Variation of the fundamental natural frequency of the clamped-clamped plate with $\alpha_2 V^2$.

our numerical routine is sensitive to the stiffness of the system of differential equations (3.17), (3.18), (3.27), and (3.28). The stiffness of these equations increases as $\alpha_2 V^2$ increases. As a result, it becomes harder to generate adequate initial guesses as pull-in is approached.

Figures 3.4 and 3.5 show the first and second mode shapes of the plate as the electrostatic force is increased from zero and approaches the pull-in level. In both figures, the mode shape is normalized with respect to the maximum deflection point. The natural frequencies and mode shapes of the free-plate vibrations compare well with those reported by Amabili et al. (1996), which we used as a bench mark to check our algorithm. We show results in Table 1 for clamped-clamped (C-C) and clamped-free (C-F) annular paltes with a radii ratio of 0.5.

Table 3.1: Nondimensional natural frequencies of an annular plate.

Material	$1stmode C-C$	$2ndmode C-C$	$3rdmode C-C$	$1stmode C-F$	$2ndmode C-F$	$3rdmode C-F$
Amabili et al. (1996)	9.447	9.498	9.660	4.220	4.691	5.667
Present algorithm	9.451	9.510	9.680	4.250	4.700	5.670

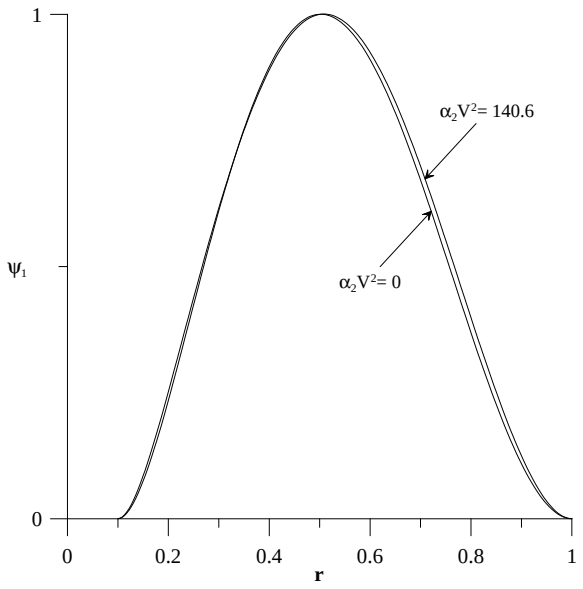

Figure 3.4: The first normalized mode shape of the clamped-clamped plate as the electrostatic force increases from zero and approaches pull-in level.

3.3 Clamped-Free Case

In this case, the plate is clamped on the outer edge and free on the inner edge. On the free edge the boundary condition of the stress function corresponds to the vanishing of the in-plane radial force N_r. Using Equation (3.7), we find that the boundary conditions at the free edge $r = b$ are

$$\begin{aligned} \frac{\partial^2 w}{\partial r^2} + \frac{\nu}{r}\frac{\partial w}{\partial r} &= 0, \\ \frac{\partial^3 w}{\partial r^3} + \frac{1}{r}\frac{\partial^2 w}{\partial r^2} - \frac{1}{r^2}\frac{\partial w}{\partial r} &= 0, \\ \text{and} \qquad \frac{\partial \Phi}{\partial r} &= 0 \end{aligned} \tag{3.31}$$

while the boundary conditions at the fixed edge $r = 1$ are the same as those in Equations (3.15) and (3.16).

We calculate the static deflection of the plate by solving Equations (3.17) and (3.18) for the bound-

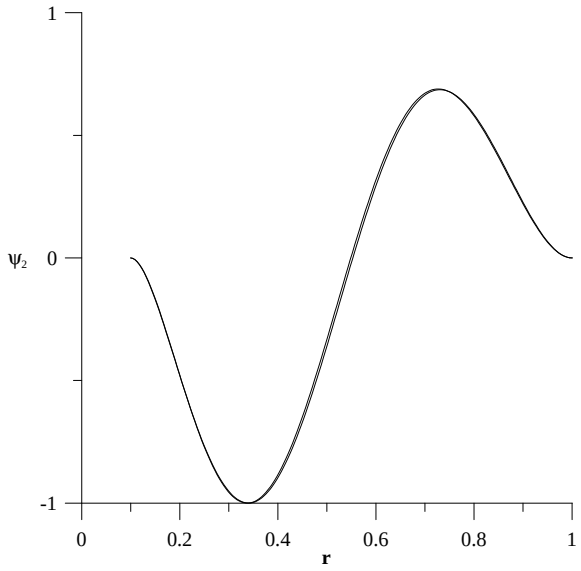

Figure 3.5: The second normalized mode shape of the clamped-clamped plate as the electrostatic force increases from zero and approaches pull-in level.

ary conditions

$$w_s'' + \frac{\nu}{r} w_s' = 0\ , \quad \Phi' = 0, \quad \text{and} \quad w_s''' + \frac{1}{r} w_s'' - \frac{1}{r^2} w_s' = 0, \quad \text{at} \quad r = b \tag{3.32}$$

$$w_s = 0\ , \quad w_s' = 0, \quad \text{and} \quad \Phi_s'' - \frac{\nu}{r} \Phi_s' = 0 \quad \text{at} \quad r = 1 \tag{3.33}$$

We solved the boundary-value problem for a range of electrostatic forces varying from zero to the forcing level where the structural instability (pull-in) develops. Figure 3.6 shows an axisymmetric cross-section of the plate as it deflects under an upward electrostatic force increasing from zero to $\alpha_2 V^2 = 21.5$. The evolution of the static deflection is most pronounced at the free edge. Figure 3.7 shows variation of the maximum nondimensional deflection $W_{Max} = w_s\,(r = b)$ with $\alpha_2 V^2$. As the electrostatic force, represented by $\alpha_2 V^2$, increases, the maximum deflection increases. This relationship is linear at low levels of electrostatic forcing; however as the electrostatic force increases, the relationship becomes increasingly nonlinear.

To calculate the mode shapes and corresponding natural frequencies, we solve Equations (3.21) and

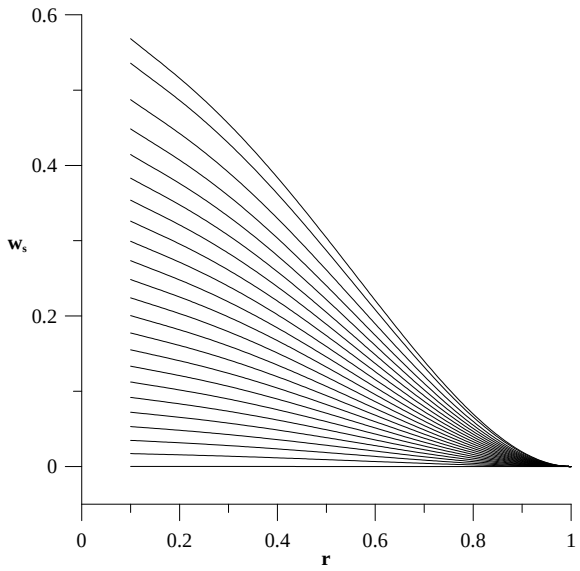

Figure 3.6: Nondimensional deflection $w_s(r)$ of the clamped-free plate under an electrostatic force ranging from $\alpha_2 V^2 = 0$ to 21.5.

(3.22) in conjunction with the boundary conditions

$$u'' + \frac{\nu}{r}u' = 0\ , \quad \frac{\partial \phi}{\partial r} = 0, \quad \text{and} \quad u''' + \frac{1}{r}u'' - \frac{1}{r^2}u' = 0, \quad \text{at} \quad r = b \tag{3.34}$$

$$u = 0\ , \quad u' = 0, \quad \text{and} \quad \phi'' - \frac{\nu}{r}\phi' = 0 \quad \text{at} \quad r = 1 \tag{3.35}$$

We assume a harmonic motion in the *nth* mode as in Equations (3.25) and (3.26). Substituting Equations (3.25) and (3.26) into Equations (3.34) and (3.35) yields

$$\psi_n'' + \frac{\nu}{r}\psi_n' = 0\ , \quad \frac{\partial \chi_n}{\partial r} = 0, \quad \text{and} \quad \psi_n''' + \frac{1}{r}\psi_n'' - \frac{1}{r^2}\psi_n' = 0 \quad \text{at} \quad r = b \tag{3.36}$$

$$\psi_n = 0\ , \quad \psi_n' = 0, \quad \text{and} \quad \chi_n'' - \frac{\nu}{r}\chi_n' = 0 \quad \text{at} \quad r = 1 \tag{3.37}$$

We solve the eigenvalue problem in Equations (3.27), (3.28), (3.36), and (3.37) by releasing one of the boundary conditions at $r = 1.0$ and solving the boundary-value problem iteratively using a shooting method until ω_n, ψ_n, and χ_n converge to within predefined tolerances. This procedure is repeated for each mode shape and associated natural frequency and stress function, using various sets of initial guesses.

Figure 3.8 shows variation of the fundamental natural frequency of the clamped-free plate with

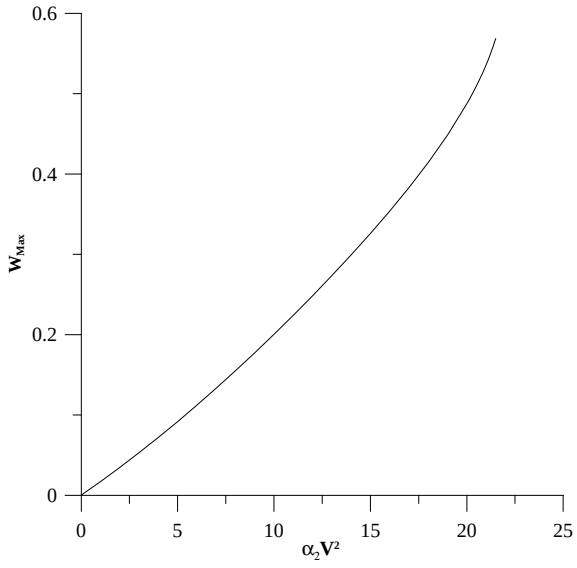

Figure 3.7: Variation of the maximum deflection W_{Max} of the clamped-free plate with $\alpha_2 V^2$.

$\alpha_2 V^2$. The fundamental frequency decreases as the electrostatic force increases and approaches zero as pull-in develops. The contrast between the natural frequency results for this case as opposed to the previous case arises from the fact that the in-plane stresses here are much less pronounced than in the previous case because of the free edge.

Figures 3.9 and 3.10 show the first and second mode shapes of the clamped-free plate as the electrostatic force is increased from zero and approaches the pull-in level. In both figures, the mode shape is normalized with respect to the absolute maximum of the mode shape for a straight plate. Significant changes are observed in the first mode shape, Figure 3.9, but not in the second mode shape, Figure 3.10. The natural frequencies and mode shapes compare well with those reported by Amabili et al. (1996).

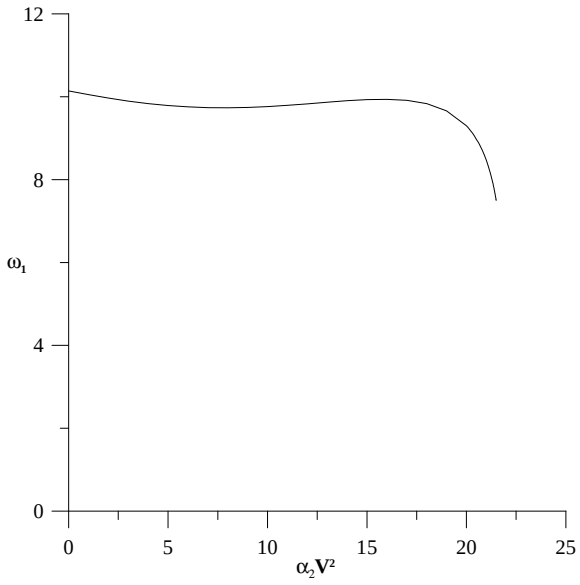

Figure 3.8: Variation of the fundamental natural frequency of the clamped-free plate with αV^2.

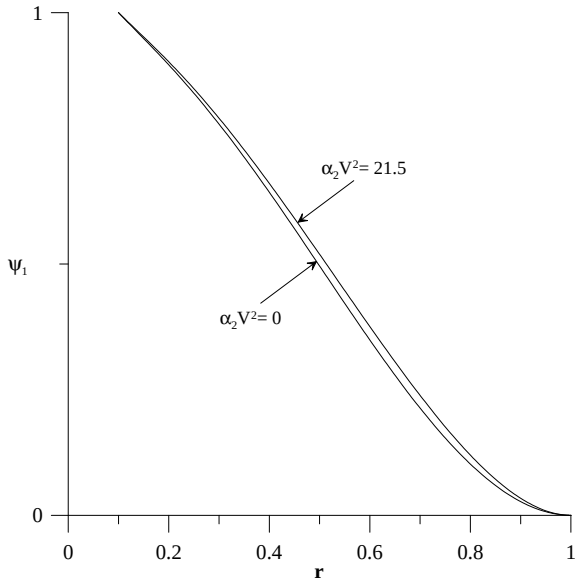

Figure 3.9: The first mode shape of the clamped-free plate as the electrostatic force increases from zero and approaches the pull-in level.

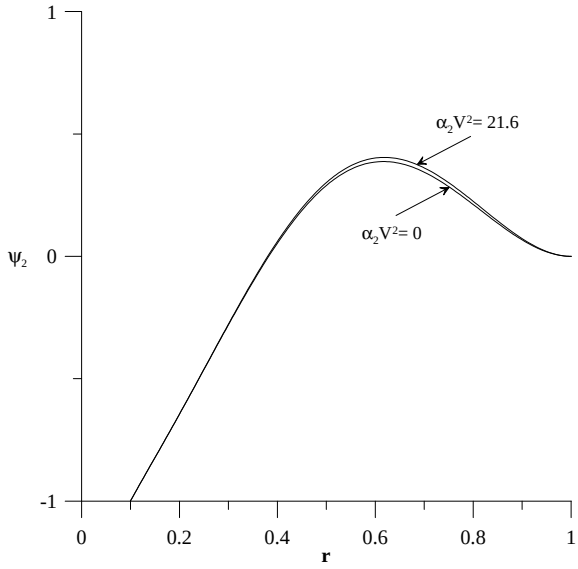

Figure 3.10: The second mode shape of the clamped-free plate as the electrostatic force increases from zero and approaches the pull-in level.

Chapter 4

Circular Plates under Thermal Loading

Thermally induced vibrations are of concern in the design of many structural elements. Most of the previous research on thermally induced vibrations in circular plates has been limited to small deflections. Moreover, the works that deal with large deflections are based on Berger's approximation. In this chapter, we investigate the nonlinear response of a circular plate to a thermal loading consisting of a steady component and a sinusoidal component. We base the analysis on the heat conduction equation and the dynamic analogue of the von Kármán equations. In Section 4.1, we present a formulation of the problem. We neglect the dissipation terms in the heat equation and solve it for the temperature distribution. Then, we substitute the resulting distribution into the equations describing the displacement and stress function. We use the method of multiple scales to determine a first-order approximation of the plate response for two cases. In the Section 4.2, we treat the case of principal parametric resonance of an axisymmetric mode in a simply supported plate with movable edges. In Section 4.3, we treat the case of combination parametric resonance of two axisymmetric modes in a clamped plate with immovable edges. The case of principal parametric resonance of an axisymmetric mode is treated as a special case.

4.1 Problem Formulation

First, we consider the coupled heat conduction equation and dynamic version of the von Kármán equations for a thermally excited circular plate. The basic geometric features are shown in Figure 4.1. We consider an axisymmetric thermal loading and axisymmetric vibrations. They are governed

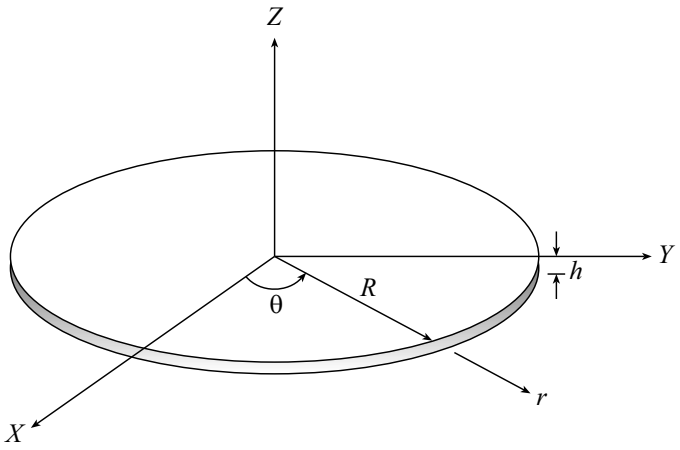

Figure 4.1: Geometry of a circular plate.

by

$$k\nabla^2 T + Q = \rho c_p \frac{\partial T}{\partial t} + \frac{E\alpha T_0}{1-2\nu}\frac{\partial e}{\partial t} \tag{4.1}$$

$$D\nabla^4 w + \rho h\ddot{w} = \frac{1}{r}\frac{\partial^2 w}{\partial r^2}\frac{\partial F}{\partial r} + \frac{1}{r}\frac{\partial w}{\partial r}\frac{\partial^2 F}{\partial r^2} - 2c\frac{\partial w}{\partial t} - \frac{1}{1-\nu}\nabla^2 M_T \tag{4.2}$$

$$\nabla^4 F = -\frac{Eh}{r}\frac{\partial^2 w}{\partial r^2}\frac{\partial w}{\partial r} - \nabla^2 N_T \tag{4.3}$$

where

$$N_T = E\alpha \int_{-\frac{1}{2}h}^{\frac{1}{2}h} [T(r,z,t) - T_0]dz \tag{4.4}$$

$$M_T = E\alpha \int_{-\frac{1}{2}h}^{\frac{1}{2}h} [T(r,z,t) - T_0]zdz \tag{4.5}$$

and $D = \frac{Eh^3}{12(1-\nu^2)}$. Here, $w(r,t)$ is the plate transverse displacement, $F(r,t)$ is the stress function, e is the dilatational strain due to the thermal effect, T is the temperature distribution, T_0 is the stress-free temperature, ρ is the material density, h is the plate thickness, c_p is the heat capacity

coefficient at constant pressure, E is the modulus of elasticity, α is the coefficient of thermal expansion, Q is the heat flux, and ν is Poisson's ratio. We consider the case in which the plate is exposed to a uniformly distributed external heat flux $Q = 4kq\cos\omega t$ and the temperature is kept constant at the plate edge at T_b.

In the axisymmetric case, the compatibility equation (4.3) can be reduced from fourth order to third order. To this end, we note that

$$\epsilon_r = \frac{1}{Eh}(N_r - \nu N_\theta) + \alpha T \tag{4.6}$$

$$\epsilon_\theta = \frac{1}{Eh}(N_\theta - \nu N_r) + \alpha T \tag{4.7}$$

$$N_r = \frac{1}{r}\frac{\partial F}{\partial r} \text{ and } N_\theta = \frac{\partial^2 F}{\partial r^2} \tag{4.8}$$

$$\epsilon_r = \frac{\partial u}{\partial r} + \frac{1}{2}\left(\frac{\partial w}{\partial r}\right)^2 \text{ and } \epsilon_\theta = \frac{u}{r} \tag{4.9}$$

where u is the radial displacement. It follows from Equations (4.6)-(4.9) that

$$\frac{\partial u}{\partial r} = -\frac{1}{2}\left(\frac{\partial w}{\partial r}\right)^2 + \frac{1}{Eh}\left(\frac{1}{r}\frac{\partial F}{\partial r} - \nu\frac{\partial^2 F}{\partial r^2}\right) + \alpha T \tag{4.10}$$

$$\frac{u}{r} = \frac{1}{Eh}\left(\frac{\partial^2 F}{\partial r^2} - \frac{\nu}{r}\frac{\partial F}{\partial r}\right) + \alpha T \tag{4.11}$$

Eliminating u from Equations (4.10) and (4.11), we obtain the compatibility equation

$$r\frac{\partial^3 F}{\partial r^3} + \frac{\partial^2 F}{\partial r^2} - \frac{1}{r}\frac{\partial F}{\partial r} = -\frac{1}{2}Eh\left(\frac{\partial w}{\partial r}\right)^2 - Eh\alpha r\frac{\partial T}{\partial r} \tag{4.12}$$

We introduce nondimensional variables, denoted by asterisks, defined as follows:

$$\begin{aligned} &r = Rr^*, \;\; t = R^2\left(\frac{\rho h}{D}\right)^{1/2} t^*, \;\; T = T_0 T^*, \\ &w = \frac{h^2}{R}w^*, \;\; z = hz^*, \;\; F = \frac{Eh^5}{R^2}F^*, \\ &c = \frac{12(1-\nu^2)}{R^4}\left(\rho h^5 D\right)^{1/2} c^*, \;\; q = \frac{h^4 q^*}{\alpha R^6} \end{aligned} \tag{4.13}$$

Substituting Equations (4.13) into Equations (4.1), (4.2), and (4.12) and dropping the asterisks, we obtain

$$\nabla^2 T + \frac{4qh^4}{\alpha T_0 R^4}\cos(\omega t) = \Gamma_1\frac{\partial T}{\partial t} + \Gamma_2\frac{\partial e}{\partial t} \tag{4.14}$$

$$\frac{\partial^2 w}{\partial t^2} + \nabla^4 w = \epsilon \left[\frac{1}{r} \frac{\partial^2 w}{\partial r^2} \frac{\partial F}{\partial r} + \frac{1}{r} \frac{\partial w}{\partial r} \frac{\partial^2 F}{\partial r^2} - 2c \frac{\partial w}{\partial t} \right] \tag{4.15}$$

$$r \frac{\partial^3 F}{\partial r^3} + \frac{\partial^2 F}{\partial r^2} - \frac{1}{r} \frac{\partial F}{\partial r} = -\frac{1}{2} \left(\frac{\partial w}{\partial r} \right)^2 - \frac{12 \alpha T_0 (1+\nu) R^3}{h^3} \int_{-\frac{1}{2}}^{\frac{1}{2}} z \nabla^2 T \, dz \tag{4.16}$$

$$r \frac{\partial^3 F}{\partial r^3} + \frac{\partial^2 F}{\partial r^2} - \frac{1}{r} \frac{\partial F}{\partial r} = -\frac{\alpha T_0 R^4}{h^4} r \int_{-\frac{1}{2}}^{\frac{1}{2}} \frac{\partial T}{\partial r} dz \tag{4.17}$$

where

$$\epsilon = \frac{12(1-\nu^2)h^2}{R^2}, \quad \Gamma_1 = \frac{\rho c_p}{k} \sqrt{\frac{D}{\rho h}}, \quad \Gamma_2 = \frac{E\alpha}{(1-2\nu)} \frac{1}{k} \sqrt{\frac{D}{\rho h}}$$

The last two terms on the right-hand side of Equation (4.14) represent the diffusion of heat and thermoelastic coupling (Hetnarski, 1987).

Usually, the materials used in plates for mechanical and MEMS applications are Steel, Aluminum (Al), and Silicon Nitride (SiNi). Using the available mechanical and thermal properties for these materials, we calculate the nondimensional coefficients Γ_1 and Γ_2, and present them in Table 4.1. For thin plates, it follows from Equation (4.14) and Table 4.1 that the thermal diffusion and thermoelastic coupling terms are negligible because Γ_1 and Γ_2 are very large. Hence, Equation (4.14) is reduced to

Table 4.1: Thermal and mechanical properties of used materials.

Material	$\rho(Kg/m^3)$	$E(GPa)$	$k(W/m.K)$	$c_p(J/Kg.K)$	α	$\Gamma 1$	$\Gamma 2$
Al	2702	70	237	903	24.0×10^{-6}	$15.86h \times 10^6$	$27.3h \times 10^6$
Steel	7800	207	60	430	12.0×10^{-6}	$97.43h \times 10^6$	$161.34h \times 10^6$
SiNi	2330	100	148	712	2.9×10^{-6}	$22.24h \times 10^6$	$9.72h \times 10^6$

$$\nabla^2 T + \frac{4qh^4}{\alpha T_0 R^4} \cos(\omega t) = 0 \tag{4.18}$$

Solving Equation (4.18) subject to the boundary conditions $T = T_b$ at $r = 1$ and $T < \infty$ at $r = 0$, we have

$$T(r,t) = T_b + \frac{h^4}{\alpha T_0 R^4} \left(1 - r^2\right) q \cos(\omega t) \tag{4.19}$$

Substituting Equation (4.19) into Equations (4.15) and (4.16) yields

$$\frac{\partial^2 w}{\partial t^2} + \nabla^4 w = \epsilon \left[\frac{1}{r} \frac{\partial^2 w}{\partial r^2} \frac{\partial F}{\partial r} + \frac{1}{r} \frac{\partial w}{\partial r} \frac{\partial^2 F}{\partial r^2} - 2c \frac{\partial w}{\partial t} \right] \tag{4.20}$$

$$r \frac{\partial^3 F}{\partial r^3} + \frac{\partial^2 F}{\partial r^2} - \frac{1}{r} \frac{\partial F}{\partial r} = -\frac{1}{2} \left(\frac{\partial w}{\partial r} \right)^2 + 2qr^2 \cos(\Omega t) \tag{4.21}$$

Next, we treat two cases of practical importance in thermally loaded circular plates: simply supported and clamped plates, starting with the first case.

4.2 Simply Supported Plate

We consider a simply supported plate with no restrictions on its in-plane displacement; that is, movable boundary condition. This case is important in the structural mechanics of planar bodies, such as plates (Vinson, 1989). In this case, the thermal stresses in the plate are self-equilibrating and the radial force N_r vanishes at the outer edge. Therefore, the boundary conditions are

$$F < \infty \text{ and } w < \infty \text{ at } r = 0 \tag{4.22}$$

$$\frac{\partial F}{\partial r} = 0 \text{ at } r = 1 \tag{4.23}$$

$$w = 0 \text{ and } \frac{\partial^2 w}{\partial r^2} + \frac{\nu}{r} \frac{\partial w}{\partial r} = 0 \text{ at } r = 1 \tag{4.24}$$

The condition in Equation (4.23) follows from Equation (4.8).

4.2.1 Perturbation Solution

We seek a first-order uniform expansion of the solution of Equations (4.20)-(4.24) in the form (Nayfeh, 1981)

$$w(r, t; \epsilon) = w_0(r, t_0, t_1) + \epsilon w_1(r, t_0, t_1) + \cdots \tag{4.25}$$

$$F(r, t; \epsilon) = F_0(r, t_0, t_1) + \cdots \tag{4.26}$$

where $t_0 = t$ and $t_1 = \epsilon t$. Hence, the time derivative is transformed into

$$\frac{d}{dt} = D_0 + \epsilon D_1 + \cdots \tag{4.27}$$

where $D_n = \partial/\partial t_n$. Substituting Equations (4.25)-(4.27) into Equations (4.20)-(4.24) and equating coefficients of like powers of ϵ, we obtain

Order ϵ^0

$$D_0^2 w_0 + \nabla^4 w_0 = 0 \tag{4.28}$$

$$r\frac{\partial^3 F_0}{\partial r^3} + \frac{\partial^2 F_0}{\partial r^2} - \frac{1}{r}\frac{\partial F_0}{\partial r} = -\frac{1}{2}\left(\frac{\partial w_0}{\partial r}\right)^2 + 2qr^2\cos(\Omega t_0) \tag{4.29}$$

$$w_0 < \infty \text{ and } F_0 < \infty \text{ at } r = 0 \tag{4.30}$$

$$F_0' = 0 \text{ at } r = 1 \tag{4.31}$$

$$w_0 = 0 \text{ and } w_0'' + \nu w_0' = 0 \text{ at } r = 1 \tag{4.32}$$

Order ϵ

$$D_0^2 w_1 + \nabla^4 w_1 = -2D_0 D_1 w_0 + \frac{1}{r}\frac{\partial^2 w_0}{\partial r^2}\frac{\partial F_0}{\partial r} + \frac{1}{r}\frac{\partial w_0}{\partial r}\frac{\partial^2 F_0}{\partial r^2} - 2cD_0 w_0 \tag{4.33}$$

$$w_1 < \infty \text{ at } r = 0 \tag{4.34}$$

$$w_1 = 0 \text{ and } w_1'' + \nu w_1' = 0 \text{ at } r = 1 \tag{4.35}$$

where the prime indicates the partial derivative with respect to r.

The solution of Equations (4.28), (4.30), and (4.32) can be expressed as

$$w_0 = \sum_{n=1}^{\infty}\left[A_n(t_1)e^{i\omega_n t_0} + \bar{A}_n(t_1)e^{-i\omega_n t_0}\right]\phi_n(r) \tag{4.36}$$

where the nth nondimensional axisymmetric mode shape is given by

$$\phi_n(r) = k_n\left[I_0\left(\sqrt{\omega_n}\right)J_0\left(\sqrt{\omega_n}r\right) - J_0\left(\sqrt{\omega_n}\right)I_0\left(\sqrt{\omega_n}r\right)\right] \tag{4.37}$$

the corresponding nondimensional natural frequency ω_n is the nth root of

$$\frac{J_1\left(\sqrt{\omega_n}\right)}{J_0\left(\sqrt{\omega_n}\right)} + \frac{I_1\left(\sqrt{\omega_n}\right)}{I_0\left(\sqrt{\omega_n}\right)} = \frac{2\sqrt{\omega_n}}{1-\nu} \tag{4.38}$$

and the k_n are chosen so that

$$\int_0^1 r\phi_n^2(r)dr = 1 \tag{4.39}$$

The lowest five nondimensional natural frequencies for the case $\nu = 0.3$ are 4.935, 29.720, 74.156, 138.318, and 222.215. Hence, the first mode is not involved in any internal resonance with any other

axisymmetric mode. Moreover, we assume that this mode is not involved in an internal resonance with any asymmetric mode. In this analysis, we consider the case of principal parametric resonance of the first mode. The analysis is also valid for any mode that is not involved in an internal resonance with other modes. For asymmetric thermal loads, one-to-one internal resonances might be activated. This case is not considered here.

Substituting Equation (4.36) into Equation (4.29) yields

$$r\frac{\partial^3 F_0}{\partial r^3}+\frac{\partial^2 F_0}{\partial r^2}-\frac{1}{r}\frac{\partial F_0}{\partial r}=-\frac{1}{2}\sum_{n,m}\phi_n'\phi_m'\times\left[A_mA_ne^{i(\omega_n+\omega_m)t_0}+A_n\bar{A}_me^{i(\omega_n-\omega_m)t_0}\right]$$
$$+cc+2qr^2\cos\omega t_0 \tag{4.40}$$

The solution of Equation (4.40) subject to the boundary conditions (4.30) and (4.31) can be expressed as

$$F_0=\sum_{m,n}\left[\ A_nA_me^{i(\omega_n+\omega_m)t_0}+A_n\bar{A}_me^{i(\omega_n-\omega_m)t_0}\right]\psi_{nm}(r)$$
$$+\ cc+\frac{1}{16}\left(r^4-2r^2\right)q\cos\omega t_0 \tag{4.41}$$

where

$$\left(r\frac{d^2}{dr^2}+\frac{d}{dr}-\frac{1}{r}\right)\frac{d\psi_{nm}}{dr}=-\frac{1}{2}\phi_n'\phi_m' \tag{4.42}$$
$$\psi_{nm}(0)<\infty \tag{4.43}$$
$$\psi_{nm}'=0\ \text{ at }\ r=1 \tag{4.44}$$

Because

$$\left(r^2\frac{d^2}{dr^2}+r\frac{d}{dr}-1\right)J_1\left(\xi_kr\right)=-\xi_k^2r^2J_1\left(\xi_kr\right) \tag{4.45}$$

we express ψ_{nm}' as

$$\psi_{nm}'(r)=\sum_{k=1}^{\infty}b_{nmk}J_1\left(\xi_kr\right) \tag{4.46}$$

Using the boundary condition (4.44), we find that the ξ_m are the roots of

$$J_1\left(\xi_k\right)=0 \tag{4.47}$$

The lowest ten roots of Equation (4.47) are 0, 3.832, 7.016, 13.324, 19.616, 22.760, 25.904, 29.047, 32.190, and 35.332. Substituting Equation (4.46) into Equation (4.42) and using Equation (4.45),

we obtain

$$\sum_{k=1}^{\infty} b_{nmk}\left[rJ_1''(\xi_k r)+J_1'(\xi_k r)-\frac{1}{r}J_1(\xi_k r)\right]=\sum_{k=1}^{\infty} b_{nmk}\xi_k^2 rJ_1(\xi_k r)=-\frac{1}{2}\phi_n'\phi_m' \tag{4.48}$$

Multiplying Equation (4.48) with $J_1(\xi_s r)$ and integrating the result with respect to r from $r=0$ to 1, we have

$$b_{nms}=\frac{\int_0^1 J_1(\xi_s r)\,\phi_n'(r)\phi_m'(r)dr}{\left[2\xi_s^2\int_0^1 rJ_1^2(\xi_s r)\,dr\right]} \tag{4.49}$$

Substituting Equations (4.36) and (4.46) into Equation (4.33) yields

$$\begin{aligned}
D_0^2 w_1+\nabla^4 w_1 &= -2i\sum_n \omega_n\left(A_n'+cA_n\right)\phi_n e^{i\omega_n t_0}\\
&+\frac{1}{8}qe^{i\omega t_0}\sum_n\left[(r^2-1)\phi_n''+\frac{3r^2-1}{r}\phi_n'\right]\left[A_n e^{i\omega_n t_0}+\bar{A}_n e^{-i\omega_n t_0}\right]\\
&+\frac{1}{r}\sum_{n,m,s}\left(\phi_s'\psi_{nm}'\right)'\left[A_sA_nA_m e^{i(\omega_n+\omega_m+\omega_s)t_0}+A_sA_n\bar{A}_m e^{i(\omega_s+\omega_n-\omega_m)t_0}\right.\\
&\left.+A_nA_m\bar{A}_s e^{i(\omega_n+\omega_m-\omega_s)t_0}+A_n\bar{A}_m\bar{A}_s e^{i(\omega_n-\omega_m-\omega_s)t_0}\right]+cc
\end{aligned} \tag{4.50}$$

Next, we consider the case of principal parametric resonance of the jth mode and assume that it is not involved in an internal resonance with any other mode. To describe the nearness of the resonance, we introduce a detuning parameter σ defined by

$$\omega=2\omega_j+\epsilon\sigma \tag{4.51}$$

Substituting Equation (4.51) into Equation (4.50) yields

$$\begin{aligned}
D^2 w_1+\nabla^4 w_1 &= -2i\sum_n \omega_n\left(A_n'+cA_n\right)\phi_n e^{i\omega_n t_0}+\frac{1}{8}q\sum_n\left[\left(r^2-1\right)\phi_n''+\frac{3r^2-1}{r}\phi_n'\right]\\
&\left[A_n e^{i(\omega_n+2\omega_j)t_0+i\sigma t_1}+\bar{A}_n e^{i(2\omega_j-\omega_n)t_0+i\sigma t_1}\right]+\frac{1}{r}\sum_{n,m,s}\left(\phi_s'\psi_{nm}'\right)'\left[A_sA_nA_m e^{i(\omega_n+\omega_m+\omega_s)t_0}\right.\\
&\left.+A_sA_n\bar{A}_m e^{i(\omega_s+\omega_n-\omega_m)t_0}+A_nA_m\bar{A}_s e^{i(\omega_n+\omega_m-\omega_s)t_0}+A_n\bar{A}_m\bar{A}_s e^{i(\omega_n-\omega_m-\omega_s)t_0}\right]+cc
\end{aligned} \tag{4.52}$$

In the presence of damping, all modes that are not directly excited or indirectly excited by an internal resonance decay with time, and hence the long-time response consists of the jth mode

only. Because the homogeneous problem consisting of Equations (4.52), (4.34), and (4.35) has nontrivial solutions, the nonhomogeneous problem has a solution only if a solvability condition is satisfied (Nayfeh, 2000).

Because the homogeneous problem is self-adjoint, the solvability condition demands that the right-hand of Equation (4.52) be orthogonal to every solution of the homogeneous problem (Nayfeh, 1981). Multiplying the right-hand side of Equation (4.52) with $r\phi_j(r)e^{-i\omega_j t_0}$, integrating the result from $r = 0$ to $r = 1$, and setting the outcome equal to zero, we obtain

$$2i\omega_j \left(A_j' + \mu_j A_j\right) + \alpha_e A_j^2 \bar{A}_j - q_e \bar{A}_j e^{i\sigma t_1} = 0 \tag{4.53}$$

where

$$\alpha_e = -\int_0^1 \phi_j \left(\phi_j' \psi_{jj}'\right)' dr = \int_0^1 \phi_j'^2 \psi_{jj}' dr \tag{4.54}$$

$$q_e = \frac{1}{8} q \int_0^1 \left(\left(r^3 - r\right)\phi_j'\right)' \phi_j dr = -\frac{1}{8} q \int_0^1 \left(r^3 - r\right)\phi_j'^2 dr \tag{4.55}$$

where $\mu_j = \int_0^1 rc\phi_j^2 dr$.

To investigate the solutions of Equation (4.53), we introduce the polar transformation

$$A_j = \frac{1}{2} a_j e^{i(\beta_j + \frac{1}{2}\sigma t_1)} \tag{4.56}$$

separate real and imaginary parts, and obtain

$$a_j' = -\mu_j a_j - \frac{q_e}{2\omega_j} a_j \sin 2\beta_j \tag{4.57}$$

$$a_j \beta_j' = -\frac{1}{2}\sigma a_j + \frac{\alpha_e}{8\omega_j} a_j^3 - \frac{q_e}{2\omega_j} a_j \cos 2\beta_j \tag{4.58}$$

The equilibrium solutions of Equations (4.57) and (4.58) correspond to periodic motions of the plate. The equilibrium solutions are given by

$$\mu_j a_j = -\frac{q_e}{2\omega_j} a_j \sin 2\beta_j \tag{4.59}$$

$$\frac{1}{2}\sigma a_j - \frac{\alpha_e}{8\omega_j} a_j^3 = -\frac{q_e}{2\omega_j} a_j \cos 2\beta_j \tag{4.60}$$

There are two possibilities: either $a_j = 0$ or $a_j \neq 0$. In the latter case, eliminating β_j from Equations (4.59) and (4.60) yields the frequency-response equation

$$\mu_j^2 + \left(\frac{1}{2}\sigma - \frac{\alpha_e}{8\omega_j} a_j^2\right)^2 = \frac{q_e^2}{4\omega_j^2} \tag{4.61}$$

or

$$a_j^2 = \frac{8\omega_j}{\alpha_e}\left[\frac{1}{2}\sigma \pm \sqrt{\frac{q_e^2}{4\omega_j^2} - \mu_j^2}\right] \tag{4.62}$$

Equation (4.62) represents the relation between the response amplitude a_j, the forcing amplitude q_e, and detuning (control) parameter σ. Next, we present results for the first mode.

4.2.2 Numerical Results

For the first mode, the first nine values of b_{ns} from Equation (4.49) are: 1.24252, -0.144995, -0.0272522, -0.0102221, 0.00702803, -0.00507591, 0.00380701, -0.00294182, and 0.00232898. Consequently, we calculate the effective nonlinearity coefficient to be $\alpha_e = 3.77941$. Also, we assume that $\mu = 0.01$ and consider nondimensional values of q ranging from 1 to 30. In Figure 4.2, we show typical frequency-response curves for $q = 10$. The curves are bent to the right, indicating a hardening-type nonlinearity. The bending of the frequency-response curves leads to multivalued amplitudes and hence to jumps. To illustrate the jump phenomenon, let us suppose that an experiment is conducted where the excitation amplitude is kept constant at $q = 10$ while the excitation frequency is varied very slowly. We start with a frequency far above the natural frequency (i.e., σ is positive) and decrease it. We choose the initial conditions so that the response amplitude is trivial. As σ is decreased, the response amplitude remains trivial untill point D is reached, where the response amplitude experiences a sudden jump up to point C. Point D is a subcritical or reverse pitchfork bifurcation. The response amplitude decreases as the frequency is further decreased untill point B is reached, where the response amplitude becomes trivial again. Point B is a supercritical pitchfork bifurcation.

Starting at point C and sweeping in the reverse direction, we note that, to the first-order approximation, the response amplitude increases without bounds as the frequency increases. In reality, the stable and unstable branches merge to produce a saddle-node bifurcation. Increasing σ above this bifurcation point results in a jump down of the response amplitude to the trivial solution. Between point D and the saddle-node bifurcation, there are three possible solutions: the trivial solution, which is stable, and two nontrivial solutions, the larger of which is stable and the smaller is unstable. In this interval, the response may be trivial or nontrivial, depending on the initial conditions.

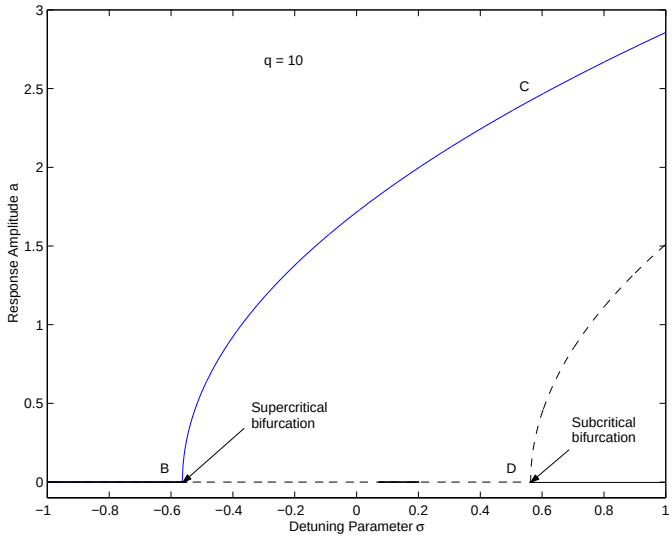

Figure 4.2: Variation of the steady-state response amplitude with the detuning parameter σ when $q = 10$.

In Figure 4.3, we show a force-response curve generated when the principal parametric resonance is negatively detuned by σ= -0.8. Starting from a forcing amplitude corresponding to point E and increasing it results in a monotonic increase in the response amplitude. Point E is a supercritical pitchfork bifurcation. For any excitation amplitude above point E, the response amplitude settles on the branch EB, irrespective of the initial conditions. Sweeping q down, one finds that the response amplitude follows the branch BE. Decreasing q below point E results in a smooth transition of the response from a nontrivial to a trivial response. Increasing the value of the detuning parameter results in a shift in the critical point E to the left.

We show in Figure 4.4 the force-response curve for the case of a positive detuning of σ=0.5. In contrast with the preceding case, there are multivalued responses. Point F is a subcritical pitchfork bifurcation and point G is a saddle-node bifurcation. Between these bifurcations, the response may be trivial or nontrivial depending on the initial conditions. Whereas the linear theory predicts stable trivial responses for forcing amplitudes below point F and unbounded responses above it, the nonlinear analysis predicts that the trivial response between points F and G is stable for small disturbances but unstable for large disturbances, a subcritical instability. Moreover, the nonlinearity puts a cap on the response amplitude. Sweeping q in the forward direction, one finds

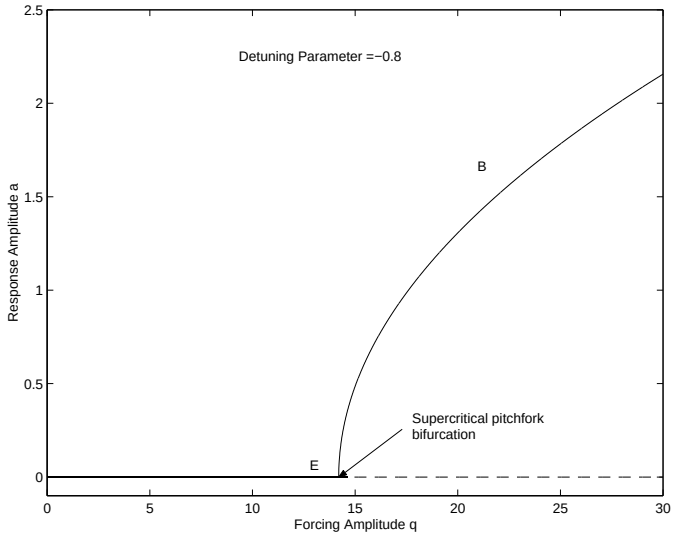

Figure 4.3: Variation of the steady-state response amplitude with the forcing amplitude for $\sigma = -0.8$.

that beyond point F the response amplitude jumps up. On the other hand, sweeping q in the reverse direction beyond point G results in a jump to the trivial response.

4.3 Clamped Circular Plate

We consider a clamped plate with an immovable edge. This case is important in most of MEMS devices, such as sensors and micropumps, as it is a more realistic representation of the actual boundary condition. The governing nondimensional Equations (4.20) and (4.21) are repeated here

$$\frac{\partial^2 w}{\partial t^2} + \nabla^4 w = \epsilon \left[\frac{1}{r}\frac{\partial^2 w}{\partial r^2}\frac{\partial F}{\partial r} + \frac{1}{r}\frac{\partial w}{\partial r}\frac{\partial^2 F}{\partial r^2} - 2c\frac{\partial w}{\partial t} \right] \tag{4.63}$$

$$r\frac{\partial^3 F}{\partial r^3} + \frac{\partial^2 F}{\partial r^2} - \frac{1}{r}\frac{\partial F}{\partial r} = -\frac{1}{2}\left(\frac{\partial w}{\partial r}\right)^2 + 2qr^2\cos(\Omega t) \tag{4.64}$$

For a clamped immovable edge, the boundary conditions are

$$w = 0 \text{ and } \frac{\partial w}{\partial r} = 0 \text{ at } r = 1 \tag{4.65}$$

$$F < \infty \text{ and } w < \infty \text{ at } r = 0 \tag{4.66}$$

$$\frac{\partial^2 F}{\partial r^2} - \frac{\nu}{r}\frac{\partial F}{\partial r} + \frac{\alpha T_0 R^4}{h^4}(T_b - 1) = 0 \text{ at } r = 1 \tag{4.67}$$

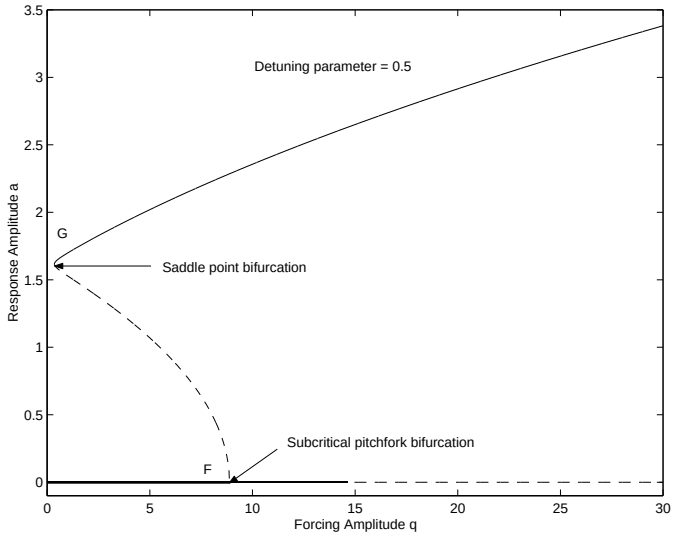

Figure 4.4: Variation of the steady-state response amplitude with the forcing amplitude for $\sigma = 0.5$.

Equation (4.67) follows from Equation (4.11) because $u = 0$.

An exact solution of Equations (4.63)-(4.67) is not available yet. To determine an approximate solution of these equations, we first transform them into a problem with homogeneous boundary conditions. To this end, we solve the linear Equation (4.64) subject to the boundary conditions (4.66) and (4.67). The general solution of the linear version of Equation (4.64), that is bounded at the origin, can be expressed as

$$F_{linear} = C_1(t)r^2 + C_2(t) + \frac{1}{16}r^4 q\cos(\Omega t) \tag{4.68}$$

Using the boundary condition, Equation (4.67), we find that

$$C_1(t) = -\frac{\alpha T_0 R^4}{2(1-\nu)h^4} - \frac{3-\nu}{8(1-\nu)}r^2 q\cos\Omega t$$

and $C_2(t)$ is an arbitrary function of time. Next, we let

$$F = \Phi + F_{linear} = \Phi - \frac{\alpha T_0 R^4}{2(1-\nu)h^4}r^2 + C_2(t) + \frac{1}{16}\left[r^4 - \frac{2(3-\nu)}{1-\nu}r^2\right] q\cos(\Omega t) \tag{4.69}$$

where Φ is the nonlinear part of the stress function. Substituting Equation (4.69) into Equations

(4.63)-(4.67) we obtain

$$\frac{\partial^2 w}{\partial t^2} + p\nabla^2 w + \nabla^4 w = \epsilon \left[\frac{1}{r}\frac{\partial^2 w}{\partial r^2}\frac{\partial \Phi}{\partial r} + \frac{1}{r}\frac{\partial w}{\partial r}\frac{\partial^2 \Phi}{\partial r^2} \right.$$
$$\left. -2c\frac{\partial w}{\partial t} + \frac{1}{4}\frac{\partial^2 w}{\partial r^2}\left[r^2 - \frac{3-\nu}{1-\nu} \right] q\cos(\Omega t) + \frac{1}{4}\frac{\partial w}{\partial r}\left[3r - \frac{3-\nu}{(1-\nu)r} \right] q\cos(\Omega t) \right. \tag{4.70}$$

$$r\frac{\partial^3 \Phi}{\partial r^3} + \frac{\partial^2 \Phi}{\partial r^2} - \frac{1}{r}\frac{\partial \Phi}{\partial r} = -\frac{1}{2}\left(\frac{\partial w}{\partial r} \right)^2 \tag{4.71}$$

$$w = 0 \text{ and } \frac{\partial w}{\partial r} = 0 \text{ at } r = 1 \tag{4.72}$$

$$w < \infty \text{ and } \Phi < \infty \text{ at } r = 0 \tag{4.73}$$

$$\frac{\partial^2 \Phi}{\partial r^2} - \frac{\nu}{r}\frac{\partial \Phi}{\partial r} = 0 \text{ at } r = 1 \tag{4.74}$$

where

$$p = \frac{12\alpha T_0 (1+\nu) R^2}{h^2}$$

4.3.1 Perturbation Solution

We seek a first-order uniform expansion of the solution of Equations (4.70)-(4.74) in the form (Nayfeh, 1981)

$$w(r,t;\epsilon) = w_0(r,t_0,t_1) + \epsilon w_1(r,t_0,t_1) + \cdots \tag{4.75}$$

$$\Phi(r,t;\epsilon) = \Phi_0(r,t_0,t_1) + \cdots \tag{4.76}$$

where $t_0 = t$ and $t_1 = \epsilon t$. Hence, the time derivative is transformed into

$$\frac{d}{dt} = D_0 + \epsilon D_1 + \cdots \tag{4.77}$$

where $D_n = \partial/\partial t_n$. Substituting Equations (4.75)-(4.77) into Equations (4.70)-(4.74) and equating coefficients of like powers of ϵ, we obtain

Order ϵ^0

$$D_0^2 w_0 + p\nabla^2 w_0 + \nabla^4 w_0 = 0 \tag{4.78}$$

$$r\frac{\partial^3 \Phi_0}{\partial r^3} + \frac{\partial^2 \Phi_0}{\partial r^2} - \frac{1}{r}\frac{\partial \Phi_0}{\partial r} = -\frac{1}{2}\left(\frac{\partial w}{\partial r}\right)^2 \tag{4.79}$$

$$w_0 = 0 \text{ and } w_0' = 0 \text{ at } r = 1 \tag{4.80}$$

$$w_0 < \infty \text{ and } \Phi_0 < \infty \text{ at } r = 0 \tag{4.81}$$

$$\Phi_0'' - \frac{\nu}{r}\Phi_0' = 0 \text{ at } r = 1 \tag{4.82}$$

Order ϵ

$$\begin{aligned} D_0^2 w_1 + p\nabla^2 w_1 + \nabla^4 w_1 = &-2D_0 D_1 w_0 + \frac{1}{r}\frac{\partial^2 w_0}{\partial r^2}\frac{\partial \Phi_0}{\partial r} + \frac{1}{r}\frac{\partial w_0}{\partial r}\frac{\partial^2 \Phi_0}{\partial r^2} \\ &-2cD_0 w_0 + \frac{1}{4}\frac{\partial^2 w_0}{\partial r^2}\left[r^2 - \frac{3-\nu}{1-\nu}\right] q\cos(\Omega t_0) + \frac{1}{4}\frac{\partial w_0}{\partial r}\left[3r - \frac{3-\nu}{(1-\nu)r}\right] q\cos(\Omega t_0) \end{aligned} \tag{4.83}$$

$$w_1 = 0 \text{ and } w_1' = 0 \text{ at } r = 1 \tag{4.84}$$

$$w_1 < \infty \text{ at } r = 0 \tag{4.85}$$

where the prime indicates the partial derivative with respect to r.

Equation (4.78) is analogous to the equation describing the dynamics of a circular plate under a uniform in-plane compressive load. Its general solution can be expressed as

$$w_0 = \sum_{n=1}^{\infty} \left[A_n(t_1)e^{i\omega_n t_0} + \bar{A}_n(t_1)e^{-i\omega_n t_0}\right] \phi_n(r) \tag{4.86}$$

where

$$\phi_n(r) = \left[B_1 J_0(\kappa_{1n} r) + B_2 Y_0(\kappa_{1n} r) + B_3 I_0(\kappa_{2n} r) + B_4 K_0(\kappa_{2n} r)\right] \tag{4.87}$$

$$\kappa_{1n}^2 = \frac{1}{2}\left[\sqrt{p^2 + 4\omega_n} + p\right], \text{ and } \kappa_{2n}^2 = \frac{1}{2}\left[\sqrt{p^2 + 4\omega_n} - p\right] \tag{4.88}$$

and B_1, B_2, B_3, and B_4 are constants. Applying the boundary condition in Equation (4.81) yields $B_2 = 0$ and $B_4 = 0$. Then, applying the boundary conditions in Equation (4.80) yields the following frequency equation:

$$\kappa_{2n} I_1(\kappa_{2n}) J_0(\kappa_{1n}) + \kappa_{1n} J_1(\kappa_{1n}) I_0(\kappa_{2n}) = 0 \tag{4.89}$$

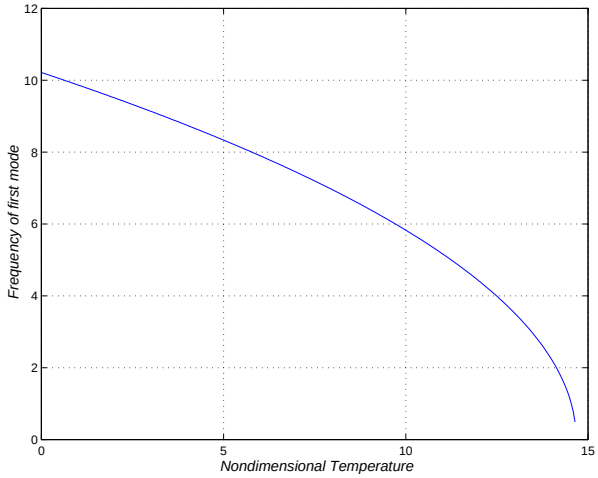

Figure 4.5: Variation of the first nondimensional frequency with the nondimensional parameter (temperature) p.

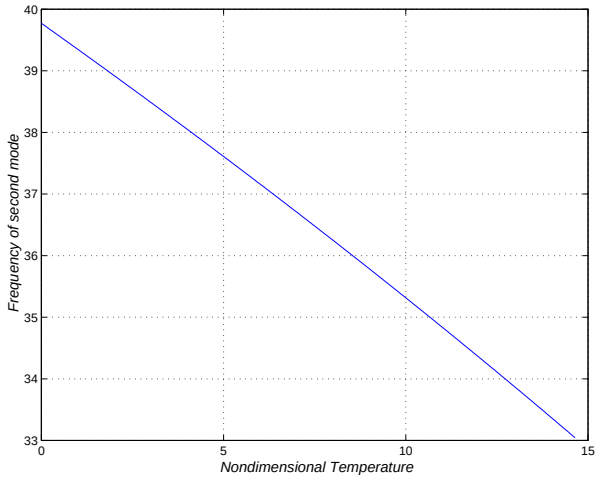

Figure 4.6: Variation of the second nondimensional frequency with the nondimensional parameter (temperature) p.

which can be solved numerically for the ω_n as a function of p and hence T_0. In Figures 4.5-7, we show variation of the first three nondimensional natural frequencies with p. Buckling occurs when the first natural frequency is zero, which corresponds to $p = 14.68$.

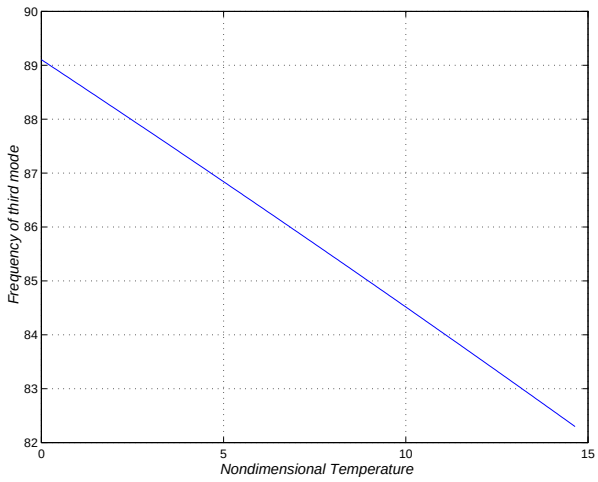

Figure 4.7: Variation of the third nondimensional frequency with the nondimensional parameter (temperature) p.

Substituting Equation (4.86) into Equation (4.79) yields

$$r\frac{\partial^3\Phi_0}{\partial r^3}+\frac{\partial^2\Phi_0}{\partial r^2}-\frac{1}{r}\frac{\partial\Phi_0}{\partial r}=-\frac{1}{2}\sum_{n,m}\phi_n'\phi_m'\left[A_mA_ne^{i(\omega_n+\omega_m)t_0}+A_n\bar{A}_me^{i(\omega_n-\omega_m)t_0}\right]+cc \tag{4.90}$$

The solution of Equation (4.90) subject to the boundary conditions (4.81) and (4.82) can be expressed as

$$\Phi_0=\sum_{m,n}\left[A_nA_me^{i(\omega_n+\omega_m)t_0}+A_n\bar{A}_me^{i(\omega_n-\omega_m)t_0}\right]\psi_{nm}(r)+cc \tag{4.91}$$

where

$$\left(r\frac{d^2}{dr^2}+\frac{d}{dr}-\frac{1}{r}\right)\frac{d\psi_{nm}}{dr}=-\frac{1}{2}\phi_n'\phi_m' \tag{4.92}$$

$$\psi_{nm}(0)<\infty \tag{4.93}$$

$$\psi_{nm}''-\nu\psi_{nm}'=0 \ \text{ at } \ r=1 \tag{4.94}$$

Because

$$\left(r^2\frac{d^2}{dr^2}+r\frac{d}{dr}-1\right)J_1\left(\xi_kr\right)=-\xi_k^2r^2J_1\left(\xi_kr\right) \tag{4.95}$$

we express ψ_{nm}' as

$$\psi_{nm}'(r)=\sum_{k=1}^{\infty}b_{nmk}J_1\left(\xi_kr\right) \tag{4.96}$$

Using the boundary condition (4.94), we find that the ξ_m are the roots of

$$\xi_k J_1(\xi_k) - (1+\nu) J_0(\xi_k) = 0 \tag{4.97}$$

The lowest ten roots of Equation (4.97) are 1.57883, 5.27284, 8.5006, 11.6802, 14.8433, 17.9988, 21.1502, 24.299, 27.4461, and 30.5921. Substituting Equation (4.96) into Equation (4.92) and using Equation (4.95), we obtain

$$\begin{aligned}&\sum_{k=1}^{\infty} b_{nmk}\left[r J_1''(\xi_k r) + J_1'(\xi_k r) - \frac{1}{r} J_1(\xi_k r)\right] \\ &= \sum_{k=1}^{\infty} b_{nmk}\xi_k^2 r J_1(\xi_k r) = -\frac{1}{2}\phi_n'\phi_m'\end{aligned} \tag{4.98}$$

Multiplying Equation (4.98) with $J_1(\xi_s r)$ and integrating the result with respect to r from $r = 0$ to 1, we have

$$b_{nms} = \frac{\int_0^1 J_1(\xi_s r)\,\phi_n'(r)\phi_m'(r)dr}{2\xi_s^2 \int_0^1 r J_1^2(\xi_s r)dr} \tag{4.99}$$

Substituting Equations (4.86) and (4.91) into Equation (4.83) yields

$$\begin{aligned}&D_0^2 w_1 + p\nabla^2 w_1 + \nabla^4 w_1 = -2i\sum_n \omega_n\left(A_n' + cA_n\right)\phi_n e^{i\omega_n t_0} \\ &+\frac{1}{8r} q e^{i\Omega t_0}\sum_n\left[\left(r^3 - \frac{3-\nu}{1-\nu}r\right)\phi_n'\right]' \times \left[A_n e^{i\omega_n t_0} + \bar{A}_n e^{-i\omega_n t_0}\right] \\ &+\frac{1}{r}\sum_{n,m,c}\left(\phi_c'\psi_{nm}'\right)'\Big[A_c A_n A_m e^{i(\omega_n+\omega_m+\omega_c)t_0} + A_c A_n \bar{A}_m e^{i(\omega_c+\omega_n-\omega_m)t_0} \\ &+A_n A_m \bar{A}_c e^{i(\omega_n+\omega_m-\omega_c)t_0} + A_n \bar{A}_m \bar{A}_c e^{i(\omega_n-\omega_m-\omega_c)t_0}\Big] + cc\end{aligned} \tag{4.100}$$

Next, we consider the cases of combination parametric resonance of the additive and difference types and principal parametric resonance.

4.3.2 Combination Parametric Resonance of the Additive Type

We consider the case of combination parametric resonance of the additive type involving the jth and kth modes and assume that neither is involved in an internal resonance with any other mode. To describe the nearness of the resonance, we introduce the detuning parameter σ defined by

$$\Omega = \omega_j + \omega_k + \epsilon\sigma \tag{4.101}$$

Because the homogeneous problem consisting of Equations (4.100), (4.84), and (4.85) has nontrivial solutions, the nonhomogeneous problem has a solution only if solvability conditions are satisfied (Nayfeh, 2000). Because the homogeneous problem is self-adjoint, the solvability conditions demand that the right-hand side of Equation (4.100) be orthogonal to every solution of the homogeneous problem. Multiplying the right-hand side of Equation (4.100) with $r\phi_s(r)e^{-i\omega_s t_0}$, integrating the result from $r=0$ to $r=1$, using Equation (4.101), and setting the result equal to zero, we obtain

$$2i\omega_j\left(A_j' + \mu_j A_j\right) + \alpha_{jj}A_j^2\bar{A}_j + \sum_{m\neq j}\alpha_{jm}A_jA_m\bar{A}_m + qf_{jk}\bar{A}_k e^{i\sigma t_1} = 0 \tag{4.102}$$

$$2i\omega_k\left(A_k' + \mu_k A_k\right) + \alpha_{kk}A_k^2\bar{A}_k + \sum_{m\neq k}\alpha_{km}A_kA_m\bar{A}_m + qf_{kj}\bar{A}_j e^{i\sigma t_1} = 0 \tag{4.103}$$

$$2i\omega_s\left(A_s' + \mu_s A_s\right) + \alpha_{ss}A_s^2\bar{A}_s + \sum_{m\neq s}\alpha_{sm}A_sA_m\bar{A}_m = 0 \text{ for } s\neq j \text{ and } k \tag{4.104}$$

where

$$\alpha_{nn} = -3\int_0^1 \phi_n\left(\phi_n'\psi_{nn}'\right)'dr = 3\int_0^1 \psi_{nn}'\phi_n'^2 dr \tag{4.105}$$

$$\begin{aligned}\alpha_{nm} &= -2\int_0^1 \phi_n\left[\psi_{mm}'\phi_n'\right]' - 4\int_0^1 \phi_n\left[\psi_{nm}'\phi_m'\right]'dr \\ &= 2\int_0^1 \psi_{mm}'\phi_n'^2 dr + 4\int_0^1 \psi_{nm}'\phi_n'\phi_m' dr\end{aligned} \tag{4.106}$$

$$\begin{aligned}f_{nm} &= -\frac{1}{8}\int_0^1 \phi_n\left[\left(r^3 - \frac{3-\nu}{1-\nu}r\right)\phi_m'\right]'dr \\ &= \frac{1}{8}\int_0^1 \left(r^3 - \frac{3-\nu}{1-\nu}r\right)\phi_m'\phi_n' dr\end{aligned} \tag{4.107}$$

$$\mu_n = \int_0^1 cr\phi_n^2 dr \tag{4.108}$$

To investigate the solutions of Equations (4.102)-(4.104), we introduce the polar transformations

$$A_j = \frac{1}{2}a_j e^{i(\beta_j + \frac{1}{2}\sigma t_1)} \tag{4.109}$$

$$A_k = \frac{1}{2}a_k e^{i(\beta_k + \frac{1}{2}\sigma t_1)} \tag{4.110}$$

$$A_s = \frac{1}{2}a_s e^{i\beta_s} \tag{4.111}$$

Substituting Equations (4.109)-(4.111) into Equation (4.104) and separating the real and imaginary parts, we obtain

$$a_s' = -\mu_s a_s \tag{4.112}$$

$$\omega_s a_s \beta_s' = \frac{1}{8}\alpha_{ss} a_s^3 + \frac{1}{8} a_s \sum_{m \neq s} \alpha_{sm} a_m^2 \tag{4.113}$$

for $s \neq k$ and j. It follows from Equation (4.112) that $a_s \to 0$ as $t_1 \to \infty$ and hence $t \to \infty$. In other words, in the presence of damping, all modes that are not directly excited by the thermal load decay exponentially with time. Hence, the long-time response consists of only the kth and jth modes, which are directly excited by the thermal load. Then, substituting Equations (4.109)-(4.111) into Equations (4.102) and (4.103), letting $A_s = 0$ for $s \neq k$ and j, and separating the real and imaginary parts, we obtain

$$a_j' = -\mu_j a_j + \frac{f_{jk}}{2\omega_j} q a_k \sin\gamma \tag{4.114}$$

$$a_j \beta_j' = -\frac{1}{2}\sigma a_j + \frac{\alpha_{jj}}{8\omega_j} a_j^3 + \frac{\alpha_{jk}}{8\omega_j} a_j a_k^2 + \frac{f_{jk}}{2\omega_j} q a_k \cos\gamma \tag{4.115}$$

$$a_k' = -\mu_k a_k + \frac{f_{kj}}{2\omega_k} q a_j \sin\gamma \tag{4.116}$$

$$a_k \beta_k' = -\frac{1}{2}\sigma a_k + \frac{\alpha_{kk}}{8\omega_k} a_k^3 + \frac{\alpha_{kj}}{8\omega_k} a_k a_j^2 + \frac{f_{kj}}{2\omega_k} q a_j \cos\gamma \tag{4.117}$$

where

$$\gamma = \beta_j + \beta_k \tag{4.118}$$

The equilibrium solutions or fixed points of Equations (4.114)-(4.118) correspond to $a_j' = 0$, $a_k' = 0$, and $\gamma' = 0$. There are two possible equilibrium solutions: (a) $a_j = 0$ and $a_k = 0$ and (b) $a_j \neq 0$ and $a_k \neq 0$. In the latter case, Equations (4.115), (4.117), and (4.118) can be combined to eliminate β_j and β_k and obtain the following equation for γ':

$$\begin{aligned}\gamma' = -\sigma &+ \left(\frac{\alpha_{jj}}{8\omega_j} + \frac{\alpha_{kj}}{8\omega_k}\right) a_j^2 + \left(\frac{\alpha_{jk}}{8\omega_j} + \frac{\alpha_{kk}}{8\omega_k}\right) a_k^2 \\ &+ \left(\frac{a_k}{2a_j\omega_j} + \frac{a_j}{2a_k\omega_k}\right) q f_{jk} \cos\gamma\end{aligned} \tag{4.119}$$

Hence, for nontrivial solutions, the modulation equations are reduced from four to three first-order differential equations. For equilibrium solutions, we set $a_j' = 0$, $a_k' = 0$, and $\gamma' = 0$ and solve

Equations (4.114), (4.116), and (4.119) for a_j, a_k, and γ. The following closed-form solution is obtained:

$$\alpha_e a_j^2 = \sigma \pm \frac{\mu_j + \mu_k}{\sqrt{\mu_j \mu_k}} \sqrt{\frac{f_{jk}^2 q^2}{4\omega_j \omega_k} - \mu_j \mu_k} \tag{4.120}$$

$$a_k^2 = \frac{\mu_j \omega_j}{\mu_k \omega_k} a_j^2 \tag{4.121}$$

$$\sin\gamma = \frac{2\mu_j \omega_j a_j}{f_{jk} a_k q} = \frac{2\mu_k \omega_k a_k}{f_{kj} a_j q} = \pm 2 \frac{\sqrt{\mu_j \mu_k \omega_j \omega_k}}{f_{jk} q} \tag{4.122}$$

where

$$\alpha_e = \frac{1}{8}\left[\frac{\alpha_{jj}}{\omega_j} + \frac{\alpha_{kj}}{\omega_k} + \left(\frac{\alpha_{jk}}{\omega_j} + \frac{\alpha_{kk}}{\omega_k}\right)\frac{\mu_j \omega_j}{\mu_k \omega_k}\right] \tag{4.123}$$

In Figure 4.8, we show the frequency-response curves obtained for $q = 0.01$ and the nondimensional temperature $p = 7.0$. The curves are bent to the right, indicating a hardening-type nonlinearity. The bending of the frequency-response curves leads to multivalued amplitudes and hence to jumps. To illustrate the jump phenomenon, let us suppose that an experiment is conducted where the excitation amplitude is kept constant while the excitation frequency is varied very slowly. We start from a frequency far above the natural frequency (i.e., a positively detuned thermal load) and decrease it. We choose the initial conditions so that the response amplitude is trivial. As σ is decreased, the response amplitudes remain trivial untill point B is reached, where they experience a sudden jump up to points C and D. Point B is a subcritical or reverse pitchfork bifurcation. The response amplitudes decrease as the frequency is further decreased untill point A is reached, where they become trivial again. Point A is a supercritical pitchfork bifurcation.

Starting at points C or D and sweeping in the reverse direction, we note that, to the first-order approximation, the response amplitudes increase without bounds as the frequency increases. In reality, the stable and unstable branches merge to produce a saddle-node bifurcation. Increasing the frequency above this point results in a jump down of the response amplitudes to the trivial solution. Between point B and the saddle-node bifurcation, there are three possible solutions: the trivial solution, which is stable, and two nontrivial solutions, the larger of which is stable and the smaller is unstable. In this interval, the response may be trivial or nontrivial, depending on the initial conditions.

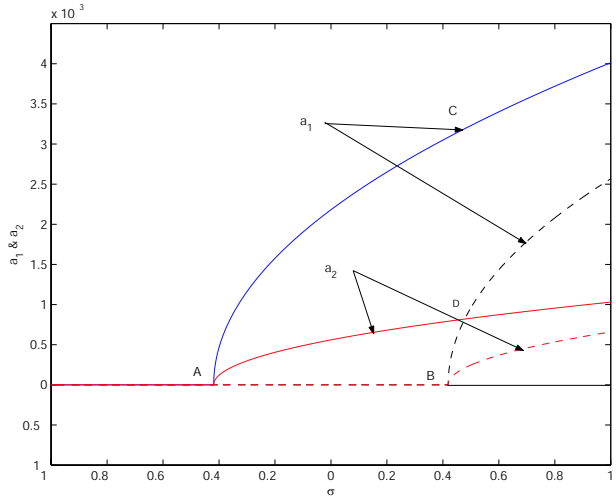

Figure 4.8: Variation of the equilibrium solutions with the detuning parameter when $p = 7.0$ and $q = 0.01$.

In Figure 4.9, we show the force-response curves generated when the system is negatively detuned by 0.8. Starting from a forcing amplitude corresponding to point A and increasing it results in a monotonic increase in the response amplitudes. Point A is a supercritical pitchfork bifurcation. For any excitation amplitude above point A, the response amplitudes settle on the branches AB and AC, irrespective of the initial conditions. Sweeping q down, one finds that the response amplitudes follow the branches BA and CA. Decreasing q below point A results in a smooth transition of the response from a nontrivial to a trivial response. Increasing the value of the detuning parameter results in a shift of the critical point A to the right.

We show in Figure 4.10 the force-response curves generated for the case of a positive detuning of 0.85. In contrast with the preceding case, there are multivalued responses. Point A is a subcritical pitchfork bifurcation and points D and E are saddle-node bifurcation. Between these bifurcations, the response may be trivial or nontrivial depending on the initial conditions. Whereas the linear theory predicts stable trivial responses for values of q below point A and unbounded responses above it, the nonlinear analysis predicts an instability of the trivial response between points A and D for large disturbances, a subcritical instability. Moreover, the nonlinearity puts a cap on the response amplitudes. Sweeping q in the forward direction, one finds that the response amplitudes

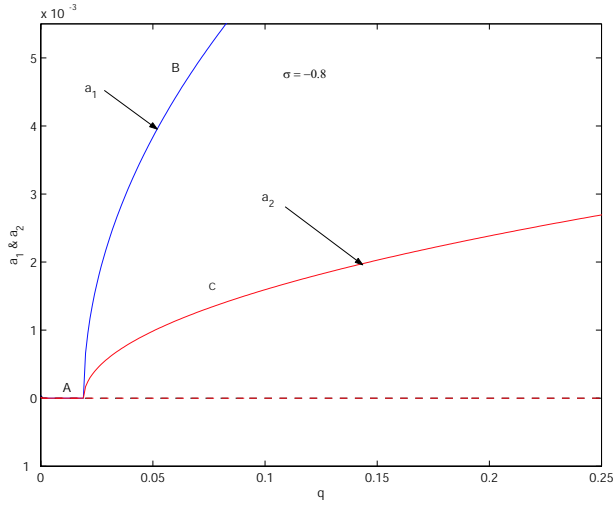

Figure 4.9: Variation of the equilibrium solutions with the forcing amplitude (force-response curves) when $\sigma = -0.8$ and $p = 7.0$.

jump up beyond point A. On the other hand, sweeping q in the reverse direction results in a jump to the trivial response beyond point D.

4.3.3 Combination Parametric Resonance of the Difference Type

The case of combination parametric resonance of the difference type

$$\Omega = \omega_k - \omega_j + \epsilon\sigma \tag{4.124}$$

can be obtained from the preceding case by changing the sign of ω_j from positive to negative. Then, it follows from Equation (4.121) that nontrivial solutions do not exist.

4.3.4 Principal Parametric Resonance

For the case of principal parametric resonance of the kth mode, we let

$$\Omega = 2\omega_k + \epsilon\sigma \tag{4.125}$$

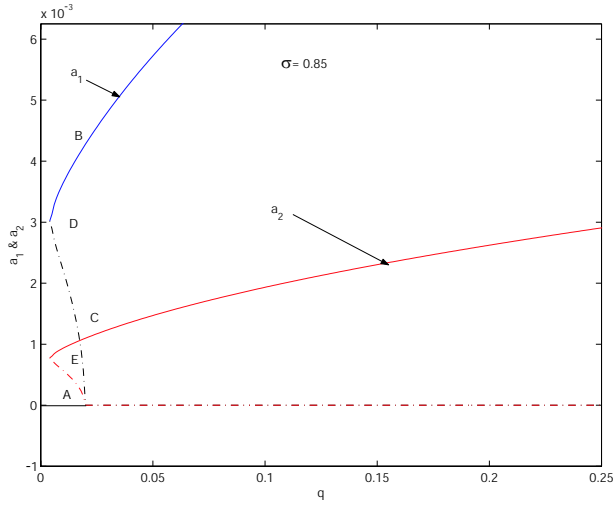

Figure 4.10: Variation of the equilibrium solutions with the forcing amplitude (force-response curves) when $\sigma = 0.85$ and $p = 7.0$.

Then, all modes except the kth mode decay exponentially with time. Then, using Equation (4.125) along with Equations (4.100), (4.84), and (4.85), we obtain

$$2i\omega_k \left(A_k' + \mu_k A_k\right) + \alpha_{kk} A_k^2 \bar{A}_k + q f_{kk} \bar{A}_k e^{i\sigma t_1} = 0 \tag{4.126}$$

where α_{kk}, f_{kk}, and μ_k are defined in Equations (4.105), (4.107), and (4.108).

Next, we substitute Equation (4.110) into Equation (4.126), separate the real and imaginary parts, and obtain

$$a_k' = -\mu_k a_k + \frac{f_{kk}}{2\omega_k} q a_k \sin(2\beta_k) \tag{4.127}$$

$$a_k \beta_k' = -\frac{1}{2}\sigma a_k + \frac{\alpha_{kk}}{8\omega_k} a_k^3 + \frac{f_{kk}}{2\omega_k} q a_k \cos(2\beta_k) \tag{4.128}$$

It follows from Equations (4.127) and (4.128) that their equilibrium solutions are given by

$$a_k^2 = \frac{8\omega_k}{\alpha_{kk}} \left[\frac{1}{2}\sigma \pm \sqrt{\frac{f_{kk}^2 q^2}{4\omega_k^2} - \mu_k^2}\right] \tag{4.129}$$

The frequency- and force-response curves generated using Equation (4.129) are qualitatively similar to those shown in Figures 4.2-4.4.

Chapter 5

Static and Dynamic Behavior of Postbuckled Circular Plates under Thermal Loading

5.1 Introduction

The vibration characteristics of thermally stressed plates have become important with the increasing flight speeds of air and space vehicles and the resulting thermal environment of the airframe. The buckling of skin panels, whether caused by air loads or by thermal stresses, causes a marked reduction in their stiffnesses. the changes in frequencies and mode shapes, which take place due to the thermal stresses, affect considerably their static and dynamic aeroelastic instabilities. These changes are the subject of this study.

The literature on the postbuckling behavior of plates, whether static or dynamic, is not as extensive as the literature on the pre-buckling behavior of plates.

5.2 Governing Equations

We consider large-amplitue deflections and vibrations of a postbuckled circular plate whose edge temperature is maintained at a constant value T_b. Neglecting thermal diffusion and thermoelastic damping, one finds that the plate temperature $T(r,t) = T_b$. We consider both clamped and simply supported boundary conditions. Axisymmetric deflections and vibrations are governed by

$$D\hat{\nabla}^4\hat{w} + \rho h\frac{\partial^2\hat{w}}{\partial\hat{t}^2} = \frac{1}{\hat{r}}\frac{\partial^2\hat{w}}{\partial\hat{r}^2}\frac{\partial\hat{F}}{\partial\hat{r}} + \frac{1}{\hat{r}}\frac{\partial\hat{w}}{\partial\hat{r}}\frac{\partial^2\hat{F}}{\partial\hat{r}^2} \tag{5.1}$$

where $\hat{w}(\hat{r},\hat{t})$ is the plate transverse displacement, $\hat{F}(\hat{r},\hat{t})$ is the stress function, ρ is the mass density, h is the plate thickness, $D = Eh^3/[12(1-\nu^2)]$ is the plate rigidity, E is the modulus of elasticity, and ν is Poisson's ratio. The compatibility equation for axisymmetric vibrations is given by

$$\hat{r}\frac{\partial^3\hat{F}}{\partial\hat{r}^3} + \frac{\partial^2\hat{F}}{\partial\hat{r}^2} - \frac{1}{\hat{r}}\frac{\partial\hat{F}}{\partial\hat{r}} = -\frac{1}{2}Eh\left(\frac{\partial\hat{w}}{\partial\hat{r}}\right)^2 \tag{5.2}$$

For a clamped plate, the boundary conditions are

$$\hat{w} = 0 \text{ and } \frac{\partial\hat{w}}{\partial\hat{r}} = 0 \text{ at } \hat{r} = R \tag{5.3}$$

$$\hat{F} < \infty \text{ and } \hat{w} < \infty \text{ at } \hat{r} = 0 \tag{5.4}$$

$$\frac{\partial^2\hat{F}}{\partial\hat{r}^2} - \frac{\nu}{\hat{r}}\frac{\partial\hat{F}}{\partial\hat{r}} + E\alpha h(T_b - T_0) = 0 \text{ at } \hat{r} = R \tag{5.5}$$

And for a simply supported plate with immovable edges, the boundary conditions are

$$\hat{w} = 0 \text{ and } \frac{\partial^2\hat{w}}{\partial\hat{r}^2} + \frac{\nu}{r}\frac{\partial\hat{w}}{\partial\hat{r}} = 0 \text{ at } \hat{r} = R \tag{5.6}$$

$$\hat{F} < \infty \text{ and } \hat{w} < \infty \text{ at } \hat{r} = 0 \tag{5.7}$$

$$\frac{\partial^2\hat{F}}{\partial\hat{r}^2} - \frac{\nu}{\hat{r}}\frac{\partial\hat{F}}{\partial\hat{r}} + E\alpha h(T_b - T_0) = 0 \text{ at } \hat{r} = R \tag{5.8}$$

where T_0 is the zero-stress temperature, α is the coefficient of thermal expansion, and R is the radius of the plate.

We introduce nondimensional variables, defined as follows:

$$\hat{r} = Rr, \;\; \hat{t} = R^2\left(\frac{\rho h}{D}\right)^{1/2}t, \;\; \hat{w} = hw, \;\; \hat{F} = Eh^3F \tag{5.9}$$

Substituting Eq. (5.9) into Eqs. (5.1)-(5.5), we obtain

$$\frac{\partial^2 w}{\partial t^2} + \nabla^4 w = \alpha_1 \left[\frac{1}{r} \frac{\partial^2 w}{\partial r^2} \frac{\partial F}{\partial r} + \frac{1}{r} \frac{\partial w}{\partial r} \frac{\partial^2 F}{\partial r^2} \right] \tag{5.10}$$

$$r \frac{\partial^3 F}{\partial r^3} + \frac{\partial^2 F}{\partial r^2} - \frac{1}{r} \frac{\partial F}{\partial r} = -\frac{1}{2} \left(\frac{\partial w}{\partial r} \right)^2 \tag{5.11}$$

$$w = 0 \text{ and } \frac{\partial w}{\partial r} = 0 \text{ at } r = 1 \tag{5.12}$$

$$F < \infty \text{ and } w < \infty \text{ at } r = 0 \tag{5.13}$$

$$\frac{\partial^2 F}{\partial r^2} - \frac{\nu}{r} \frac{\partial F}{\partial r} + \frac{\alpha (T_b - T_0) R^2}{h^2} = 0 \text{ at } r = 1 \tag{5.14}$$

where

$$\alpha_1 = 12(1 - \nu^2).$$

We transform Eqs. (5.10-14) first into a problem with homogeneous boundary conditions. To this end, we solve the linear part of Eq. (5.11) subject to the boundary conditions (5.13) and (5.14). The general solution of the linear part of Eq. (5.11), which is bounded at the origin, can be expressed as

$$F = C_1(t) r^2 + C_2(t) \tag{5.15}$$

Using the boundary condition, Eq. (5.14), we find that

$$C_1(t) = -\frac{\alpha (T_b - T_0) R^2}{2(1 - \nu) h^2}$$

and $C_2(t)$ is an arbitrary function of time. Next, we let

$$F = \Phi - \frac{\alpha (T_b - T_0) R^2}{2(1 - \nu) h^2} r^2 + C_2(t) \tag{5.16}$$

in Eqs. (5.10)-(5.14) and obtain

$$\frac{\partial^2 w}{\partial t^2} + p \nabla^2 w + \nabla^4 w = \alpha_1 \left[\frac{1}{r} \frac{\partial^2 w}{\partial r^2} \frac{\partial \Phi}{\partial r} + \frac{1}{r} \frac{\partial w}{\partial r} \frac{\partial^2 \Phi}{\partial r^2} \right] \tag{5.17}$$

$$r \frac{\partial^3 \Phi}{\partial r^3} + \frac{\partial^2 \Phi}{\partial r^2} - \frac{1}{r} \frac{\partial \Phi}{\partial r} = -\frac{1}{2} \left(\frac{\partial w}{\partial r} \right)^2 \tag{5.18}$$

$$w = 0 \text{ and } \frac{\partial w}{\partial r} = 0 \text{ at } r = 1 \tag{5.19}$$

$$w < \infty \text{ and } \Phi < \infty \text{ at } r = 0 \tag{5.20}$$

$$\frac{\partial^2 \Phi}{\partial r^2} - \frac{\nu}{r} \frac{\partial \Phi}{\partial r} = 0 \text{ at } r = 1 \tag{5.21}$$

where

$$p = \frac{12\alpha(T_b - T_0)(1+\nu)R^2}{h^2}.$$

The nondimensional parameter p depends on the temperature and thermal properties of the material.

REDUCED-ORDER MODEL

A general analytical solution of the nondimensional coupled Eqs. (5.17)-(5.21) is not available yet, hence we seek an approximate analytical solution in the form

$$w(r,t) = \sum_{m=1}^{N} \eta_m(t)\phi_m(r) \tag{5.22}$$

where $\phi_m(r)$ is the mth shape function, $\eta_m(t)$ is the mth generalized coordinate for the mth shape function, and N is the number of retained shape functions. As N approaches infinity, the approximation in Eq. (5.22) becomes exact if the chosen shape functions form a complete set. Once we solve for all the $\phi_m(r)$ and $\eta_m(t)$, we calculate an approximation to the deflection $w(r,t)$ from Eq. (5.22).

We choose the shape functions $\phi_m(r)$ to be the first N axisymmetric modes of the linear undamped plate with the in-plane load due to temperature. For this case, the mode shapes are given by

$$\phi_m(r) = \frac{J_0(r\lambda_{1m})}{J_0(\lambda_{1m})} - \frac{I_0(r\lambda_{2m})}{I_0(\lambda_{2m})} \tag{5.23}$$

where J_0 is the Bessel function of the first kind, I_0 is the modified Bessel function of the first kind,

$$\lambda_{1m} = \frac{1}{2}\left[\sqrt{p^2+4\omega_m}+p\right], \quad \lambda_{2m} = \frac{1}{2}\left[\sqrt{p^2+4\omega_m}-p\right] \tag{5.24}$$

and ω_m is the known mth nondimensional natural frequency associated with the mth linear undamped axisymmetric mode $\phi_m(r)$. We note that the mode shapes are orthonormal; that is,

$$\int_0^1 r\phi_m(r)\phi_n(r)dr = \delta_{mn} \tag{5.25}$$

where δ_{mn} is the Kronecker delta.

Substituting Eq. (5.22) into Eq. (5.18) and integrating, we have (Vogl and Nayfeh, 2003)

$$\Phi(r,t) = \sum_{m,n=1}^{N} \eta_m(t)\eta_n(t)\psi_{mn}(r) \tag{5.26}$$

where $\psi_{mn}(r)$ is given by (Nayfeh and Pai, 2003)

$$\begin{aligned}\psi'_{mn}(r) = \quad & -\tfrac{r}{4}\int_0^r \tfrac{\phi'_m\phi'_n}{\xi}d\xi + \tfrac{1}{4r}\int_0^r \xi\phi'_m\phi'_n d\xi \\ & +\tfrac{r}{4}\int_0^1 \tfrac{\phi'_m\phi'_n}{\xi}d\xi + \tfrac{r}{4}\tfrac{1+\nu}{1-\nu}\int_0^1 \xi\phi'_m\phi'_n d\xi\end{aligned} \tag{5.27}$$

Here, the prime denotes differentiation with respect to the space variable r and the overdot denotes differentiation with respect to the time variable t. We note that ψ'_{mn} is symmetric in m and n for $m, n = 1, 2, \ldots, N$.

We then substitute Eqs. (5.22), (5.23), and (5.26) into Eq. (5.17) and obtain

$$\begin{aligned}\sum_{m=1}^{N}\left(\ddot{\eta}_m + \omega_m^2\eta_m\right)\phi_m + p\sum_{m=1}^{N}\eta_m\left(\phi''_m + \frac{1}{r}\phi'_m\right) = \\ \alpha_1\left[\frac{1}{r}\sum_{m,n,p=1}^{N}\eta_m\eta_n\eta_p\Big(\phi''_m\psi'_{np} + \phi'_m\psi''_{np}\Big)\right]\end{aligned} \tag{5.28}$$

We multiply Eq. (5.28) with $r\phi_q(r)$, integrate the outcome over $r \in [0,1]$, use the orthonormality condition (5.25), and obtain

$$\left(\ddot{\eta}_q + \omega_q^2\eta_q\right) - p\sum_{m=1}^{N}\eta_m\int_0^1 r\phi'_m\phi'_q dr = -\alpha_1\sum_{m,n,p=1}^{N}\eta_m\eta_n\eta_p\int_0^1 \phi'_q\phi'_m\psi'_{np}dr \tag{5.29}$$

where $q = 1, 2, \ldots, N$. Consequently, the discretizations of $w(r,t)$ and $\Phi(r,t)$ in Eqs. (5.22) and (5.26), respectively, have reduced the general nonlinear distributed-parameter system, Eqs. (5.17)-(5.21), into the system of N nonlinearly coupled ordinary-differential Equations (5.29).

Once the ϕ_n and ψ'_{np} are calculated for $n, p = 1, 2, \ldots, N$, one evaluates the integrals in Eq. (5.29). Then, the system of equations (5.29) is solved for the $\eta_m(t)$. Then, once all of the $\eta_m(t)$ are determined, the plate deflection $w(r,t)$ can be calculated using Eq. (5.22).

STATIC BEHAVIOR

Setting all of the time derivatives equal to zero, we reduce the system of coupled differential equations (5.29) into a system of coupled algebraic equations. Choosing values for the parameters

ν and N, we solve this algebraic system for the η_m and then the static deflection using Eq. (5.22). In what follows, we choose $\nu = 0.3$ (a very common value for metals) and $N = 15$. Figure 5.1

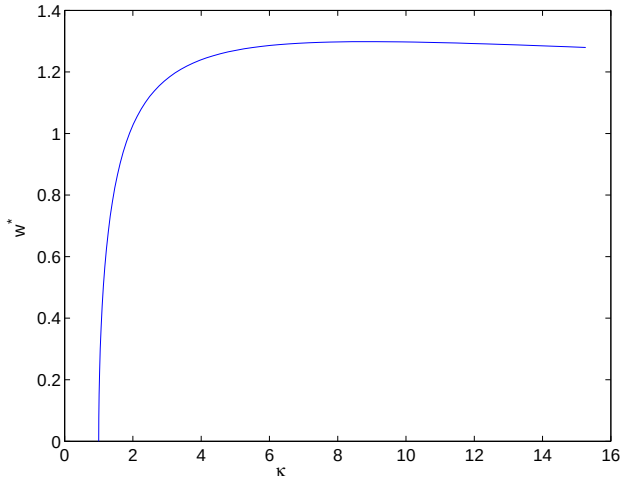

Figure 5.1: Normalized maximum postbuckling deflection vs. load level κ.

shows variation of the maximum postbuckling deflection with the load level $\kappa = \frac{p}{p_{cr}}$, where p_{cr} is the first buckling load. Convergence was obtained using five modes, including more modes does not affect the converged results. Figure 5.2 shows variation of the normalized radial stresses Λ with the number of modes N retained in the approximation. The significance of the shown results lies in the fact that the value of N needed for the radial stress to converge is higher than the value of N needed for the deflection to converge. Also, the number of modes needed for convergence depends on the load level, the higher the load level is the higher N is.

Bodner (1954) solved for the radial stress of a clamped plate using a power-series solution. He could not carry out the solution for higher load levels because of convergence problems. Figure 5.3 shows a comparison between our solution and Bodner's. It is clear that our solution can reach higher load levels easily with less number of modes compared with the number of terms one needs for the power-series solution. Also, it indicates that the power-series solution starts to deviate from our results for $\kappa > 3$.

For the sake of comparison, we solved the same simply supported plate problem of Friedrichs and Stoker (1942) and reproduce their power-series solution results. They used a maximum of 23 terms

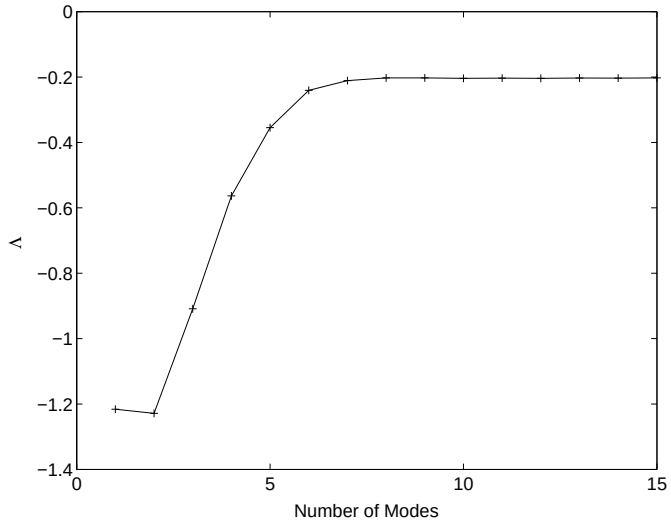

Figure 5.2: Normalized edge load vs. number of modes needed for convergence at $\kappa = 15$

in their solution and in our reproduction we used 50. The number of modes N retained in our solution is 15. The results compare fairly well for much less computational effort. Figure 5.4 shows this bench mark comparison.

NATURAL FREQUENCIES

In this section, we determine the natural frequencies of the axisymmetric modes of the deflected plate. The procedure followed here is similar to that of Vogl and Nayfeh (2003). First, we perturb each coefficient function $\eta_m(t)$ with a harmonic term from its equilibrium value η_m^{eq}; that is,

$$\eta_m(t) = \eta_m^{eq} + \beta_m e^{i\omega t}, \tag{5.30}$$

Then, we substitute Eq. (5.30) into the reduced-order model, Eq.(5.29), and keep only the linear terms in β_m. Because the constant terms, which are due to equilibrium, cancel out, the reduced-order model becomes a system of N linear homogeneous algebraic equations in the unknowns β_m and ω; that is,

$$[Z(\omega)]\{\beta_m\} = \{0\}, \tag{5.31}$$

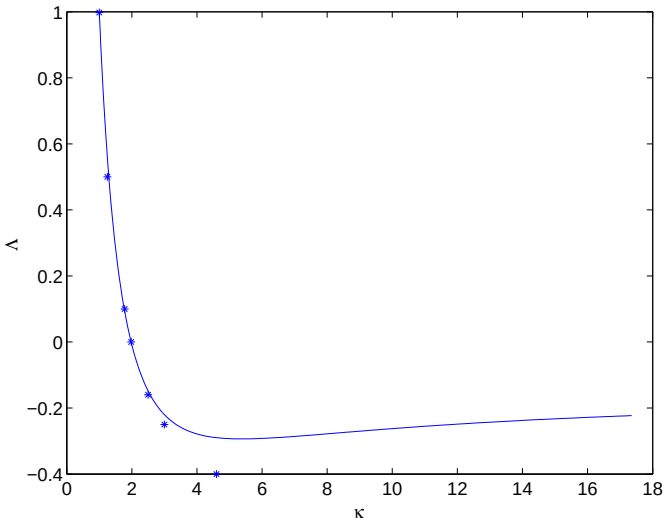

Comparison of the power series solution with our solution for the case of a clamped plate.

where $[Z(\omega)]$ is an $N \times N$ constant matrix, which is a function of ω. For nontrivial β_m, the determinant of $[Z(\omega)]$ must be zero; that is,

$$\det([Z(\omega)]) = 0. \tag{5.32}$$

Equation (5.32) is an algebraic equation of order $2N$ with N roots associated with unique modes of vibration. The positive roots correspond to the natural frequencies of the deflected plate and the negative roots correspond to unstable equilibrium states.

Figure 5.5 shows variation of the first nondimensional axisymmetric natural frequency with the load level κ and Figure 5.6 shows variation of the square value of the first natural frequency with the load level κ. The reason for showing both results is that some previous publications mixed both results and showed the squared value in place of the value of the frequency, both behviors are clearly different. Figure 5.7 shows variation of the first four nondimensional axisymmetric natural frequencies with the load level κ.

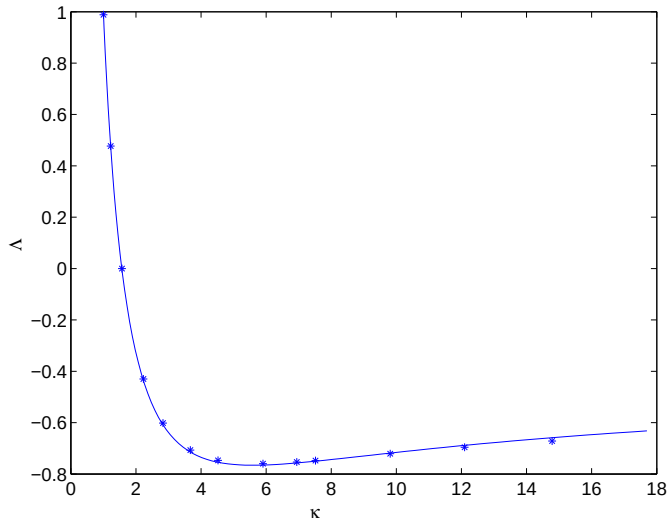

Figure 5.3: Comparison of the power-series solution with our solution for a simply supported plate; solid curve: present solution, stars: power-series solution.

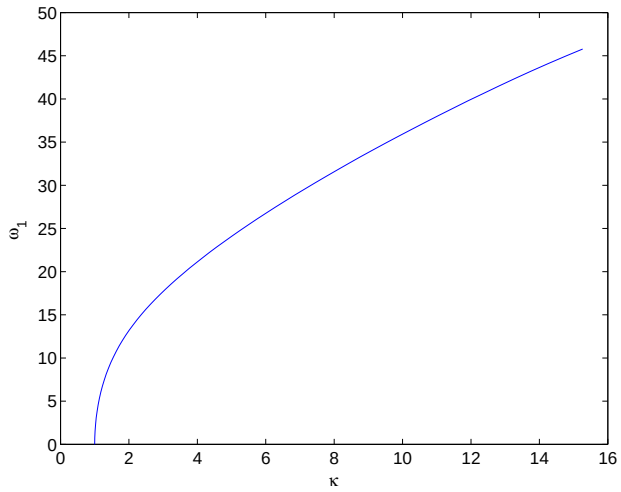

Figure 5.4: Variation of the first natural frequency with the load level κ.

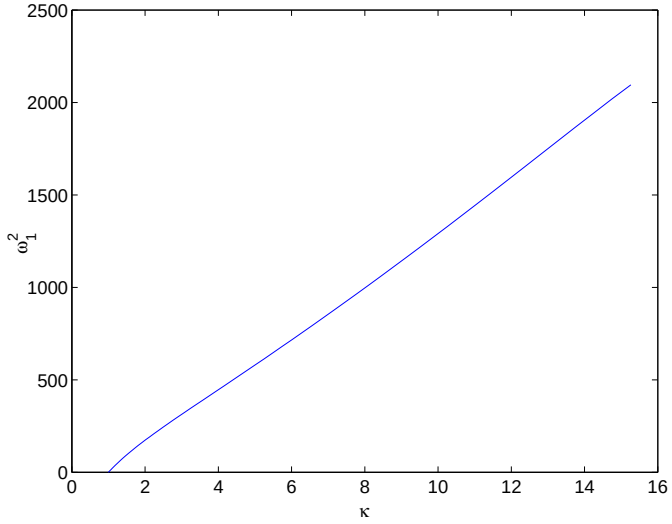

Figure 5.5: Variation of the first natural frequency sqaured with the load level κ.

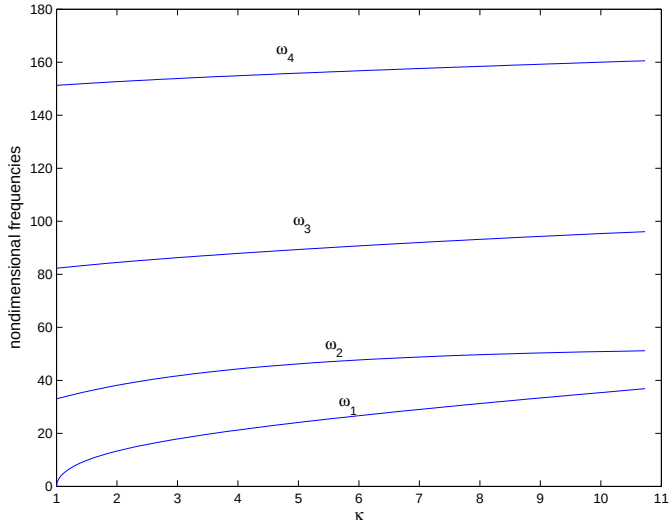

Figure 5.6: Variation of the first four natural frequencies with the load level κ.

Chapter 6

Circular Plates under Thermal and Electrostatic Loadings

6.1 Introduction

Sensors are one of the most commonly used devices in industry. They are composed of several components and the heart of them is the sensing element, which may be either a beam, or a bridge, or a diaphragm. Sensors are increasingly used as a major safeguard against thermal disasters, especially after the disaster of the Space Shuttle Columbia (Frauenfelder, 2003). High-performance sensors capable of operating at temperatures as high as 300 C and in corrosive environments are in demand in many industries, such as automotive engine control, subterranean heat exploration, and industrial pressure instruments (Ishida, 2001). Also, pressure and vibration-measurement sensors in gas-turbine engines of manned aircraft operate in high-temperature environments (up to 600 C); they are based on measurements of the lower natural frequencies of diphragms. Therefore, there is a wide interest in analyzing, controlling, and compensating for the influence of temperature on sensor performance (Smith and Senturia, 1995). The focus of this paper is on the modeling and analysis of such an influence on a circular diaphragm sensor.

6.2 Problem Formulation

We consider large-amplitued deflections and vibrations of an electrostatically actuated clamped circular plate whose edge temperature is maintained at a constant value T_b. Neglecting the thermal diffusion and thermoelastic damping, one finds that the plate temperature $T(r,t) = T_b$. The clamped boundary condition is important in many MEMS devices, such as sensors and micropumps, as it is a more realistic representation of the actual boundary conditions. Under electrostatic actuation, axisymmetric deflections and vibrations are governed by

$$D\hat{\nabla}^4\hat{w} + \rho h\frac{\partial^2\hat{w}}{\partial\hat{t}^2} = \frac{1}{\hat{r}}\frac{\partial^2\hat{w}}{\partial\hat{r}^2}\frac{\partial\hat{F}}{\partial\hat{r}} + \frac{1}{\hat{r}}\frac{\partial\hat{w}}{\partial\hat{r}}\frac{\partial^2\hat{F}}{\partial\hat{r}^2} + \frac{\epsilon V^2}{2(d-\hat{w})^2} \tag{6.1}$$

where $\hat{w}(\hat{r},\hat{t})$ is the plate transverse displacement, $\hat{F}(\hat{r},\hat{t})$ is the stress function, ρ is the mass density, h is the plate thickness, $D = Eh^3/[12(1-\nu^2)]$ is the plate rigidity, E is the modulus of elasticity, ν is Poisson's ratio, d is the initial gap between the electrodes, V is the applied voltage, and ϵ is the dielectric constant of the medium.

As shown in Chapter 2, the compatibility relation can be expressed as

$$\hat{r}\frac{\partial^3\hat{F}}{\partial\hat{r}^3} + \frac{\partial^2\hat{F}}{\partial\hat{r}^2} - \frac{1}{\hat{r}}\frac{\partial\hat{F}}{\partial\hat{r}} = -\frac{1}{2}\left(\frac{\partial w}{\partial r}\right)^2 \tag{6.2}$$

For a clamped plate, the boundary conditions are

$$\hat{w} = 0 \text{ and } \frac{\partial\hat{w}}{\partial\hat{r}} = 0 \text{ at } \hat{r} = R \tag{6.3}$$

$$\hat{F} < \infty \text{ and } \hat{w} < \infty \text{ at } \hat{r} = 0 \tag{6.4}$$

$$\frac{\partial^2\hat{F}}{\partial\hat{r}^2} - \frac{\nu}{\hat{r}}\frac{\partial\hat{F}}{\partial\hat{r}} + E\alpha h(T_b - T_0) = 0 \text{ at } \hat{r} = R \tag{6.5}$$

where T_0 is the zero-stress temperature, R is the radius of the plate, and α is the coefficient of thermal expansion.

We introduce nondimensional variables, defined as follows:

$$\hat{r} = Rr, \quad \hat{t} = R^2\left(\frac{\rho h}{D}\right)^{1/2}t, \quad \hat{w} = dw, \quad \hat{F} = Ehd^2F \tag{6.6}$$

Substituting Equation (6.6) into Equations (6.1)-(6.5), we obtain

$$\frac{\partial^2 w}{\partial t^2} + \nabla^4 w = \alpha_1\left[\frac{1}{r}\frac{\partial^2 w}{\partial r^2}\frac{\partial F}{\partial r} + \frac{1}{r}\frac{\partial w}{\partial r}\frac{\partial^2 F}{\partial r^2}\right] + \frac{\alpha_2 V^2}{(1-w)^2} \tag{6.7}$$

$$r\frac{\partial^3 F}{\partial r^3}+\frac{\partial^2 F}{\partial r^2}-\frac{1}{r}\frac{\partial F}{\partial r}=-\frac{1}{2}\left(\frac{\partial w}{\partial r}\right)^2 \tag{6.8}$$

$$w=0 \text{ and } \frac{\partial w}{\partial r}=0 \text{ at } r=1 \tag{6.9}$$

$$F<\infty \text{ and } w<\infty \text{ at } r=0 \tag{6.10}$$

$$\frac{\partial^2 F}{\partial r^2}-\frac{\nu}{r}\frac{\partial F}{\partial r}+\frac{\alpha(T_b-T_0)R^4}{h^4}=0 \text{ at } r=1 \tag{6.11}$$

where

$$\alpha_1=\frac{12(1-\nu^2)d^2}{h^2} \text{ and } \alpha_2=\frac{\epsilon R^4}{2Dd^3}$$

and the coefficient α_1 represents the strength of the nonlinear terms. In general the gap to thickness ratio can be the order of 1-2. and it can be less than one in case of what is called Touch Mode Capacitive Sensors.

We transform Equations (6.7)-(6.11) first into a problem with homogeneous boundary conditions. To this end, we solve the linear part of Equation (6.8) subject to the boundary conditions (6.10) and (6.11). The general solution of the linear part of Equation (6.8), which is bounded at the origin, can be expressed as

$$F=C_1(t)r^2+C_2(t) \tag{6.12}$$

Using the boundary condition, Equation (6.11), we find that

$$C_1(t)=-\frac{\alpha(T_b-T_0)R^4}{2(1-\nu)h^4}$$

and $C_2(t)$ is an arbitrary function of time. Next, we let

$$F=\Phi-\frac{\alpha(T_b-T_0)R^4}{2(1-\nu)h^4}r^2+C_2(t) \tag{6.13}$$

into Equations (6.7)-(6.11) and obtain

$$\frac{\partial^2 w}{\partial t^2}+p\nabla^2 w+\nabla^4 w=\alpha_1\left[\frac{1}{r}\frac{\partial^2 w}{\partial r^2}\frac{\partial \Phi}{\partial r}+\frac{1}{r}\frac{\partial w}{\partial r}\frac{\partial^2 \Phi}{\partial r^2}\right]+\frac{\alpha_2 V^2}{(1-w)^2} \tag{6.14}$$

$$r\frac{\partial^3\Phi}{\partial r^3}+\frac{\partial^2\Phi}{\partial r^2}-\frac{1}{r}\frac{\partial\Phi}{\partial r}=-\frac{1}{2}\left(\frac{\partial w}{\partial r}\right)^2 \tag{6.15}$$

$$w=0 \text{ and } \frac{\partial w}{\partial r}=0 \text{ at } r=1 \tag{6.16}$$

$$w<\infty \text{ and } \Phi<\infty \text{ at } r=0 \tag{6.17}$$

$$\frac{\partial^2\Phi}{\partial r^2}-\frac{\nu}{r}\frac{\partial\Phi}{\partial r}=0 \text{ at } r=1 \tag{6.18}$$

where

$$p=\frac{12\alpha(T_b-T_0)(1+\nu)R^2}{h^2}$$

The coefficient p depends on the temperature and thermal properties of the material. For example, in case of RF MEMS capacitive switches where either aluminium or gold membranes are used and the temperature varies between 50 and 70 C, p can take values ranging from 5 to 16. This is a wide range covering prebuckling, postbuckling, and collapse of the plate.

REDUCED-ORDER MODEL

A general analytical solution of the nondimensional coupled Equations (6.14)-(6.18) is not available yet, hence we seek an approximate analytical solution in the form

$$w(r,t)=\sum_{m=1}^{N}\eta_m(t)\phi_m(r) \tag{6.19}$$

where $\phi_m(r)$ is the mth shape function, $\eta_m(t)$ is the mth generalized coordinate for the mth shape function, and N is the number of retained shape functions. As N approaches infinity, the approximation in Equation (6.19) becomes exact if the chosen shape functions form a complete set. Once we solve for all the $\phi_m(r)$ and $\eta_m(t)$, we calculate an approximate deflection $w(r,t)$ from Equation (6.19).

We choose the shape functions $\phi_m(r)$ to be the first N axisymmetric modes of the linear undamped case ($\alpha_1=0$) with the in-plane load due to temperature and no electrostatic forcing ($V=0$). For this case, the mode shapes are given by

$$\phi_m(r)=\frac{J_0(r\lambda_{1m})}{J_0(\lambda_{1m})}-\frac{I_0(r\lambda_{2m})}{I_0(\lambda_{2m})} \tag{6.20}$$

where J_0 is the Bessel function of the first kind, I_0 is the modified Bessel function of the first kind, and

$$\lambda_{1m} = \frac{1}{2}\left[\sqrt{p^2 + 4\omega_m} + p\right] \quad \text{and} \quad \lambda_{2m} = \frac{1}{2}\left[\sqrt{p^2 + 4\omega_m} - p\right]$$

and ω_m is the known mth nondimensional natural frequency associated with the mth linear undamped axisymmetric mode $\phi_m(r)$. We note that the mode shapes are orthonormal; that is,

$$\int_0^1 r\phi_m(r)\phi_n(r)dr = \delta_{mn} \tag{6.21}$$

where δ_{mn} is the Kronecker delta.

Substituting Equation (6.19) into Equation (6.15) and integrating, we have (Vogl and Nayfeh, 2003)

$$\Phi(r,t) = \sum_{m,n=1}^{N} \eta_m(t)\eta_n(t)\psi_{mn}(r) \tag{6.22}$$

where $\psi_{mn}(r)$ is given by (Nayfeh and Pai, 2003)

$$\begin{aligned}\psi'_{mn}(r) = &-\frac{r}{4}\int_0^r \frac{\phi'_m\phi'_n}{\xi}d\xi + \frac{1}{4r}\int_0^r \xi\phi'_m\phi'_n d\xi \\ &+ \frac{r}{4}\int_0^1 \frac{\phi'_m\phi'_n}{\xi}d\xi + \frac{r}{4}\frac{1+\nu}{1-\nu}\int_0^1 \xi\phi'_m\phi'_n d\xi\end{aligned} \tag{6.23}$$

Here, the prime denotes differentiation with respect to the space variable r and the overdot denotes differentiation with respect to the time variable t. We note that ψ'_{mn} is symmetric in m and n for $m, n = 1, 2, \ldots, N$.

We then substitute Equations (6.19), (6.20), and (6.23) into Equation (6.14) and obtain

$$\begin{aligned}\sum_{m=1}^{N}\left(\ddot{\eta}_m + \omega_m^2\eta_m\right)\phi_m + p\sum_{m=1}^{N}\eta_m\left(\phi''_m + \frac{1}{r}\phi'_m\right) = \alpha_2 V^2\left(1 - \sum_{i=1}^{N}\eta_i\phi_i\right)^{-2} + \\ \alpha_1\left[\frac{1}{r}\sum_{m,n,p=1}^{N}\eta_m\eta_n\eta_p\left(\phi''_m\psi'_{np} + \phi'_m\psi''_{np}\right)\right]\end{aligned} \tag{6.24}$$

We multiply Equation (6.24) with $r\phi_q(r)\left(1 - \sum_{i=1}^{N}\eta_i\phi_i\right)^2$, integrate the outcome over $r \in [0,1]$,

use the orthogonality condition (6.21), and obtain

$$\left(\ddot{\eta}_q+\omega_q^2\eta_q\right)-2\sum_{i,m=1}^{N}\left(\ddot{\eta}_m+\omega_m^2\eta_m\right)\eta_i\int_0^1 r\phi_i\phi_m\phi_q dr+\sum_{i,j,m=1}^{N}\left(\ddot{\eta}_m+\omega_m^2\eta_m\right)\eta_i\eta_j\int_0^1 r\phi_i\phi_j\phi_m\phi_q dr$$
$$-p\sum_{m=1}^{N}\eta_m\int_0^1 r\phi_m'\phi_q' dr+2p\sum_{i,m=1}^{N}\eta_i\eta_m\int_0^1 r\phi_m'\left(\phi_i\phi_q\right)' dr-p\sum_{i,j,m=1}^{N}\eta_i\eta_j\eta_m\int_0^1 r\phi_m'\left(\phi_i\phi_j\phi_q\right)' dr=$$
$$\alpha_1\Bigg[-\sum_{m,n,p=1}^{N}\eta_m\eta_n\eta_p\int_0^1\phi_q'\phi_m'\psi_{np}' dr+2\sum_{i,m,n,p=1}^{N}\eta_i\eta_m\eta_n\eta_p\int_0^1\left(\phi_i\phi_q\right)'\phi_m'\psi_{np}' dr$$
$$-\sum_{i,j,m,n,p=1}^{N}\eta_i\eta_j\eta_m\eta_n\eta_p\int_0^1\left(\phi_i\phi_j\phi_q\right)'\phi_m'\psi_{np}' dr\Bigg]+\alpha_2V^2\int_0^1 r\phi_q dr \tag{6.25}$$

where $q=1,2,\ldots,N$. Consequently, the discretizations of $w(r,t)$ and $\Phi(r,t)$ in Equations (6.19) and (6.22), respectively, have reduced the general nonlinear distributed-parameter system, Equations (6.14)-(6.18), into the system of N nonlinearly coupled ordinary-differential equations (6.25).

The system of equations (6.25) can be solved for the $\eta_m(t)$ once the ϕ_n and ψ_{np}' are calculated for $n,p=1,2,\ldots,N$. Also, using the definitions of ϕ_m and ψ_{mn}', one can evaluate the integrals in Equation (6.25). Then, once all $\eta_m(t)$ are determined by solving the N coupled equations (6.25), the plate deflection $w(r,t)$ can be calculated using Equation (6.19).

STATIC BEHAVIOR

Setting all time derivatives equal to zero, we reduce the system of coupled differential equations (6.25) into a system of coupled algebraic equations. Choosing values for the parameters α_1, ν, p, and N, we solve this algebraic system for the η_m and then the static deflection using Equation (6.19). In what follows, we choose $\alpha_1=1$ corresponding to a gap the order of the plate thickness, $\nu=0.3$ (a very common value for metals), and $N=5$. We present results for different values of p below the critical (buckling) value p_{cr}.

Figure 6.1 shows the interplay between the electrostatic and thermal loadings. For each thermal load level $\kappa=\frac{p}{p_{cr}}$, we plot variation of the maximum plate deflection $w_m=w(0)$ with the electrostatic load coefficient α_2V^2. For each α_2V^2, there are two values of w_m, the smaller value is stable and the larger one is unstable. For each κ, the stable value of w_m increases with increasing α_2V^2 up

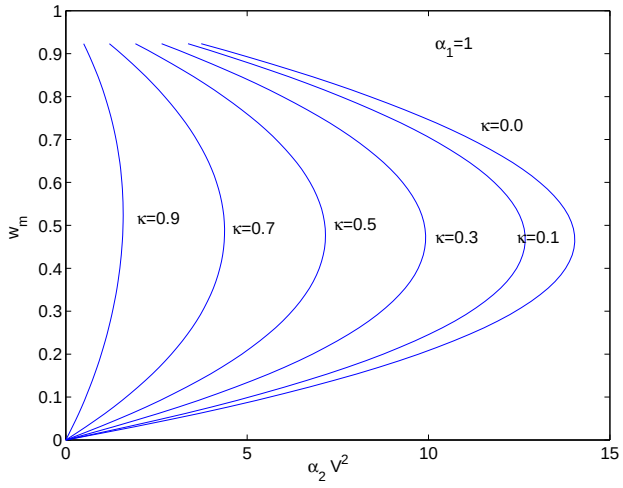

Figure 6.1: Variation of the normalized maximum deflection with the electrostatic coefficient.

to a critical value $\alpha_2 V_p^2$ beyond which the plante collapses. The voltage V_p is known as the pull-in voltage. At this value, the stable solution branch (solid line) collides with the unstable branch (dashed line) and destroy each other in a saddle-node bifurcation.

In Figure 6.2, we plot variation of the maximum plate deflection $w_m = w(0)$ with the electrostatic load coefficient $\alpha_2 V^2$ for $\alpha_1 = 0.0$, 3.0, and 8.0. As mentioned above, the coefficient α_1 represents the strength of the geometric nonlinearity. As α_1 increases, the pull-in voltage increases. Also, as α_1 increases, the value of w_m at which pull-in occurs increases. It follows from Figure 6.2 that α_1 does not have a significant effect on the stable maximum deflection below $\alpha_2 V^2 \approx 10$.

NATURAL FREQUENCIES

In this section, we determine the natural frequencies of the axisymmetric modes of the deflected plate. The procedure followed here is similar to that reported by Vogl and Nayfeh (2003). First, we perturb each coefficient function $\eta_m(t)$ with a harmonic term from its equilibrium value η_m^{eq}; that is,

$$\eta_m(t) = \eta_m^{eq} + \beta_m e^{i\omega t} \tag{6.26}$$

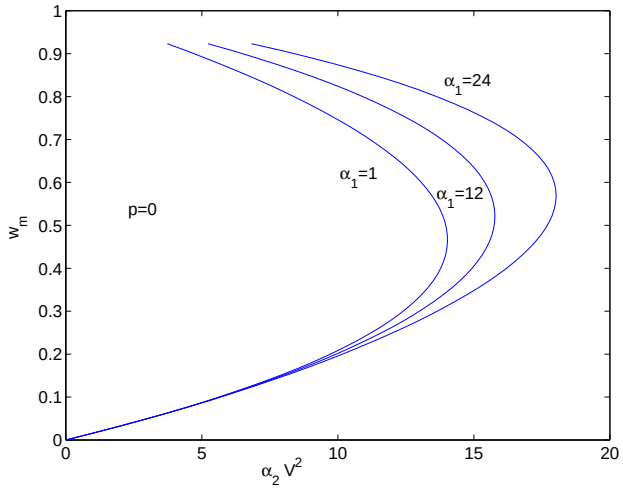

Figure 6.2: Effect of α_1 on the electrostatic coefficient-displacement behavior.

Then, we substitute Equation (6.26) into the reduced-order model (6.25) and keep only the linear terms in β_m. Because the constant terms, which are due to equilibrium, cancel out, the reduced-order model becomes a system of N linear homogeneous algebraic equations in the unknowns β_m and ω; that is,

$$[Z(\omega)]\{\beta_m\} = \{0\}, \tag{6.27}$$

where $[Z(\omega)]$ is an $N \times N$ constant matrix, which is a function of ω. For nontrivial β_m, the determinant of $[Z(\omega)]$ must be zero; that is,

$$\det([Z(\omega)]) = 0. \tag{6.28}$$

Equation (6.28) is an algebraic equation of order $2N$ with N roots associated with unique modes of vibration. The positive roots correspond to the natural frequencies of the deflected plate and the negative roots correspond to unstable equilibrium states.

Figure 6.3 shows variation of the first five nondimensional axisymmetric natural frequencies with the nondimensional temperature p. Figures 6.4 and 6.5 show variation of the first natural frequency with the electrostatic coefficient for three thermal load levels, namely, 0.0,0.3, and 0.7. In Figure 6.4, $\alpha_1 = 1$; it indicates a weak nonlinear effect. In Figure 6.5, $\alpha_1 = 12$; it indicates a strong effect of the nonlinearity. It follows from both figures that increasing the thermal load decreases the first

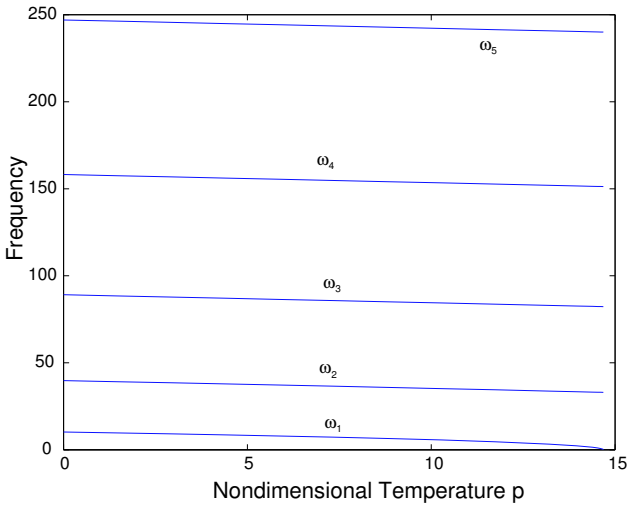

Figure 6.3: Variation of the first five frequencies with the nondimensional temperature p.

natural frequency as well as the pull-in voltage. Moreover, increasing the strength of the mid-plane stretching nonlinearity increases the natural frequency and the pull-in voltage.

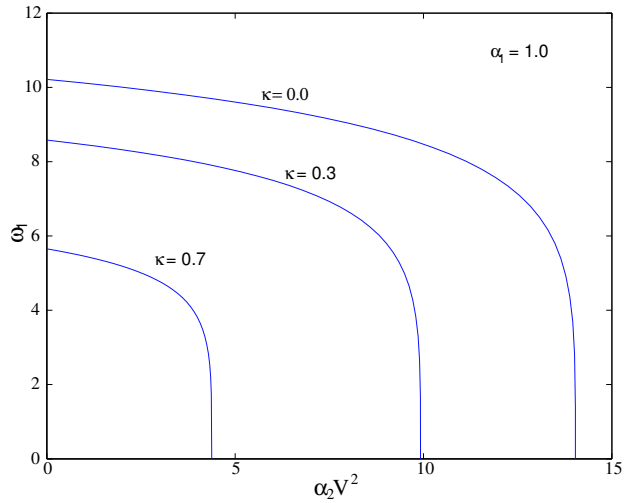

Figure 6.4: Effect of κ on the electrostatic coefficient-frequency behavior for $\alpha_1 = 1$.

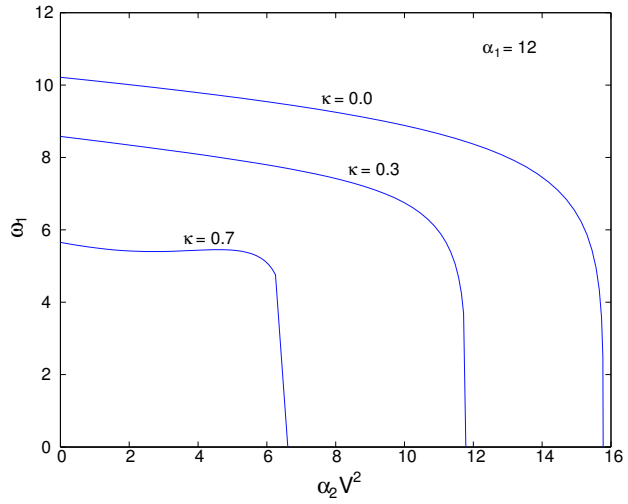

Figure 6.5: Effect of κ on the electrostatic coefficient-frequency behavior for $\alpha_1 = 12$.

Chapter 7

Summary and Recommendations for Future Work

7.1 Summary

In the first two chapters of this work we reviewed the relevant literature and formulated the general von Kármán equations for circular plates under both thermal and electrostatic loadings.

In Chapter 3, we studied the mechanical behavior of an electrostatically actuated micropump. We modeled the actuating element as an annular plate using the von Kármán nonlinear model for plates to account for in-plane stresses and moderately large deformations. The electrostatic forcing adds another nonlinearity to the model. We solved for the nonlinear static deflection first and then solved the linearized eigenvalue problem around the calculated deflected shape. We presented results describing the static characteristics and the linear natural frequencies and the corresponding mode shapes of the actuating element under two different boundary conditions.

Most of the previous research on thermally induced vibrations in circular plates has been limited to small deflections. Moreover, the works that deal with large deflections were based on Berger's approximation. In Chapter 4, we investigated the nonlinear response of a circular plate to a thermal loading consisting of a steady component and a sinusoidal component. We based the analysis on the

heat conduction equation and the dynamic analogue of the von Kármán equations. We neglected the dissipation terms in the heat equation and solved it explicitly for the temperature distribution. Then, we substituted the resulting distribution into the equations describing the displacement and the stress function. We used the method of multiple scales to determine a first-order approximation of the plate response with simply supported boundary conditions in the case of principal parametric resonance of an axisymmetric mode, which is not involved in an internal resonance with any other mode, and obtained two first-order nonlinear ordinary-differential equations governing the amplitude and phase of the response. We used these modulation equations to generate frequency-and force-response curves. The numerical results showed that the heat variation can lead to large-amplitude responses, including multivalued responses and jumps. We followed the same procedure for the second case of a clamped circular plate to investigate combination parametric resonances of the additive and difference types and also principal parametric resonance.

In Chapter 5, we investigated the static and dynamic behavior of postbuckled circular plates under a thermal load using the Galerkin approximation. We formulated the dynamic postbuckling problem of a circular plates under a constant temperature using the von Karman plate model. We used the Galerkin procedure to reduce the distributed-parameter problem into a finite system of ordinary-differential equations in time. The linear undamped modes with in-plane loading were used as basis functions in the discretization. For given system parameters, the reduced-order system was used to calculate approximations to the plate static as well as dynamic deflections. First, we solves for the equilibrium state due to the thermal load. We concluded that five modes are adequate for determining the static deflection, but they were not adequate for calculating the radial stresses, which needed 15 modes for convergence. Then, we repeated the calculations for the simply supported case and comapared the results with those obtained using the power-series solution. We used five modes to determine the natural frequencies of the axisymmetric modes for the deflected plate under an electrostatic actuation. As expected, the fundamental natural frequency decreases as the load level increases in the post-buckling regime.

The present analysis shows that the one-term Galerkin approximation might yield misleading results. Using a three-mode approximation might produce acceptable deflections, but not radial stresses. The present analysis also provides designers with a tool that can be used to analyze the

dynamic postbuckling of circular plates.

In Chapter 6, we formulated the dynamic problem of a circular plate with a constant temperature under an electrostatic load using the von Karman plate model. Again, we used the Galerkin procedure to reduce the distributed-parameter problem into a finite system of ordinary-differential equations in time. The linear undamped modes accounting for the in-plane loading were used as basis functions in the discretization. For given system parameters, the reduced-order system was used to calculate approximations to the plate static as well as dynamic deflections. First, we solved for the two equilibrium states (stable and unstable) due to a general electric potential between the plate and the electrode using a varaying number of modes in the discretization. We concluded that five modes are adequate for determining the stable static deflection up to pull-in and most of the unstable static-deflection curve. We used five modes to determine the natural frequencies of the axisymmetric modes for the deflected plate under an electrostatic actuation. As expected, the fundamental natural frequency decreases as the electrostatic coefficient increases for the same plate temperature and approaches zero at pull-in. Then, we repeated the calculations for different plate temperatures below the temperature corresponding to plate buckling. We found that the pull-in voltage decreases with increasing temperature. We also found that the plate deflection at pull-in increases slightly with increasing temperature. Increasing the strength of nonlinearity, by increasing the nondimensional gap to thickness ratio α_1, increases the pull-in voltage.

The present analysis provides designers with a tool to optimize the geometry and performance of sensors operating in a high-temperature environment. Also, this analysis can help designers control and compensate for the detrimental effect of temperature on the accuracy of measurements of such devices in uncontrolled thermal environments.

7.2 Future Work

We recommend the following topics as a continuation of this thesis. They will provide a complete picture of the modeling and analysis of the cases examined above.

1. We recommend experiments to verify the frequency change due to thermal effects.

2. We recommend examination of the effect of thermal distribution through thickness on the static and dynamic behavior of plates.

3. We recommend development of a more sophisticated and accurate electrostatic force model to assess the accuracy of the parallel plate model.

References

1. A. Abe, Y. Kobayashi, and G. Yamada, Three-mode response of simply supported rectangular laminated plates, *JSME International Journal* **41** (1998), 51-59.

2. A. Abe, Y. Kobayashi, and G. Yamada, Analysis of subharmonic resonance of moderately thick antisymmetric angle-ply laminated plates by using method of multiple scales, *Journal of Sound and Vibration* **217** (1998), 467-484.

3. J. Ahmed, Dynamic post-buckling characteristics of circular plates, *Journal of the Franklin Institute* **289** (1970), 57-66.

4. G. A. Altay and M. C. Dokmeci, Kármán-Mindlin plate equations for thermoelastic vibrations of temperature dependent materials, *ARI* **50** (1997), 110-126.

5. M. Amabili, G. Frosali, and M.K. Kwak, Free vibrations of annular plates coupled with fluids, *Journal of Sound and Vibration* **191** (1996), 825-846.

6. L. Azrar, E. H. Boutyour, and M. Potier-Ferry, Nonlinear forced vibrations of plates by an asymptotic-numerical method, *Journal of Sound and Vibration* **252** (2002), 657-674.

7. K. Bairagi, *Textbook of Plates*, Khanna, Bombay, 1986.

8. P. Biswas and P. Kapoor, Nonlinear vibrations of circular plates at elevated temperature, *4th International Conference on Numerical Methods in Thermal Problems* Swansea, UK (1985), 1493-1501.

9. F. Bloom and D. Coffin, *Handbook of Thin Plate Buckling and Postbuckling*, Chapman and Hall/CRC, Boca Raton, Florida, 2001.

10. R. Bodner, The post-buckling behavior of a clamped circular plate, *Quarterly of Applied Mathematics* **12** (1954), 397-401.

11. B. A. Boley and J. H. Weiner, *Theory of Thermal Stresses*, Wiley, New York, 1960.

12. T. Bourouina and J-P. Grandchamp, Modeling micropumps with electrical equivalent networks, *Journal of Micromechanics and Microengineering* **6** (1996), 398-404.

13. M. E. Brewster, The post-buckling behavior of a clamped circular plate, *SIAM Journal on Applied Mathematics* **51** (1991), 1255-1283.

14. F. Buckens, Vibrations in a thermally stressed thin plate, *Journal of Thermal Stresses* **2** (1979), 367-385.

15. W. P. Chang and S. M. Wan, Thermomechanically coupled non-linear vibration of plates, *International Journal of Non-Linear Mechanics* **21**(5) (1986), 375-389.

16. C-Y. Chia, *Nonlinear Analysis of Plates*, McGraw-Hill, New York, 1980.

17. H-N. Chu and G. Herrmann, influence of large amplitudes of free flexural vibrations of rectangular elastic plates, *Journal of Applied Mechanics* **23** (1956), 532-542.

18. A. Cozma and R. Puers, Electrostatic actuation as a self-testing method for silicon pressure sensors, *Sensors and Actuators A* **60**(5) (1997), 32-36.

19. E. M. Dombourian, C. V. Smith, and R. L. Carlson, A Perturbation solution to a plates postbuckling problem, *International Journal of Non-Linear Mechanics* **11** (1976), 49-58.

20. P. C. Dumir, Nonlinear vibration and postbuckling of isotropic thin circular plates on elastic foundations, *Journal of Sound and Vibration* **107** (1986), 253-263.

21. P. C. Dumir, R. Kumar, and M. L. Ghandi, Nonlinear axisymmetric vibration of orthotropic thin circular plates on elastic foundation, *Journal of Sound and Vibration* **103** (1985), 273-283.

22. P. C. Dumir, R. Kumar, and M. L. Ghandi, Nonlinear axisymmetric vibration of orthotropic thin circular plates with elastically restrained edges, *Journal of Computers and Structures* **26** (1986), 677-686.

23. O. Francais, I. Dufour, and E. Sarraute, Analytical static modeling and optimization of electrostatic micropump, *Journal of Micromechanics and Microengineering* **7** (1997), 183-185.

24. O. Francais and I. Dufour, Dynamic simulation of an electrostatic micropump with pull-in and hystersis phenomena, *Sensors and Actuators A* **70** (1998), 56-60.

25. O. Francais and I. Dufour, Normalized abacus for the global behavior of diaphragms: pneumatic, electrostatic, piezoelectric, or electromagnetic actuation, *Journal of Modeling and Simulation of Microsystems* **1** (1999), 149-160.

26. K. O. Friedrichs and J. J. Stoker, Buckling of the circular plate beyond the critical thrust, *Journal of Applied Mechanics* **9** (1942), A7-A14.

27. B. E. Gatewood, *Thermal Stresses*, McGraw-Hill, New York, 1957.

28. R. C. Gauss and S. S. Antman, Large thermal buckling of nonuniform beams and plates, *International Journal of Solids and Structures* **20** (1982), 979-1000.

29. C. Gehin, C. Barthod, and Y. Teisseyre, Design and characterization of a force resonant sensor, *Sensors and Actuators A: Physical* **84** (2000), 65-69.

30. M. L. Gossard, P. Seide, and W. M. Roberts, *Thermal Buckling of Plates*, NACA Technical Note 2771, 1952.

31. J. Hadian and A. H. Nayfeh, Modal interaction in circular plates, *Journal of Sound and Vibration* **142** (1990), 279-292.

32. R. R. Heldenfels and W. M. Roberts, *Experimental and theoretical determination of thermal stresses in a flat plate*, NACA Technical Note 3578, 1956.

33. G. Herrmann, *Influence of large amplitudes on flexural motions of elastic plates*, NACA Technical Note 2769, 1952.

34. R. B. Hetnarski, *Thermal Stresses II*, North-Holland, The Netherlands, 1987.

35. C-L. Huang and B. E. Sandman, Large amplitude vibrations of a rigidly clamped circular plates, *International Journal of Non-Linear Mechanics* **6** (1971), 451-468.

36. T. Irie and G. Yamada, Thermally induced vibration of circular plate, *Bulletin of the Japanese Society of Mechanical Engineers* **21** (1978), 1703-1709.

37. T. Y. Jiang, T. Y. Ng, and K. Y. Lam, Dynamic analysis of an electrostatic micropump, *3rd International Conference on Modeling and Simulation of Microsystems, MSM2000* California 2000.

38. R. Jones, J. Mazumdar, and Y. K. Cheung, Vibration and buckling of plates at elevated temperatures, *International Journal of Solids and Structures* **16** (1980), 61-70.

39. E. R. Konig and G. Wachutka, Analysis of unstable behavior occurring in electro-mechanical microdevices, *2nd International Conference on Modeling and Simulation of Microsystems, MSM1999* California 1999.

40. A. Y. T. Leung and S. G. Mao, A symplectic Galerkin method for non-linear vibration of beams and plates, *Journal of Sound and Vibration* **183** (1995), 475-491.

41. L. Librescu, *Plates and Shells*, Unpublished Lecture Notes, 2001.

42. L. Librescu and W. Lin, Non-linear response of laminated plates and shells to thermomechanical loading: Implications of violation of interlaminar shear traction continuity requirement, *International Journal of Solids and Structures* **36** (1999), 4111-4147.

43. R. M. Lin, M. K. Lim, and H. Du, Large deflection analysis of plates under thermal loading, *Computer Methods in Applied Mechanics and Engineering* **117** (1994), 381-390.

44. S. P. Maganty and W. B. Bickford, Large amplitude oscillation of thin circular rings, *Journal of Applied Mechanics* **54** (1987), 315-322.

45. E. H. Mansfield, On the large-deflexion vibrations of heated plates, *Proceedings of the Royal Society of London, Series A* **379** (1982), 15-39.

46. K. Marguerre, Thermo-elastische platten-gleich-ungen, *Zeitschrift fur Angewandte Mathematik und Mechanik* **15** (1935), 369-372.

47. M. A. Michalicek, *Introduction to Microelectromechanical Systems: A Short Course*, Air Force Research Laboratory, New Mexico, 2000.

48. Y. Nath and R. S. Alwar, Nonlinear dynamic analysis of orthotropic circular plates, *International Journal of Solids and Structures* **16** (1980), 433-443.

49. Y. Nath, Large amplitude response of circular plates on elastic foundation, *International Journal of Non-Linear Mechanics* **17** (1982), 285-296.

50. Y. Nath and S. Kumar, Large amplitude response of layered circular plates, *Journal of Engineering Mechanics* **121** (1995), 37-49.

51. A. H. Nayfeh, *Introduction to Perturbation Techniques*, Wiley, New York, 1981.

52. A. H. Nayfeh, *Nonlinear Interactions*, Wiley, New York, 2000.

53. A. H. Nayfeh and D. T. Mook, *Nonlinear Oscillations*, Wiley, New York, 1979.

54. M. Newman and M. Forray, Axisymmetric large deflections of circular plates subjected to thermal and mechanical loads, *Journal of Aerospace Science* **29** (1962), 1060-1066.

55. C. F. Ng and R. G. White, Dynamic behavior of postbuckled isotropic plates under in-plane compression, *Journal of Sound and Vibration* **120** (1988), 1-18.

56. J. L. Nowinski, Nonlinear transverse vibrations of circular elastic plates built-in at the boundary, *4th US National Congress on Applied Mechanics* **1** (1962), 325-332.

57. J. L. Nowinski and H. Ohnabe, On certain inconsistencies in Berger equations for large deflections of elastic plates, *International Journal of Mechanical Science* **14** (1972), 165-170.

58. K. Oh and A. H. Nayfeh, High- to low frequency modal interactions in a cantilever composite plate, *Journal of Vibration and Acoustics* **120** (1998), 579-587.

59. M. C. Pal, Large deflections of heated circular plates, *Acta Mechanica* **8** (1969), 82-103.

60. M. C. Pal, Large amplitude free vibration of circular plates subjected to aerodynamic heating, *International Journal of Solids and Structures* **6** (1970), 301-313.

61. M. C. Pal, Static and dynamic non-linear behaviour of heated orthotropic circular plates, *International Journal of Non-Linear Mechanics* **8** (1973), 489-504.

62. V. Panc, *Theories of Elastic Plates*, Noordhoff, Leyden, 1975.

63. R. Puers, A. Cozma, and D. De Bruyker, On the mechanisms in thermally actuated composite diaphragm, *Sensors and Actuators A* **67** (1998), 13-17.

64. H. Qiang, Z. Nianmei, and Y. Guitong, Chaotic motion of a nonlinear thermo-elastic elliptic plate, *Applied Mathematics and Mechanics* **20** (1999), 960-966.

65. C. Rajalingham and R. B. Bhat, Influence of an electric field on diaphragm stability and vibration in a condenser microphone, *Journal of Sound and Vibration* **211** (1998), 819-827.

66. G. Ramesh and C. S. Krishnamoorthy, Geometrically non-linear analysis of plates and shallow shells by dynamic relaxation, *Computer Methods in Applied Mechanics and Engineering* **123** (1995), 15-32.

67. J.N. Reddy, *Theory and Analysis of Elastic Plates*, Hemisphere, New York, 1999.

68. C. A. Rossit and P. A. A. Laura, A unified polynomial approach for the approximate solution of thermoelastic problems in rectangular plates, *Ocean Engineering* **24** (1997), 543-549.

69. M.T.A. Saif, B.E. Alaca, and H. Sehitoglu, Analytical modeling of electrostatic membrane actuator for micropumps, *IEEE Journal of Microelectromechanical Systems* **8** (1999), 335-345.

70. M. Sathyamoorthy, Effect of thermal loading on large amplitude vibration of clamped circular plates, *Design and Analysis of Plates and Shells*, ASME, Chicago, Illinois, (1986), pp. 137-141.

71. M. Sathyamoorthy, Nonlinear vibration analysis of plates: A review and survey of current developments, *Applied Mechanics Review* **40** (1987), 1553-1561.

72. M. Sathyamoorthy, *Nonlinear Analysis of Structures*, CRC Press, Boca Raton, Florida, 1998.

73. J. I. Seeger and B. E. Boser, Parallel-plate driven oscillations and resonant pull-in, *Solid-State Sensor, Actuator and Microsystems Workshop*, Hilton Head Island, South Carolina 2002.

74. H-S. Shen, Thermal post-buckling analysis of imperfect laminated plates using a higher-order shear deformation theory, *International Journal of Non-Linear Mechanics* **32** (1997), 1035-1050.

75. Y. Shulman, *On the Vibration of Thermally Stressed Plates in the Pre-Buckling and Post-Buckling States*, MIT Technical Report 25-25, 1958.

76. I. S. Sokolnikoff and E. S. Sokolnikoff, Thermal stresses in elastic plates, *Transactions of the American Mathematical Society* **45** (1939), 235-255.

77. S. Sridhar, D. T. Mook, and A. H. Nayfeh, Nonlinear resonances in the forced responses of plates, Part I: Symmetric responses of circular plates, *Journal of Sound and Vibration* **41** (1975), 359-373.

78. S. Sridhar, D. T. Mook, and A. H. Nayfeh, Nonlinear resonances in the forced responses of plates, Part II: Asymmetric responses of circular plates, *Journal of Sound and Vibration* **59** (1978), 159-170.

79. A. V. Srinivasan, Nonlinear vibrations of beams and plates, *International Journal of Non-Linear Mechanics* **1** (1966), 179-191.

80. E. Suhir, *Structural Analysis in Microelectronic and Fiber-Optic Systems*, van Nostrand Reinhold, New York, 1991.

81. M. Sunakawa, Influence of temperature changes and large amplitude on free flexural vibration of rectangular elastic plates, *Transactions of JSME* **30** (1964), 558-566.

82. T. R. Tauchert, Thermally induced flexure, buckling, and vibration of plates, *Applied Mechanics Review* **44** (1991), 347-360.

83. E.H. Tay and K.H. Phoon, Review of the technology of micropumps, *Journal of Institution of Engineers, Singapore* **37** (1997), 68-72.

84. E. A. Thornton, Thermal buckling of plates and shells, *Applied Mechanics Review* **46** (1993), 485-506.

85. D. Trajkovski and R. Cukic, A coupled problem of thermoelastic vibrations of a circular plate with exact boundary conditions, *Mechanics Research Communications* **26** (1999), 217-224.

86. A. C. Ugural, *Stresses in Plates and Shells*, McGraw-Hill, New York, 1981.

87. K. L. Verma, Thermoelastic vibration of a transversely isotropic plate with thermal relaxations, *International Journal of Solids and Structures* **38** (2001), 8529-8546.

88. J. R. Vinson, *The Behavior of Thin Walled Structures*, Kluwer, Amsterdam, The Netherlands, 1989.

89. Vogl, G. W. and Nayfeh, A. H., A reduced-order model for electrically actuated clamped circular plates, *ASME International 19th Biennial Conference on Mechanical Vibration and Noise (VIB)*, September 2-6, 2003, Chicago, Illinois.

90. T. Wah, Vibration of circular plates at large amplitudes, *Journal of Engineering Mechanics Division, Proceedings of American Society of Civil Engineers* EM **5** (1963), 1-15.

91. A. Wang, Axisymmetric postbuckling and secondary bifurcation buckling of circular plates, *International Journal of Non-Linear Mechanics* **35** (2000), 279-292.

92. P. K. C. Wang and F. Y. Hadaegh, Computation of static shapes and voltages for micromachined deformable mirrors with nonlinear electrostatic actuators, *IEEE Journal of Microelectromechanical Systems* **5** (1996), 205-220.

93. J. E. Warren, A. M. Brzezinski, and J. F. Hamilton, Capacitance-microphone static membrane deflections, *Journal of the Acoustical Society of America* **52** (1972), 711-719.

94. J. E. Warren, A. M. Brzezinski, and J. F. Hamilton, Capacitance-microphone dynamic membrane deflections, *Journal of the Acoustical Society of America* **54** (1973), 1201-1213.

95. Z. Wei, Analysis of global dynamics in a parametrically excited thin plate, *Acta Mechanica Sinica (English Series)* **17** (2001), 71-85.

96. S. Xuefeng, C. Yiping, and Z. Xiaoqing, The study of nonlinear thermoelastic vibration of circular plate, *Acta Mechanica Solida Sinica* **20** (1999), 245-250.

97. N. Yamaki, Influence of large amplitudes on flexural vibrations of elastic plates, *Zeitschrift fur Angewandte Mathematik und Mechanik* **41** (1961), 501-510.

98. Y-L. Yeh, C-K. Chen, and H-Y. Lai, Chaotic and bifurcation dynamics for a simply supported rectangular plate of thermo-mechanical coupling in large deflection, *Chaos, Solitons and Fractals* **13** (2002), 1493-1506.

99. P. Yu, W. Zhang, and Q. Bi, Vibration analysis on a thin plate with the aid of computation normal forms, *International Journal of Non-Linear Mechanics* **36** (2001), 597-627.

100. W. Zhang, Global and chaotic dynamics for a parametrically excited thin plates, *Journal of Sound and Vibration* **239** (2001), 1013-1036.

101. J. Zhu, S. K. Datta, and A. H. Shah, Modal representation of transient dynamics of laminated plates, *Journal of Composite Engineering* **5** (1995), 949-963.

Vita

Waleed Fekry Faris was born on December 15, 1966 in Sharkia, Egypt. He joined the College of Engineering at Zagzig University in 1984 and graduated from the Department of Mechanical Engineering in 1989 with honors and he was ranked the first in the graduating class at Zagzig University. After finishing his military service, he joined the Mechanical Engineering Department as an instructor. He finished his MS in 1996. In 1999, he joined the Department of Engineering Science and Mechanics at Virginia Tech to pursue a PhD in nonlinear dynamics, which he earned in December 2003.